2022-01

CLASSICAL STABILITY AND FORMATION OF BLACK HOLES BEYOND GENERAL RELATIVITY

RODRÍGUEZ BAEZ, YOLBEIKER

UNIVERSIDAD TECNICA
FEDERICO SANTA MARIA

PONTIFICIA
UNIVERSIDAD
CATÓLICA DE
VALPARAÍSO

Classical stability and formation of black holes beyond general relativity

A thesis submitted in partial fulfillment for the degree of Doctor in Physical Sciences.

Author:
Yolbeiker Rodríguez Baez

Advisor:
Dr. Radouane Gannouji

Valparaíso, Chile

January 2022

Director of Thesis:

Dr. Radouane Gannouji
Instituto de Física
Pontificia Universidad Catolica de Valparaíso

Comission:

Dr. Gustavo Dotti
Facultad de Matemática, Astronomía, Física y Computación
Universidad Nacional de Córdoba

Dr. Julio Oliva
Departamento de Física
Universidad de Concepción

Dr. Olivera Miskovic
Instituto de Física
Pontificia Universidad Catolica de Valparaíso

Dr. Dumitru Astefanesei
Instituto de Física
Pontificia Universidad Catolica de Valparaíso

Abstract

In this thesis, we will discuss the formation, classical stability, and an observational signature of black holes in the presence of additional degrees of freedom. Adding additional degrees of freedom though extra fundamental fields in the action seems to be the most promising way to construct theories of gravity beyond general relativity.

Firstly, we present a numerical study of the gravitational collapse of *k-essence* model, in which a scalar field with a non-canonical kinetic term is added into the action. We will show that the scalar field propagates in the so-called emergent spacetime described by a metric different from the gravitational one, the effective metric. In this theory, two horizons emerge, known as the apparent and sonic horizon, related to the collapse of the gravitational and the effective metric, respectively. For numerical purposes, we will focus on a particular Lagrangian $K(X) = X + \beta X^2$, and study the formation and universal structure dynamics of the horizons at the threshold of the formation of these objects.

However, the addition of scalar degrees of freedom is not the only alternative. Higher dimensions, supergravity and string theories naturally lead to additional scalar and vector fields in the action when we consider the low-energy limit of such theories. To construct viable theories of gravity with additional fundamental fields, a review of the stability of black holes must be a necessary task to ensure the absence of Ostrogradsky instability. In this sense, we study the classical stability of the generalized Einstein-Maxwell-Scalar theory. We will develop a perturbation formalism on a static and spherically symmetric background and show that black holes are generically stable under certain conditions.

Finally, we will discuss a physical observable of black holes, namely the quasinormal modes for pure Lovelock black holes in some particular dimensions. It is well-known that the set of quasinormal modes frequencies depends on the intrinsic parameter of the black hole. We will analyze how the spacetime dimension affects the characteristic time and oscillation frequency of the ringdown signal, the final state of a perturbed black hole.

The results of this thesis are published in:

- R. Gannouji, Y. Rodríguez Baez and N. Dadhich, *Pure Lovelock black holes in dimensions $d = 3N + 1$ are stable*, *Phys. Rev. D* **100** (2019) 084011 [arXiv: 1907.09503].
- R. Gannouji and Y. Rodríguez Baez, *Critical collapse in K-essence models*, *JHEP* **07** (2020) 132 [arXiv: 2003.13730].
- R. Gannouji, and Y. Rodríguez Baez, *Stability of generalized Einstein-Maxwell-scalar black holes*, *JHEP (to appear)* (2021) [arXiv: 2112.00109].

Acknowledgements

Quiero agradecer en primer lugar a mi tutor Radouane Gannouji, por su constante apoyo durante estos años de formación profesional. Por estar siempre disponible en esos momentos donde los cálculos y códigos no parecían ir por buen camino. Por ser un ejemplo a seguir en la academia. Por transmitirme esos conocimientos que unicamente se dan en esas horas de discusiones.

A mi familia, que a pesar de la distancia, me apoyaron en cada momento. Ellos fueron el motor que me impulsaba cada día en esta travesía del doctorado.

A mis compañeros y colegas del Doctorado, que me brindaron su apoyo incondicional. En especial, quiero agradecer a Juan Manuel Calles, por todos eso momentos en los que compartimos fuera de la universidad. Por ayudarme a entender y organizar muchas de esas ideas que surgen al momento de programar. Por dedicar parte de su tiempo a leer esta tesis. Gracias amigo por todo ese apoyo.

También quiero agradecer a los profesores de la UTFSM y la PUCV que contribuyeron en mi formación académica durante los primeros años del Doctorado.

La presente tesis fue financiada por la Agencia Nacional de Investigación y Desarrollo (ANID), y la Dirección General de Investigación, Innovación y Postgrado (DGIIP) de la UTFSM.

Contents

Chapter 1

Introduction

1.1 A brief review of general relativity

Einstein's theory of general relativity (GR) is based on the Equivalence Principle, which led to the realization that gravity is best described and understood as a manifestation of the geometry and curvature of spacetime itself. Spacetime is the unification of space and time in one entity. It is the domain in which we live. General relativity describes spacetime as a four-dimensional pseudo-Riemannian manifold: a differential manifold endowed with a Lorentzian geometry. This manifold is equipped with a metric tensor that enables us to define notions of distance, time, the angle at an intersection and other geometric quantities.

The metric tensor $g_{\mu\nu}$ is defined by[1]

$$\mathrm{d}s^2 = g_{\mu\nu}\mathrm{d}x^\mu \mathrm{d}x^\nu \tag{1.1}$$

where $\mathrm{d}s$ is the infinitesimal distance measured between two neighboring points in the spacetime. The dynamics of the gravitational field, the spacetime metric, are prescribed by the Einstein Equations

$$G_{\mu\nu} \equiv R_{\mu\nu} - \frac{1}{2}Rg_{\mu\nu} = \frac{8\pi G}{c^4}T_{\mu\nu} \tag{1.2}$$

where G is the Newton's constant and c is the speed of light in vacuum. $T_{\mu\nu}$ is the stress-energy tensor, it is a physical quantity that encodes the density and flux of energy and momentum present in spacetime. $R_{\mu\nu}$ is the Ricci tensor, it is the contraction of the Riemann

[1] In this thesis we work in the $(-,+,+,+)$ metric signature convention.

tensor $R^{\alpha}{}_{\mu\nu\beta}$ which express the curvature of the spacetime. Mathematically

$$R^{\mu}{}_{\nu\alpha\beta} = \partial_\alpha \Gamma^{\mu}_{\nu\beta} - \partial_\beta \Gamma^{\mu}_{\nu\alpha} + \Gamma^{\mu}_{\sigma\alpha}\,\Gamma^{\sigma}_{\nu\beta} - \Gamma^{\mu}_{\sigma\beta}\,\Gamma^{\sigma}_{\nu\alpha} \tag{1.3}$$

$$\Gamma^{\alpha}_{\mu\nu} = \frac{1}{2} g^{\alpha\sigma}(\partial_\mu g_{\sigma\nu} + \partial_\nu g_{\sigma\mu} - \partial_\sigma g_{\mu\nu}) \tag{1.4}$$

$$R_{\mu\nu} = R^{\alpha}{}_{\mu\alpha\nu}\,. \tag{1.5}$$

In the above expressions, $\Gamma^{\alpha}_{\mu\nu}$ are the metric connections also called Christoffel symbols. Using the Bianchi identity[2], it can be checked that the Einstein tensor $G_{\mu\nu}$, defined in (1.2), is divergenceless $\nabla^\mu G_{\mu\nu} = 0$;[3] therefore, by the Einstein equations, we get that the energy-momentum tensor satisfies the same condition, $\nabla^\mu T_{\mu\nu} = 0$.

Einstein's equations reduce to Poisson equation for the Newtonian potential in the limit where the gravitational field is weak and static. Therefore, GR reproduces the observational test made by Newtonian physics. Moreover, this theory brings new predictions, like the deflection of light and the perihelion shift of Mercury, that help to validate the theory. But, one of the most intriguing predictions of Einstein's theory of general relativity is the existence of black holes. A Black Hole (BH) is a region from which a signal can't be sent to future null infinity. The boundary of this region is called the *event horizon*. It defines the point of no return in which no observer, lightray, and information can escape from the interior of this region. Strong evidence indicates that black holes are common astrophysical objects. They are present in the center of most galaxies and can be formed through the gravitational collapse of massive stars [4].

A remarkable property of a black hole is that its gravitational field is entirely determined by three asymptotically measurable parameters: its mass M, angular momentum J, and electric charge Q. In 4 dimensions and in electro-vacuum spacetime (with $\Lambda = 0$), GR states that black holes cannot carry any other charge. This is the so-called *no-hair conjecture* or the *uniqueness theorem* [5]. This stunning result, together with the striking analogy between the laws of black hole physics and the laws of equilibrium thermodynamics, make black holes the simplest and most exciting objects to test gravity in the strong-field regime.

Another exciting prediction of Einstein's theory of general relativity is the emission of Gravitational Waves (GWs), which are little ripples that propagate through spacetime. These waves are caused by the time-varying curvature of the spacetime produced by massive accelerating objects. But spacetime is a rigid entity; it requires a large amount of energy to generate significant waves. Therefore, the collisions of black holes or a star and a black hole

[2] $\nabla_\sigma R_{\mu\nu\alpha\beta} + \nabla_\alpha R_{\mu\nu\beta\sigma} + \nabla_\beta R_{\mu\nu\sigma\alpha} = 0$

[3] We employ the notation $\nabla_\mu V^\nu = \partial_\mu V^\nu + \Gamma^{\nu}_{\mu\alpha} V^\alpha$

are the phenomena that produce gravitational waves with significant amplitude. Clearly, the final result of a collision is a black hole with a higher mass but fewer to the sum of the individual masses. Since gravitational waves quickly decay on time, the final stage of this process — known as the *ringdown* — can be considered as small perturbations of the final black hole. The ringdown signal can be modeled as a superposition of damping oscillations characterized by complex frequencies, called *quasinormal modes*. The real part describes the oscillation frequency, while the imaginary part is the decay rate of the signal.

It turns out that general relativity predicts that the late-time behavior of the gravitational perturbations does not depend on the way they were induced. The quasinormal frequencies depend only on the black hole parameters (M, J, Q).[4] Therefore, detection of quasinormal modes allows us to determine the intrinsic parameters of such objects and detect any deviation from GR with great accuracy. The existence of BHs and GWs, which are a direct test of GR in the strong-field regime, have been proven notably through the imaging of a black hole shadow in the electromagnetic spectrum by the Event Horizon Telescope [6] and through the observation of coalescing binary black holes by the LIGO/Virgo Collaboration [7, 8].

Since its publication in 1915, General relativity has been kept under extensive experimental scrutiny, passing all experimental tests to date with great accuracy [9]. However, all attempts to quantize gravity and to unify it with the other interactions of nature have failed, suggesting that the standard GR may not be the final theory to describe gravity. Power-counting arguments indicate that GR is an effective field theory and needs to be modified at low and high energies. For example, in the high energy limit, GR does not address the problem of singularities inside BHs [10]. As shown in [11], the theory becomes renormalizable if we modify the Einstein-Hilbert action by adding quadratic curvature terms. In the cosmological scenario, GR does not offer a solution (accepted by all) to the horizon and flatness problem [12, 13], or explain the late-time acceleration of the universe [14, 15]. Since GR contains no adjustable constants, nothing can be changed. Any other attempt to describe gravity necessarily modifies GR.

1.2 Theories beyond general relativity

In 4-dimensions, Einstein's theory of general relativity is the unique interacting theory of a Lorentz-invariant massless spin-2 particle on a pseudo-Riemannian manifold, and any modification inevitably introduces new degrees of freedom. In order to construct a relativistic theory of gravity, it is necessary to review the bases that ensure that any modification could

[4] From the astrophysical point of view, BHs have no electric charge, so they are described uniquely with two parameters.

be considered a viable theory. Any theory of gravity must be constructed from the metric tensor; it encodes the geometrical properties of spacetime. Lovelock's theorem [16, 17] collects all the bases on which we can build a theory of gravity. It states that [18]:

> *The only divergence-free symmetric rank-2 tensor constructed solely from the metric and its derivatives up to second order in four dimensions, preserving diffeomorphism invariance, is the Einstein tensor plus a cosmological term.*

Despite the powerful restrictions imposed by this theorem, it does not imply that the Einstein-Hilbert action is the only action constructed from $g_{\mu\nu}$ that results in the Einstein equations. Giving up each assumption made by this theorem gives a hint to construct modifications of general relativity. Specifically, there are at least four inequivalent ways to circumvent Lovelock's theorem [18]:

- Consider other fields beyond the metric tensor
- Include higher dimensions
- Violate diffeomorphism invariance
- Violate the weak equivalence principle

In this thesis, we will study three theories of gravity beyond general relativity that include new degrees of freedom (adding extra fundamental fields) and higher spacetime dimensions. These are the most common and conservative ways to construct theories of gravity beyond GR.

1.2.1 *k-essence* theory

Dropping the assumption that "a theory of gravity must depend only on the metric tensor $g_{\mu\nu}$" opens a route to consider new fundamental fields. The simplest field to add is a scalar field. This modification gives the well-known Scalar-Tensor theories of gravity. In general, these theories allow for exact analytical solutions. It would be impossible to cite all the different origins for the scalar field, but Brans-Dicke theory of gravity [19] was one of the first theories beyond GR that introduced a scalar field with non-minimal coupling to gravity. This theory was constructed with the intention that the scalar field plays some role in the late-time evolution of the universe. However, as shown in [20] and references therein, cosmological observations impose strong restrictions on this model to the point of being discarded.

After this proposal, other scalar-tensor theories have been constructed. For example, Horndeski theory [21] is the most general action that leads to second-order equations of

motion for a metric and a scalar field in 4 dimensions, although the scalar field is coupled to gravity and higher curvature terms appear in the Lagrangian. Detection of the gravitational waves GW170817 [22] coming from the collision of a binary neutron star system, in combination with its electromagnetic counterpart [23], have served to put constraints in the tensor mode propagation speed, restricting the parameter space of Horndeski theory [24, 25, 26, 27].

In this thesis, we will consider a simple class of Horndeski gravity, the *k-essence* theory, whose Lagrangian contains the non-standard kinetic term of the scalar field. The action is given by

$$\mathcal{S}[g_{\mu\nu}, \phi] = \int d^4x\sqrt{-g}\left[\frac{1}{2}R + K(\phi, X)\right] \tag{1.6}$$

where $X = -1/2(\partial_\mu\phi)^2$ is the standard kinetic term of the scalar field ϕ. As shown in [28], under particular choices of the Lagrangian K, this theory leads to the suppression of the sound speed, giving a small value of the tensor-to-scalar ratio, which is strongly favored by observations. Another motivation to study the *k-essence* model comes from string and supergravity theories. Non-standard kinetic terms of the massless scalar degrees of freedom generically appear in the low energy limit of such theories [29]. In cosmology, *k-essence* Lagrangian was first studied in the context of *k-inflation* [30]. Then these types of models were suggested as dynamical Dark Energy for solving the late-time acceleration of the universe and the cosmic coincidence problem [31].

An attractive property of *k-essence* theories is that the inclusion of non-canonical terms in the action makes that perturbations of the field propagate in the so-called *emergent spacetime* described by a metric different from the gravitational one, the *effective metric*. As we stated before, black holes are some of the most intriguing solutions of Einstein's equations. It has been found that the dynamical evolution of a *k-essence* scalar field coupled to gravity allows for the existence of two horizons, one corresponding to the fluctuations of the *k-essence* scalar field, called the sonic horizon, and the other being the usual light horizon [32].

Physically, these horizons can be formed by the gravitational collapse of the scalar field. Gravitational collapse has been one of the most studied subjects in General Relativity since it has profoundly impacted our understanding of astrophysical phenomena. Einstein's equations form a highly complex system of differential equations; therefore, we frequently impose some symmetries on the spacetime to make the problem more tractable. Spacetimes with spherical symmetry are one of the cases. The numerical study of spherical gravitational collapse has a long history which began with the work of the collapse of ideal fluid spheres with an equation of state $P = 2\rho/3$ [33]. They found that collapse could lead to the formation of a black hole or a bounce according to initial conditions. Many new codes have been later developed with a focus on applications to realistic stellar collapse. But there has also been

considerable interest in more theoretical problems such as critical phenomena. Choptuik [34] has shown that if p is a parameter describing some aspect of the initial distribution of scalar field energy, there exists a critical value $p^\star$ which denotes the threshold of black hole formation. For $p < p^\star$, the scalar field disperses to infinity while for $p > p^\star$ black hole forms. In the supercritical regime, meaning for $p > p^\star$ but very close to the threshold, a universal behavior appears (i.e., independent of the initial data) relating the mass M of black holes to a universal scaling behavior

$$M \propto (p - p^\star)^\gamma \ , \quad \gamma \simeq 0.37 \tag{1.7}$$

This solution has been repeatedly verified, also by using a fully 3D code [35]. But as in critical phenomena, there exist classes of universality. Adding a mass term to the theory [36], which introduces a length scale, produces also a universal behavior but with a different scaling parameter γ. See also studies with a massive complex scalar field [37], with radiation fluid [38] or with extra dimensions [39].

The Choptuik problem has been one of the most significant works done in the context of Numerical relativity. Applying numerical techniques, it is possible to solve the time evolution of Einstein's equations. Since part of our investigation is inspired by these results, in Chapter 2, we review the Choptuik problem in more detail. Breaking the explicit general covariance of Einstein equations using the 3+1 formalism, we rewrite these equations as a system of partial differential equations in which the time coordinate plays a special role. In Chapter 3, we show the numerical techniques that we employed to develop a numerical code to solve the numerical evolution in time.

In this thesis, we study a natural extension of the work performed by Choptuik by studying models known as *k-essence*. For this purpose, in Chapter 4, we will describe the generic theory and summarize the various conditions for the viability of these models at classical as well as quantum level. We will derive the characteristics for these models and therefore their hyperbolicity. Using a spherically symmetric spacetime, we will obtain the constraints and evolution equations. In chapter 5, for numerical purposes, we will assume a particular *k-essence* model which will be studied in the weak as well as the strong gravitational regime. We have published the main results of this investigation in Ref. [1].

1.2.2 Generalized Einstein-Maxwell-scalar gravity

Adding extra fundamental fields in the action seems to be the most promising way to modify GR. However, adding extra degrees of freedom can affect the stability of the theory since

these new fields can be coupled to the metric tensor in unconventional ways, giving higher-order derivatives in the Lagrangian. When this happens, the Hamiltonian usually depends linearly on the canonical momentum (this dependence cannot be eliminated with integration by parts), and the system is kinetically unbounded from below. Therefore, nondegenerate Lagrangians with higher-order time derivatives lead to ghost-like instabilities, also known as Ostrogradsky instabilities [40, 41]. To avoid ghost degrees of freedom in the theory, all we need to ensure is that equations of motion remain up to second-order derivatives. Well-known examples are the Galileon models [42] and Horndeski theory, which lead to second-order equations of motion despite the presence of higher-order derivatives in their Lagrangian.

In the same way, as we introduced a scalar field, we can add a vector field. In this context, we have the generalized Proca theories [43], which are the most general vector-tensor theories with second-order equations of motion. However, we do not have to limit ourselves to include only one field. Adding a scalar field plus a vector field into the gravity sector, we can construct a Scalar-Vector-Tensor (SVT) theory [44].

Among all possible choices for a SVT theory, in this thesis we will deal with the so-called Einstein-Maxwell-Scalar (EMS) theory. This theory can be thought of as the generalization of the Einstein-Maxwell theory since we add a scalar field in the action with its corresponding kinetic energy term and with a coupling to the Maxwell field. Adding a scalar field in the action enhances the solutions of the field equations compared to the Reissner-Nordström solution, which is the charged black hole solution of the Einstein-Maxwell theory. The EMS theory arises as the effective action in the low-energy limit of string theories, in which the coupling between the scalar and Maxwell field typically has the form of an exponential function; here, the scalar field is dubbed as the dilaton since it describes how the extra dimensions dilate along the four-dimensional spacetime.

The EMS theory has its roots in the Kaluza-Klein models [45, 46]. Immediately after the publication of Einstein's theory of general relativity, which considers gravity as an effect of the curvature of the spacetime, Kaluza-Klein models suggested that the electromagnetic and gravitational fields were thought to be the components of a five-dimensional gravitational field. In fact, considering a five-dimensional theory of gravity, with the extra dimension compactified on a circle, the reduction of the theory to a four-dimensional spacetime gives the Einstein gravity coupled to a $U(1)$ vector field plus a single massless scalar field. In consequences, Maxwell's theory of electromagnetism arises naturally from a higher-dimensional theory.

The history of black hole solutions in EMS theory is fascinating since this theory provides

black hole solutions with mass, rotation, charge, and scalar hair. Therefore, it provides an attractive theoretical and computational playground to explore possible deviations from GR prediction. Nevertheless, given any black hole solution, it is necessary to check its dynamical stability to ensure that this solution would describe a physical phenomenon. The classical stability analysis is performed by making linear perturbations around the background solution; therefore, the problem changes to studying how small perturbations propagate on the background of a stationary BH. Studying wave propagation in black hole geometries gives an understanding of several topics in theoretical physics as the radiation from a slightly non-spherical gravitational collapse, scattering and absorption of waves by black holes, the generation of gravitational waves by coalescing binary systems.

Theoretical studies of BH linear perturbation theory to Schwarzschild spacetime date back to 1957 due to the pioneering work done by Regge-Wheeler [47] and Zerilli [48]. This theory was summarized in an influential monograph by Chandrasekhar [49], and it has been applied to many different physical situations.

In a spherically symmetric spacetime, the formalism consists in decomposing the perturbations in terms of spherical harmonics. In four dimensions, the metric perturbations are classified —according to their transformation properties under two-dimensional rotations— as odd (axial or vector) perturbations and even (polar or scalar) perturbations. A third type of perturbations emerges in dimensions larger than 4, known as tensor perturbations. The key point of this formalism is that the gravitational perturbation equation is reduced to a master linear differential equation similar to the Schrödinger equation with a scattering potential, from which the stability of the solution can be derived following the work done by Vishveshwara [50], Price [51] and Wald [52].

Using linear perturbation theory, in Chapter 6, we study the stability of black holes in generalized Einstein-Maxwell-Scalar theories around static spherically symmetric spacetimes, the simplest non-trivial theories including a scalar and Maxwell fields. To investigate whether or not BH solutions in this theory suffer from ghost or Laplacian instabilities, we extend the Regge-Wheeler formalism to include perturbations of the new fields. This makes the mathematical analysis more involved.

Since perturbations are decoupled at the level of the action, we discuss odd- and even-parity modes separately. In both cases, we reduce the linearized field equations to coupled differential equations for the dynamical variables corresponding to the GW and the scalar and vector field degrees of freedom. Requiring the absence of ghost instabilities in the second-order Lagrangian, we derive conditions to get the stability of BH solutions in this theory. We will also see that the propagation speeds of the GWs are the same in both types

of perturbations, giving a consistent relation that holds in any second-order SVT theories. However, the propagation speed of the scalar wave is generically different from the other fields. This yields another condition to avoid gradient instabilities, restricting further the form of the EMS action.

We published the main results of this investigation in Ref. [2].

1.2.3 Pure Lovelock theory

As stated before, the Lovelock theorem guarantees that Einstein's theory of general relativity represents the most general theory of gravity with a single metric tensor that has field equations with at most second-order derivatives in four dimensions. Therefore, another way to construct theories beyond GR is to extend the spacetime dimension. Gravitational theories in dimensions other than four have a strong theoretical interest since they offer a solution to the hierarchy problem: why gravity is the weakest interaction of nature.

Dropping the assumption of the dimension in the Lovelock theorem and preserving the others, we get that Einstein-Hilbert action is not the most general action in higher dimensions. In fact, the quadratic Gauss-Bonnet term, given by $R^2 - 4R_{\mu\nu}R^{\mu\nu} + R_{\mu\nu\alpha\beta}R^{\mu\nu\alpha\beta}$, preserves the divergence-free symmetric rank-2 tensor required by the Lovelock theorem. In this sense, there is no reason to exclude higher-order curvature terms in the action. Hence, for $d > 4$, the most general theory of gravity is obtained by adding higher curvature corrections to the Einstein-Hilbert action, which is unique in $d = 4$ and none else.

Under plausible assumptions, David Lovelock [6] obtained, for any dimension d, the most general, symmetric and conserved tensor, which is quasi-linear in the second derivatives of the metric. It is the generalization of the Einstein tensor $G_{\mu\nu}$ in higher dimensions. He also showed that this tensor could be derived from the action principle in which the Lagrangian is a homogeneous polynomial in the Riemann curvature of arbitrary degree N. It is a linear combination of $N = [\frac{d-1}{2}]$ dimensionally continued Euler densities. In five- and six-dimensions, the explicit form of the Lovelock Lagrangian is a linear combination of the Einstein-Hilbert term plus the quadratic Gauss-Bonnet term and the cosmological constant. Due to their properties, the Lovelock Lagrangian is the most natural generalization of Einstein-Hilbert theory to describe pure gravity in dimensions larger than four.

Since its publication, much attention has been applied to study the main properties of Lovelock's theories of gravity: their vacuum structure, hamiltonian formalism, dimensional reduction, induced cosmologies, wormhole configurations, and their black hole solutions, including their formation, stability and thermodynamics.

However, this generalization obscures the simplicity of general relativity. Every term in

the Lovelock Lagrangian is multiplied by a dimensionful coupling constant. Therefore, in addition to the Newton and the cosmological constants, this theory has $[\frac{d-3}{2}]$ dimensionful parameters that can be adjusted. Finding solutions to this theory is not an easy task. Many investigations centered on black hole solutions in Lovelock gravity restrict the space of parameters to simplify the mathematical analysis. This is the case of *Pure Lovelock gravity*. Instead of considering the full Lovelock polynomial, the Lagrangian —and consequently equations of motion— has only the Nth order term. There is no sum over lower orders. Remarkably, black hole solutions of this theory are asymptotically indistinguishable from those appearing in General Relativity [53].

In this thesis, we will focus on particular dimensions $d = 3N + 1$, in which the BH solution corresponds to the Schwarchild geometry even though the action does not contain the Einstein-Hilbert term. In such dimensions, the potential falls off exactly as four-dimensional GR, $1/r$. Based on this surprising property, we would address the question: would pure Lovelock black hole in $d = 3N + 1$ be stable? For this purpose, in Chapter 7, we will focus on the study of stability of pure Lovelock black holes with horizon having spherical topology. We apply perturbation theory to the background solution. We will continue the formalism of linear perturbation theory presented in Chapter 6 and extend it to higher dimensions.

As we stated before, following the gauge-invariant formalism developed in [54, 55], perturbations can be decomposed into tensor, vector and scalar perturbations according to their transformation properties with respect to $(d-2)$-dimensional rotations. The last two types correspond, respectively, to odd- and even-parity modes in the four-dimensional case, while tensor perturbations are new and emerge only in higher dimensions.

Despite the complicated form of Pure Lovelock equations, all perturbation equations are reduced to a Schrödinger-type equation

$$\Big[-\frac{d^2}{dr_*^2} + V(r)\Big]\psi = \omega^2\psi \tag{1.8}$$

from which the stability of the solution can be easily derived. The above equation can be treated as an eigenvalue problem, where the wavefunction ψ is the eigenvector and ω is the eigenvalue of the corresponding operator.

A remarkable outcome obtained from the analysis of this equation (first showed by Vishveshwara [50], which studies the Schwarzschild BH in four-dimension) is that the eigenvalues that solve equation (1.8) are discrete complex quantities. This result is obtained after imposing physical boundary conditions at the horizon and at spatial infinity. The set of these discrete complex frequencies are called quasi-normal modes (QNMs). The real part describes the oscillation frequency, while the imaginary part is the decay rate of the signal.

Since we considered a time dependence of the form $e^{-i\omega t}$, we should find that the imaginary part of these frequencies must be negative to obtain a mode decaying with time, signaling the stability of the solution.

Centered on this result, besides proving the stability of Schwarzschild-type black holes in dimension $d = 3N + 1$ from the analytical point of view in Sec. 7.2, we compute the set of quasinormal modes frequencies, in Sec. 7.6 and 7.7, to demonstrate the stability of these BHs using numerical techniques. This numerical analysis will give us more relevant conclusions above the properties of these BHs. In particular, we will focus on studying how the dimension affects the frequency and the decay rate of the oscillation.

Determining quasinormal mode frequencies has become one of the primary goals in any theory of gravity since this set of frequencies depends on the intrinsic properties of the black hole. For this reason, this set is also known as the spectrum/fingerprint of the BH. Although QNMs are well described by linear approximation theory, they can be used to test general relativity in the non-linear regime. Through this approach, we can study some aspects of the gravitational field that cannot be experimentally confirmed without considering the strong gravity regime.

We have published the main results of this investigation in Ref. [3].

As we have seen, this thesis addresses three issues around black holes. Through gravitational collapse, we will analyze the local properties at the threshold of BH **formation**. By applying linear perturbation theory, we will explore the **existence** and the **signature** of black holes. Since general relativity is a well-tested theory, we consider modifications adding new fundamental fields and increasing the spacetime dimension. Therefore our research is devoted to study the *Classical stability and formation of Black holes beyond general relativity*.

Chapter 2

Massless Scalar Field: review

Understanding gravitational collapse phenomena have been a key point to understand the nature of the gravitational field. Based on general relativity, the dynamics of an isolated system that interacts only through the gravitational field typically ends up in one of these three possibilities: the system collapses into a black hole, produces a self-sustained object like a star, or it is dispersed to infinity leaving a flat spacetime. Thus, it is through gravitational collapse that objects like stars, clusters of stars, galaxies, and black holes are formed. Understanding these phenomena is of great interest in the astrophysical community.

One of the simplest ansatz to understand gravitational collapse is to consider a scalar field as the matter content that interacts with gravity. With this simplification, we avoid effects that come from internal degrees of freedom of matter. One of the first people to study the evolution of this system from the analytic point of view was D. Christodoulou [56, 57, 58]. He studied the initial value problem for Einstein's equations in the spherically symmetric case with a massless scalar field minimally coupled to gravity. Studying the evolution of this system, he concluded, in a pair of theorems, that if the initial Cauchy data describing the scalar field is sufficiently small, there exists a global classical solution which disperses in the infinite future. On the contrary, for a high initial data, the field collapsed forming a black hole. From the analytical point of view, it was not possible to conclude the final state of the system for an intermediate value between these two cases.

Since General relativity is a theory formulated in a covariant way, it is not simple to obtain analytical solutions except when the spacetime has a lot of symmetries, as we saw in the previous example. One way to overcome this issue, and gain some understanding of the evolution of the system given any spacetime, is to apply numerical techniques to solve the dynamics. *Numerical relativity* is, in principle, a way to understand physical problems brought up in General Relativity; it is a tool that focuses on resolving Einstein equations

using algorithms and numerical approximations. One of the pionering works in this area was performed by M. Choptuik [34], who solved the dynamical evolution of a scalar field minimally coupled to gravity from the numerical point of view. To model this collapse, Choptuik considered a massless spherically symmetric scalar field. These considerations have the advantages of reducing the collapse to a problem in 1+1 dimensions. In this case, there is no gravitational radiation; this feature is important because it simplifies the problem focusing only on the collapse itself. However, since the scalar field depends on spacetime coordinates, this system has a lot of freedom that overcomplicates the solution. To simplify even more the problem, Choptuik chooses an initial scalar field described by a unique parameter, known as *1-parameter family* of initial data. One example of these configurations is a scalar field with the form of a Gaussian distribution, in which the amplitude, position or width is the variable that characterized the family (refered as p) that he could control to fix the value of the scalar field at each point in space. As we described, Choptuik's investigations were the continuation of Christodoulou's conclusions. He wanted to know if the parameter had a critical value ($p^\star$) and answer the question: how is the behavior of the black hole mass when the parameter is moved from the BH side towards the dispersion side?

To obtain conclusions that were not family dependent, tens of 1-parameter families were considered, each of them forming a BH or leaving a flat spacetime depending on the initial parameter. Choptuik found, by fine-tuning the initial data, three highly convincing numerical conclusions [34]:

1. **Scaling relation**

   When the parameter of the initial data approaches the critical values from above (in the BH side), we can produce infinitesimal black holes, with the property that its mass satisfy the scaling relation

   $$M_{BH} \approx C(p - p^\star)^\gamma \tag{2.1}$$

   where C is a constant and $p^\star$ is the critical parameter, both depending on the chosen particular 1-parameter family. γ is a critical exponent that is universal; it means that it is independent of the initial family, having a value of $\gamma \approx 0.37$ for this particular type of matter. This phenomenon of universality implies that one can tune the black hole mass to zero.

2. **Universality**

   For a finite time and a finite region in space, the solution obtained for all near-critical data was the same. This universality of the solution ends when the system's evolution decides between the BH formation or dispersion.

3. **Scale-echoing**

   The critical solution is the same when a rescaling of space and time is performed by a factor of e^{Δ}

   $$\phi_*(t, r) = \phi_*(e^{\Delta}t, e^{\Delta}r)\,, \tag{2.2}$$

   where Δ is another universal dimensionless parameter. For a massless scalar field, $\Delta \approx 3.44$.

As a summary, and making a qualitative description, what happens is the following:

For a massless scalar field, the phase space of solutions is divided into two regimes, one for which all trajectories result in a black hole formation, the other in the dispersal of the field to infinity. The connection between them is a critical surface in which a critical point acts as an attractor. Any solution that starts near the critical surface evolves almost parallel to the critical solution; after a finite time, the system chooses one of the two possible endpoints; see Figure 2.1 for a schematic representation. As described in [59], the property of Universality can be explained in a similar way. Any solution that evolves near the critical surface loses all its initial configuration details, except the distance from the black hole threshold.

After the empirical discovery made by Choptuik, gravitational collapse was discovered in many other types of matter coupled to gravity, and even in gravitational waves [61], that can collapse to a BH even in the absence of matter. Thanks to these later studies, it was obtained that the parameters γ and Δ are not universal, their values depend on the type of matter that is contained in the spacetime, but the general conclusions remain unchanged. Based on these properties and the existence of a critical value, the collapse of some type of matter coupled to gravity is known as critical collapse. The critical phenomena can be understood from the pull between the kinetic and potential energy; the former tends to disperse the scalar field to infinity while the gravitational potential tries to trap some energy of the field; if the potential is strong, a black hole can be formed.

Based on the scaling relation (2.1) and its similarity with phase transition observed in statistical mechanics, this type of collapse is known as Type II: the mass of the BH starts from an infinitesimal value and the transition is smooth. Another type of transition, known as Type I, was discovered in other types of matter. In this case, the solution is not characterized by a scaling relation; the solution is static: the BH mass has a finite (non zero) value, so the transition between solutions is not continuous. This type of critical phenomena are observed when there is a preferred length scale within the theory, such in the gravitational collapse of a massive scalar field, for example.

The mathematical theory of both types of gravitational collapse is well described in [62].

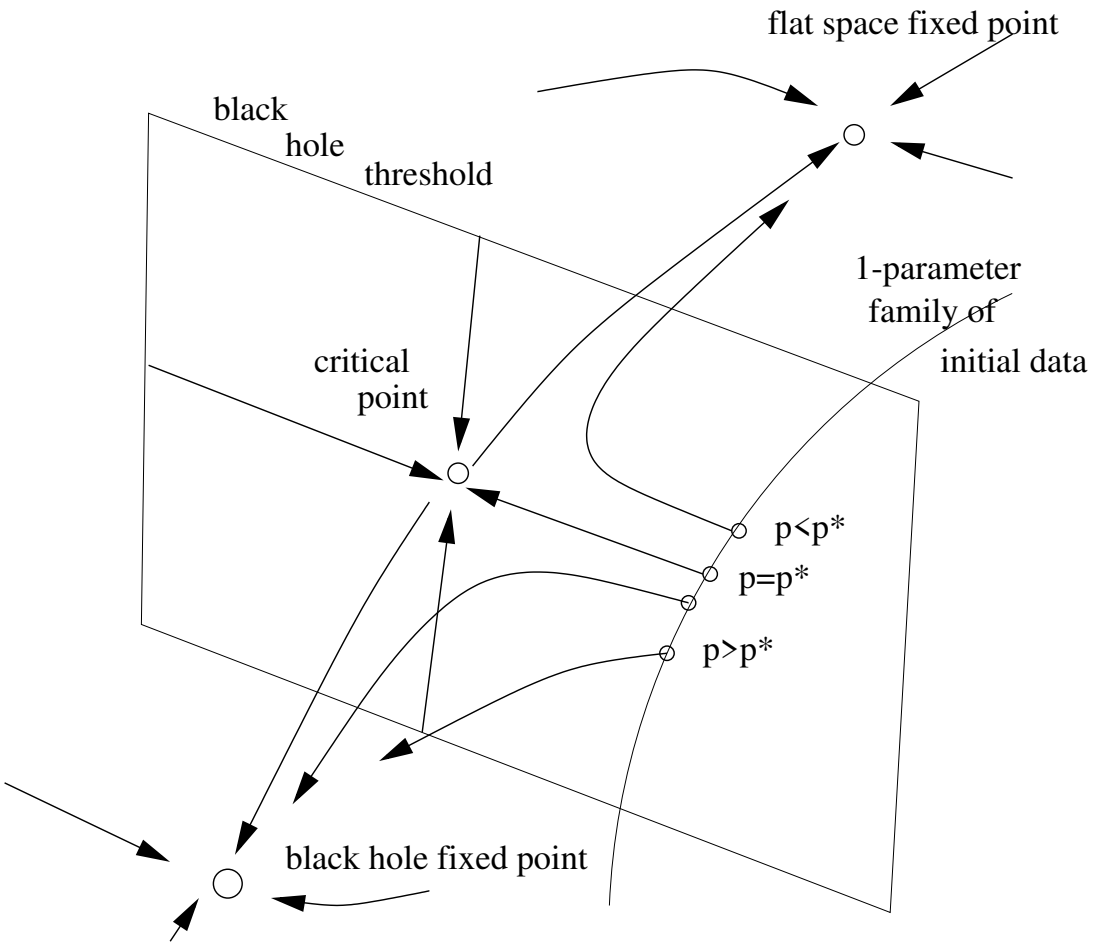

Figure 2.1: *The phase space picture for the black hole threshold in the presence of a critical point. The arrow lines are time evolutions, corresponding to spacetimes. The line without an arrow is not a time evolution, but a 1-parameter family of initial data that crosses the black hole threshold at* $p = p^\star$ *(Figure from [60]).*

2.1 Description of the Problem

Before describing the numerical procedure that we employ to solve the evolution of the system, first, we will explain the physical situation and determine the equations that Choptuik used to describe the coupling between gravity and a real massless scalar field. A more extended review of this topic can be found in [59, 60, 62].

We start by introducing the action of the system

$$\mathcal{S} = S_{EH} + S_{\phi} = \int d^4x\sqrt{-g}\left(\frac{R}{2\kappa} - \frac{1}{2}\partial_\mu\phi\partial^\mu\phi\right) \tag{2.3}$$

where g is the determinant of the metric $g_{\mu\nu}$, R is the Ricci scalar curvature, ϕ the scalar field, and $\kappa = 8\pi G$, with G the gravitational constant. We will consider geometrized units, where $c = G = 1$. We apply the standard procedure of the minimal action principle, first with respect to the metric field to obtain the Einstein equations of motion that describe the dynamics of the spacetime, and next to the scalar field to obtain the Klein-Gordon equation that describes the evolution for the scalar field. Together they describe the dynamics of the system. Explicitly, they read

$$G_{\mu\nu} = 8\pi\left(\nabla_\mu\phi\nabla_\nu\phi - \frac{1}{2}g_{\mu\nu}\nabla_\alpha\phi\nabla^\alpha\phi\right), \tag{2.4}$$

$$\Box\phi = 0\,. \tag{2.5}$$

These equations are written in a fully covariant way, where there is no clear distinction between space and time. Although this form of the equations is quite natural from the point of view of differential geometry —which has been a key feature to understand how gravity works— in particular cases it is more convenient to return to the classical picture of studying the problem in terms of the dynamical evolution of the field in "time". It can be done by rewriting the four-dimensional Einstein field equations as a Cauchy problem where the system of equations is transformed into a system of partial differential equations in which a unique solution is obtained if we provide initial conditions. Clearly, this process breaks the explicit covariance of general relativity.

In the literature, we can find various formalisms to break the covariance of the equations; we will apply the $3+1$ formalism, also known as ADM (Arnowit-Deser-Misner) formulation [63]. The formalism consists in a foliation of the spacetime in hypersurfaces of constant time, because time coordinate acquires a special role. Each hypersurface is described by a 3-Riemaniann metric. Since this formulation is so important to numerical relativity, we will

review the crucial aspects in the next section. It is useful to mention that this foliation is possible for any globally hyperbolic spacetime; see Appendix D of reference [64].

2.1.1 ADM metric

The ADM formalism is only one of the different approaches to break the covariance of Einstein field equations[1]. It consists of a foliation where we split spacetime into

$$\text{three-dimensional space} \quad + \quad \text{time coordinate} \, .$$

As we stated before, the main goal of this formalism is to rewrite the Einstein field equations in a way that allows us to give a set of initial Cauchy data that determines the evolution of the gravitational field at any later time t.

The foliation starts by considering a globally hyperbolic spacetime with metric $g_{\mu\nu}$. The slicing of the manifold into a one-parameter family of three-dimensional hypersurfaces is done by imposing some restriction on the coordinates

$$\Phi(x^\mu) = ctte.$$

Since we are interested in a foliation in which the time coordinate plays a special role, we choose space-like hypersurfaces that are parameterized by $\Phi(x^\mu) \equiv t = ctte$ (see Figure 2.2). Therefore, the hypersurfaces have time-like normal vectors and space-like tangent vectors.

Going further into the analysis, we can characterize this foliated spacetime as follows: let n^α be a unit normal vector field to the hypersurface Σ_t and let t^a be a vector field on the spacetime manifold (see Figure 2.3). We can interpret t^a as being the "flow of time" through spacetime[2]. To deduce the metric in this foliated spacetime, we can employ the geometric analysis (see also [67]):

- Consider a hypersurface Σ_t at some coordinate time t in which we define a spatial coordinates basis $x^i(t)$. The proper distance in this slice is determined by a $3-$dimensional spatial metric
$$dl^2 = \gamma_{ij} dx^i dx^j \, . \tag{2.6}$$

- Now, consider the subsequent hypersurface Σ_{t+dt}. An observer traveling through the normal direction will experience some proper time $d\tau$, which is some multiple of the

[1] Other two alternatives are the *characteristic formalism* [65] and *conformal formalism* [66].

[2] In general, the normal direction of the hypersurface is not necessarily the same as the t^a coordinate direction.

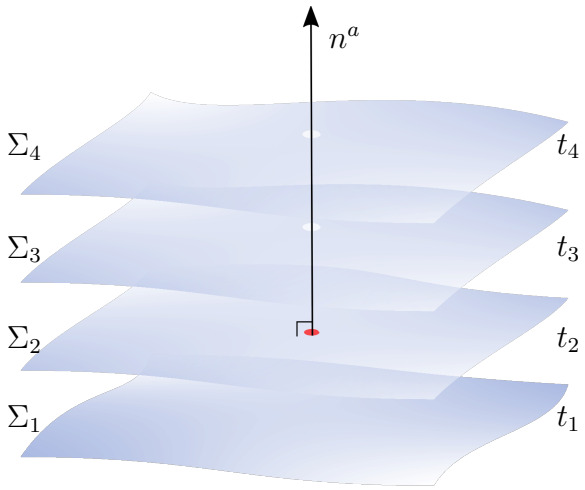

Figure 2.2: *Foliation of spacetime into three-dimensional spacelike hypersurfaces.*

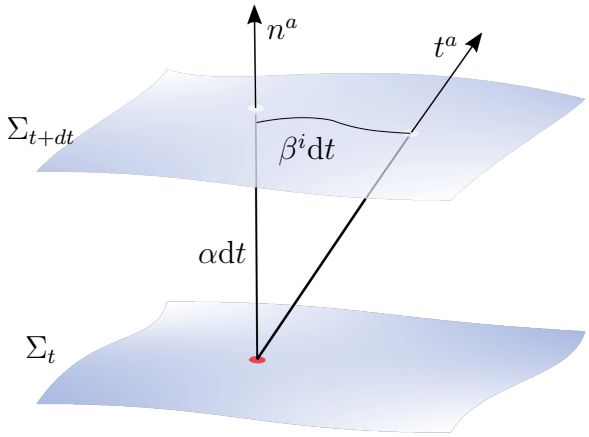

Figure 2.3: *Two adjacent hypersurfaces. We show the lapse function α and shift vector β^i.*

change in the time coordinate

$$d\tau = \alpha(t, x^i)dt \tag{2.7}$$

where α is called the lapse function, it measures the ratio between proper time and coordinate time. The lapse encodes our freedom to slice the time-like evolution, it is a gauge variable.

- On the other hand, an observer which travels through t^a, will arrive at the coordinates

$$x^i_{t+dt} = x^i_t - \beta^i(t, x^j)dt \tag{2.8}$$

where β is the shift vector that measures the spacelike shift of the coordinates while traveling normally and along the t^a direction (see Figure 2.3).

In terms of the functions $\{\alpha, \beta^i, \gamma_{ij}\}$, the metric of spacetime, in the coordinates $x^\mu = (t, x^i)$, can be written as

$$ds^2 = -\alpha^2\, dt^2 + \gamma_{jk}(dx^j + \beta^j dt)(dx^k + \beta^k dt)\,. \tag{2.9}$$

Note that the lapse function α and the shift vector β, usually referred as gauge variables, completely determine the foliation of the spacetime by the $t = constant$ spacelike hypersurfaces. Equation (2.9) is then the most general form of the metric for any foliated spacetime.

2.1.2 Spherically symmetry metric

Although the form of the line element (2.9) gives the most general metric, it overcomplicates the solutions for a spherically symmetry spacetime. This spacetime has extra degrees of freedom —invariance under rotations— that we can use to simplify this line element. Consider a spherically symmetry space given by the coordinates $x^i = (r, \theta, \phi)$. If θ and ϕ are chosen as the polar-angular coordinates on the hypersurface, we can set the gauge in which the shift vector has r-component only, since any displacement in the angular coordinates can be obtained by a rotation of the space. Thus

$$\beta^i = \beta\, \delta^i_r \,.$$

We can rewrite the metric on the hypersurface as

$$\mathrm{d}l^2 = \gamma_{ij} dx^i dx^j = \gamma_{rr} dr^2 + \gamma_{\theta\theta} \mathrm{d}\sigma^2$$

where $\mathrm{d}\sigma^2$ is the standart metric on the unit sphere. Inserting this form in (2.9), we obtain

$$\begin{aligned} \mathrm{d}s^2 &= -\alpha^2 \mathrm{d}t^2 + \gamma_{rr}(\mathrm{d}r + \beta \mathrm{d}t)(\mathrm{d}r + \beta \mathrm{d}t) + \gamma_{\theta\theta}\mathrm{d}\sigma^2 \\ &= -(\alpha^2 - \gamma_{rr}\beta^2)\mathrm{d}t^2 + 2\gamma_{rr}\beta \mathrm{d}t\mathrm{d}r + \gamma_{rr}\mathrm{d}r^2 + \gamma_{\theta\theta}\mathrm{d}\sigma^2 \end{aligned}$$

where we have supressed the coordinate dependence of each function to simplify the notation. We can rename the metric component as: $\gamma_{rr} = a^2(t, r)$ and $\gamma_{\theta\theta} = r^2 b^2(t, r)$, so

$$\mathrm{d}s^2 = -(\alpha^2 - a^2\beta^2)\mathrm{d}t^2 + 2a^2\beta \mathrm{d}t\mathrm{d}r + a^2 \mathrm{d}r^2 + r^2 b^2 \mathrm{d}\sigma^2 \,.$$

Notice that to get the above line element, we used the gauge degrees of freedom associated to coordinates θ and ϕ to eliminate two components of the shift vector. Therefore, we have two remaining functions linked with the coordinates t and r. We can chose the radial coordinate in such a way that it gives the correct area of the unit surface sphere; thus, we set $b^2(t, r) = 1$. The remaining function is used in a way that one requires that each hypersurface be a maximal hypersurface; this means that coordinates t and r are perpendicular to each other, which implies that $\beta(t, r) = 0$. Thus, the final metric is

$$\mathrm{d}s^2 = -\alpha^2(t, r)\mathrm{d}t^2 + a^2(t, r)\mathrm{d}r^2 + r^2 \mathrm{d}\sigma^2 \,. \tag{2.10}$$

This is the most general metric with spherical symmetry for a foliated spacetime. It

is also referred to as a metric in *polar-areal coordinates*. This is the metric that Choptuik employed to solve numerically the evolution of the system described in the above section.

2.2 Evolution equations

The above line element gives the metric in polar-areal coordinates; it is the generalization of Schwarzschild coordinates in the numerical relativity scheme. Using this metric (2.10), the Klein-Gordon equation (2.5) takes the simple form

$$0 = \Box\phi = \frac{1}{\sqrt{-g}}\partial_\mu\left[\sqrt{-g}g^{\mu\nu}\partial_\nu\phi\right] = \frac{1}{r^2 a\alpha}\left(-r^2\partial_t\left[\frac{a}{\alpha}\partial_t\phi\right] + \partial_r\left[r^2\frac{\alpha}{a}\partial_r\phi\right]\right). \tag{2.11}$$

To solve this equation, it is convenient to introduce two auxiliary fields

$$\Phi(t,r) = \partial_r\phi(t,r)\,, \qquad \Pi(t,r) = \frac{a}{\alpha}\partial_t\phi(t,r) \tag{2.12}$$

in order to rewrite the second-order Klein-Gordon equation as a system of two one order partial differential equations

$$\partial_t\Phi = \partial_r\left(\frac{\alpha}{a}\Pi\right) \tag{2.13}$$

$$\partial_t\Pi = \frac{1}{r^n}\partial_r\left(r^n\frac{\alpha}{a}\Phi\right) = (n+1)\frac{\partial}{\partial r^{n+1}}\left(r^n\frac{\alpha}{a}\Phi\right) \tag{2.14}$$

where $n = d-2$ is the dimension of the sphere. In the above equations, we have generalized the line element (2.10) to any dimension d, in order to study gravitational collapse in higher dimensions, see Appendix A. For $d = 4$ ($n = 2$) we recover Choptuik's equations [34]. The last equality in (2.14) is helpful for the computational solution; this is a common practice in spherically symmetric codes. On the other hand, the first two components of the Einstein tensor are

$$G_{tt} = \frac{n}{r}\frac{\alpha^2}{a^2}\left[\frac{a'}{a} + (n-1)\frac{a^2-1}{2r}\right], \tag{2.15}$$

$$G_{rr} = \frac{n}{r}\left[\frac{\alpha'}{\alpha} + (n-1)\frac{1-a^2}{2r}\right], \tag{2.16}$$

where a prime denotes derivative with respect to r. The last remaining pieces of the evolution are the components of the energy-momentum tensor. For a massless scalar field, the non-

vanishing components are

$$\begin{aligned} T_{tt} &= \frac{1}{2}\frac{\alpha^2}{a^2}\left[\Pi^2+\Phi^2\right], & T_{rr} &= \frac{1}{2}\left[\Pi^2+\Phi^2\right], \\ T_{tr} &= \frac{\alpha}{a}\Pi\Phi, & T_{ij} &= \frac{1}{2}\frac{r^2}{a^2}\left[\Pi^2-\Phi^2\right]\bar{\gamma}_{ij}, \end{aligned} \tag{2.17}$$

where indices (i,j) denote angular coordinates, $x^i = (\theta,\varphi)$, $\bar{\gamma}_{ij}$ is the metric of the unit sphere, and we have employed definitions (2.12). With all these quantities on hand, the $tt-$ and $rr-$component of Einstein equations (2.4) become

$$\frac{a'}{a} + (n-1)\frac{a^2-1}{2r} - \frac{4\pi r}{n}\left(\Pi^2+\Phi^2\right) = 0, \tag{2.18}$$

$$\frac{\alpha'}{\alpha} + (n-1)\frac{1-a^2}{2r} - \frac{4\pi r}{n}\left(\Pi^2+\Phi^2\right) = 0, \tag{2.19}$$

which has no time derivatives; therefore, these equations do not describe evolution in time. They are constraint equations that must be satisfied at each hypersurface (at each time). In the language of $(3+1)-$formalism, these equations are the Hamiltonian and Momentum constraints in GR.

At the end, the gravitational collapse of a massless scalar field coupled to gravity is described completely by equations (2.13), (2.14), (2.18) and (2.19); they form a fully constrained evolution scheme to solve for the coupled system of equations. In this scheme, the metric variables are determined using the Hamiltonian and momentum constraint equations, and the scalar equation is treated as hyperbolic, which determines the time evolution of the system.

2.2.1 Initial Conditions

The foliation of the spacetime allowed us to rewrite Einstein equations in a set of partial differential equations (2.13, 2.14, 2.18, 2.19). To completely specify the Cauchy problem, we need to provide initial data to obtain exact solutions. This can be done by fixing the form of the scalar field at the initial time, $\phi(t=0,r)$. We follow the same scheme that Choptuik used in [34], in which a smooth function parameterizes the initial distribution of the scalar field. This function depends on one parameter, refered as p, that characterizes the strength of the initial conditions. A simple example is a Gaussian distribution

$$\phi(t_0,r) = \phi_0 r^3 \exp\left[-\left(\frac{r-r_0}{\delta}\right)^q\right] \tag{2.20}$$

where t_0 is the initial time and ϕ_0, r_0, δ and q are constant. In this case, Choptuik found that the *control parameter* p (which describes the family) can be any of the four

$$p \in \{\phi_0, r_0, \delta, q\}\,.$$

That is, fixing any three of them, we shall obtain a family of initial data, $S[p]$. We will take the overall amplitude factor (ϕ_0) to be the parameter that characterized the family. Once the initial data for the scalar field is established, we are free to choose the initial data for the auxiliary fields (2.12). For example we can set

$$\Phi(t_0, r) = \partial_r \phi(t_0, r)\,, \qquad \Pi(t_0, r) = \frac{\phi(t_0, r)}{r} + \partial_r \phi(t_0, r)\,. \tag{2.21}$$

These conditions describe a scalar field that is initially ingoing; the shape of this field is shown in Fig. 2.4. Another choice of initial data, commonly taken in gravitational collapse, is $\Pi(t_0, r) = 0$; in this case, the field comprises two small packages, one traveling to the origin and the other one to infinity.

In order to obtain results that are family independent, i.e. conclusions do not depend on the initial data that is chosen; it is necessary to consider another type of family to describe the initial scalar field. We also perform the evolution of the system using

$$\phi(t_0, r) = \phi_0 \tanh\left(\frac{r - r_0}{d}\right), \tag{2.22}$$

where r_0, d and ϕ_0 are constants. Again we used the amplitude of the field to describe the family. We will identify the Gaussian profile (2.20) as **Family A** and the other one (2.22) as **Family B**. It should be mentioned that these choices of the initial data are not unique. In Appendix B, we review other choices of the initial conditions typically found in the literature.

2.2.2 Boundary Conditions

Although spacetime is infinite, we have limited computational resources to solve equations in a numerical scheme. For this reason, we have to restrict our solution to a finite range, $r \in (0, r_{max})$; where r_{max} simulates the infinity and numerically has to be chosen in a way that our solutions do not depend on this parameter. This can be done by imposing boundary conditions at the edges of this range.

The first boundary is located at $r = 0$, which is the origin of the spherically symmetric coordinate system, it is not a physical boundary. One can impose regularity conditions to

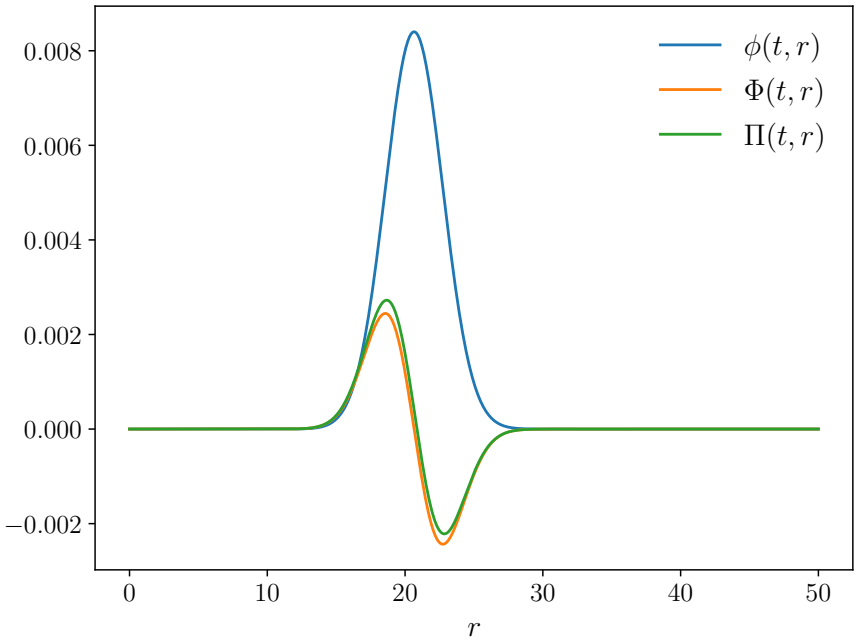

Figure 2.4: *Scalar field and auxiliary fields at initial time. The numerical integration of all the equations are performed between $r \in (0, 50]$. The shape of the scalar field is shon in (2.20) where we choose $r_o = 20$, $\delta = 3$ and $q = 2$.*

ensure that fields at this point are not ill-defined. We require spacetime to be locally flat there

$$ds^2 = -dt^2 + dr^2 + r^2 d\Omega^2 \,.$$

In this case, the Klein-Gordon equation of the scalar field is

$$\Box\phi = 0 \qquad \longrightarrow \qquad \partial_t^2\phi = \frac{1}{r^2}\partial_r(r^2\partial_r\phi) \tag{2.23}$$

which can be rewritten as the ordinary one-dimensional wave equation, $\partial_t^2(r\phi) = \partial_r^2(r\phi)$. The general solution of this equation is

$$\phi(t,r) = \frac{1}{r}[f(t+r) + g(t-r)] \tag{2.24}$$

where f and g are two arbitrary differentiable functions. The former describes an ingoing wave to the center, $r = 0$, and the latter describes an outgoing wave from the center. Let us now examine the behaviour near $r = 0$ assuming that $\phi(t, 0)$, as well as f and g, are smooth.

Making a Taylor expansion around $r \to 0$, we obtain

$$f(t+r) = f(t) + r\partial_r f(t,r)|_{r\to 0} + \frac{1}{2}r^2\partial_r^2 f(t,r)\Big|_{r=0} + \dots$$
$$g(t-r) = g(t) - r\partial_r g(t,r)|_{r\to 0} + \frac{1}{2}r^2\partial_r^2 g(t,r)\Big|_{r=0} + \dots$$

it follows for the general solution

$$\lim_{r\to 0}\phi(t,r) = \frac{1}{r}[f(t)+g(t)] + f'(t) - g'(t) + \frac{r}{2}(f''(t)+g''(t)) + \dots .$$

Therefore, in order for the solution to be well defined at the origin $r = 0$, we must impose $f(t) = -g(t)$. As a consequence of this regularity condition, it follows that $f^{(n)}(t) = -g^{(n)}(t)$. Thus

$$\lim_{r\to 0}\phi(t,r) = 2f'(t) + \frac{r^2}{3}f'''(t) + \dots .$$

From this last result we can conclude

$$\partial_r\phi(t,r)|_{r=0} = 0 + \mathcal{O}(r)\,. \tag{2.25}$$

On the other hand, if we set a distance far enough from the origin, we can guarantee that our spacetime is asymptotically flat, e.g. Minkowski. In this case, the dynamic equation is given by (2.23) and its solution by (2.24). At infinity, we must impose boundary conditions to have a zero amplitude for signals entering the integration domain. In contrast, information leaving the domain is unaffected; no boundary conditions are specified for outgoing waves. This condition is known as the radiation boundary condition [68] and can be applied to our problem by imposing

$$\lim_{r\to\infty} r\phi(t,r) = g(t-r)\,.$$

From this relation we can easily compute that

$$\partial_t[r\phi(t,r)] = \partial_t g(t-r)\ , \qquad \partial_r[r\phi(t,r)] = \partial_r g(t-r) \tag{2.26}$$

since $\partial_t g(t-r) = -\partial_r g(t-r)$, we get

$$\lim_{r\to\infty}\left(\partial_t[r\phi(t,r)] + \partial_r[r\phi(t,r)]\right) = 0\,.$$

This condition can be re-written in terms of our domain variables as

$$\frac{\partial\phi(t,r_{max})}{\partial t}+\frac{\partial\phi(t,r_{max})}{\partial r}+\frac{\phi(t,r_{max})}{r}=0\,. \tag{2.27}$$

Notice that this boundary condition is exact only for spherically symmetric waves, characterized by the property that they are incident normal to the boundary $r = r_{max}$. Since auxiliary fields also approach the right boundary, the same conditions must be applied to $\Phi(t, r)$ and $\Pi(t, r)$.

As we will see in the next chapter, we will discretize the spacetime in a fixed integration domain to solve evolution equations. Although we cannot dwell on this issue in much detail, it should be pointed out that the above boundary conditions have to be well integrated into the discretization scheme to perfectly couple the data provided by the interior evolution and constrain equations in order to have a stable evolution scheme.

2.2.3 Regularity Conditions

As the origin is not a special point, we require spacetime to be locally flat there, like all other non-singular points. This condition implies $a(t, r = 0) = 1$; otherwise, a conical singularity develops at the origin. To understand where this condition comes from, let us consider a circle at the origin (with $\theta = \pi/2$) that is parametrized by φ. The proper circumference is given by

$$\int_0^{2\pi} r\sin(\pi/2)d\varphi = 2\pi r$$

while the proper radius is

$$\int_0^{r}\big(a(t,0)+ra'(t,0)+\mathcal{O}(r^2)\big)dr = a(t,0)r+\mathcal{O}(r^2)\,.$$

As $r \to 0$, their ratio approaches to the value $2\pi/a(t, 0)$, which is not the locally flat value of 2π unless $a(t, 0) = 1$. On the other hand, since the equation for $\alpha(t, r)$ is also first order, we need one initial condition for it, as well. This condition can be motivated by the requirement that our metric approaches the Schwarzschild form as $r \to \infty$, that is

$$a(r_{max})\alpha(r_{max}) = 1\,. \tag{2.28}$$

Given this initial conditions, the Hamiltonian constraint (2.18) can be integrated radially outwards (starting at $r = 0$) and no additional condition is required at $r = r_{max}$. When $a(t, r)$ is known, we can compute the initial condition (2.28) for $\alpha(t, r)$ and the slicing condition

(2.19) can be integrated radially inwards (starting from $r = r_{max}$ to $r = 0$). However, the equation (2.19) is linear in $\alpha(t, r)$ and it is invariant under the rescaling $\alpha(t, r) \to \kappa\alpha(t, r)$ where κ is a constant. Therefore, instead of integrating equation (2.19) radially inwards, we can obtain the solution for the metric function $\alpha(t, r = 0)$, giving an arbitrarily initial value for $\alpha(t, r = 0)$, then rescale the solution with the constant κ chosen in a way that condition (2.28) is satisfied.

2.3 Black hole detection

In the weak-field regime (when the amplitude of the scalar field is close to zero), the physical situation is as follows: the initial imploding scalar field travels towards the origin, increases its amplitude as it approaches $r = 0$, and then, as the gravitational interaction is weak, the scalar field is reflected with the same shape but inverted (i.e. $\phi \to -\phi$). After enough time, all the scalar field is dispersed to infinity (traveling towards $r \gg 0$), leaving a Minkowski spacetime in the interior, see Fig 2.5.

As we increase the initial amplitude of the scalar field ϕ_0, we increase the amount of matter in spacetime. When the scalar field collapses near the origin, the ensuing gravitationally-induced self-interaction of the scalar field gets stronger. Therefore, we can reach the limit where a black hole forms in the evolution. However, as we stated before, our metric —written in the polar/areal coordinates (2.10)— cannot penetrate apparent horizons; time evolution breaks down at this point. Nevertheless, we can detect signals that indicate the formation of a black hole: the lapse function goes to zero, signaling that the coordinate system starts to become singular near what would be the radius of the black hole.

In spherical symmetry, we can monitor the *Misner-Sharp mass* [69] (see Appendix C)

$$m_{MS}(t, r) = \frac{r}{2}\left(1 - (\nabla r)^2\right) = \frac{r}{2}\left(1 - \frac{1}{a^2(t, r)}\right) \tag{2.29}$$

which has been used for a long time in the context of gravitational collapse. It satisfies several useful criteria for a quasi-local mass. For example, in asymptotically flat spacetimes it reduces to the ADM mass at spatial infinity and the Bondi-Sachs mass at future null infinity.

In a collapse simulation where a black hole is formed, we will see that the function $2m_{MS}/r$ rapidly tends to 1 at some specific radius, $r = R_{BH}$ (see Fig 2.6), where R_{BH} is precisely the radius of the black hole and, in addition, the mass of the hole is then immediately given by

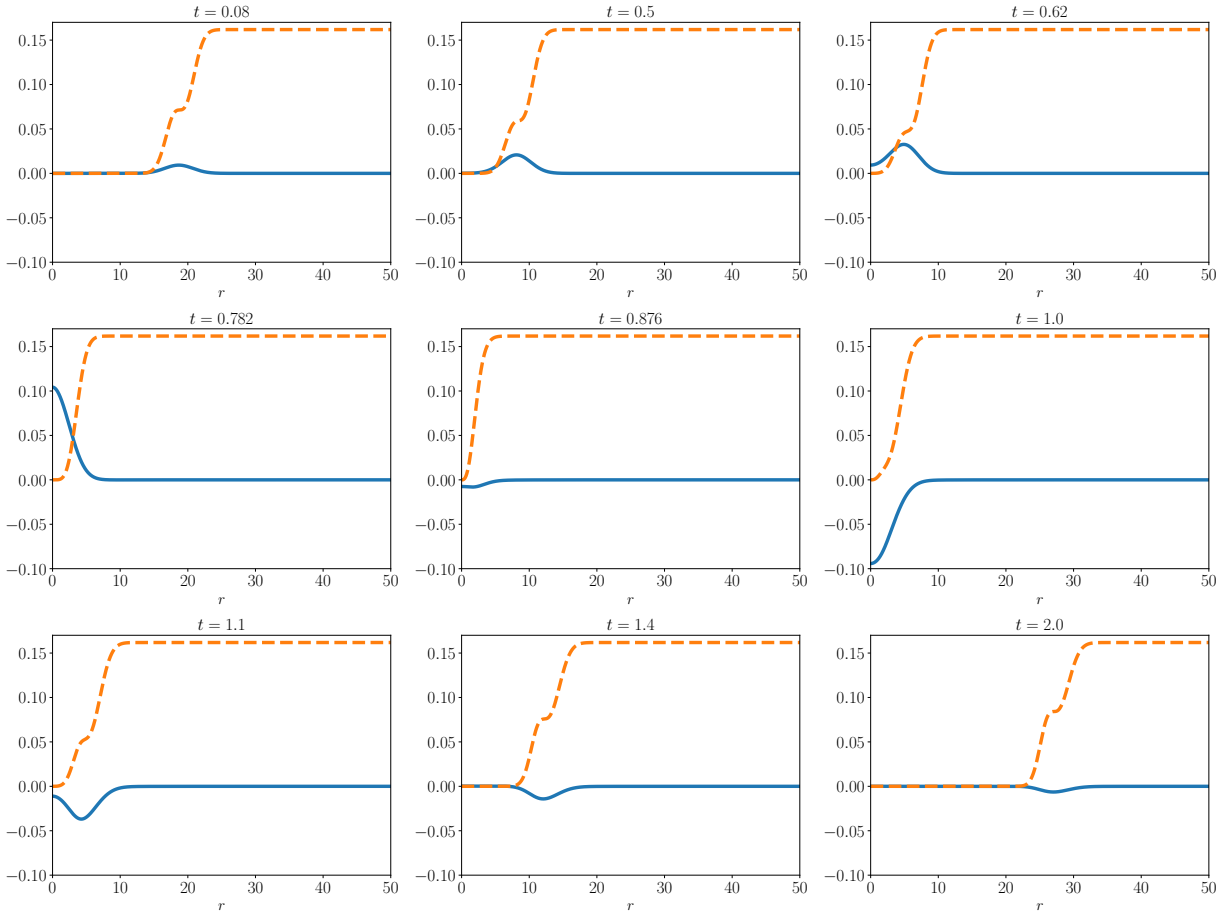

Figure 2.5: *The scalar field profile $\phi(t, r)$ (blue solid line) and Misner-Sharp mass $m_{MS}(t, r)$ (orange dashed line) for a weak field. The reported time is the iteration step (not proper time), normalized in terms of the number of points where the coordinate r is discretized. The metric fields (not shown) remain smooth and close to their Minkowksi spacetime values throughout.*

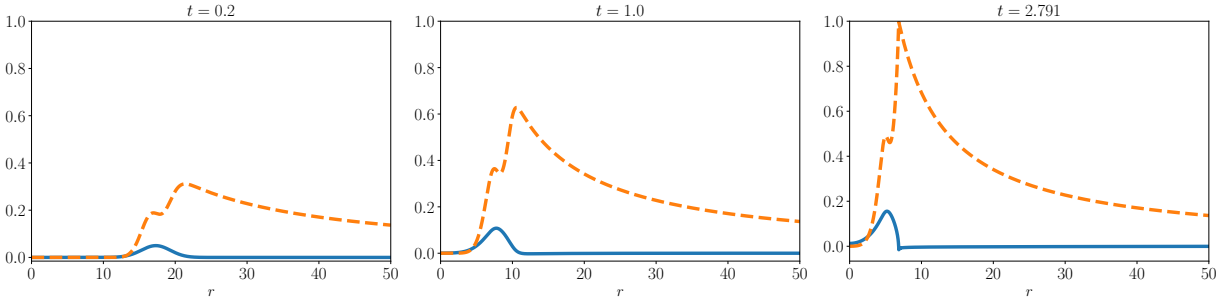

Figure 2.6: *The scalar field profile $\phi(t, r)$ (blue solid line) and the ratio $2m_{MS}/r$ (orange dashed line) for a strong field.*

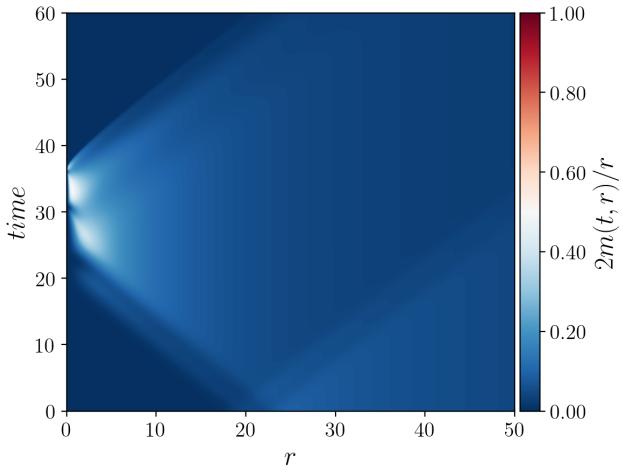

Figure 2.7: *Dispersion of the field. Evolution of the mass function when $p < p^*$.*

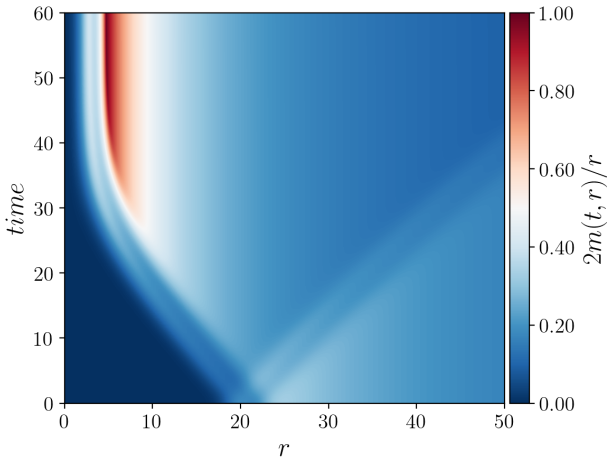

Figure 2.8: *Black hole formation. Evolution of the mass function when $p > p^*$.*

the expected expression

$$M_{BH} = \frac{R_{BH}}{2}\,. \tag{2.30}$$

Numerically, we can say that we have detected a black hole if $2m_{MS}/r \geq 0.995$.

2.4 Final comments - results of our code

As we mentioned during this chapter, the gravitational collapse of a scalar field has two possible final states: dispersion of the field or formation of a black hole. We have already shown some results of the scalar field evolution in each case, Fig 2.5 and Fig 2.6. However, as we mentioned in the above section, instead of studying the evolution of the scalar field or the auxiliary quantities, it is better to monitor the *mass function*: $2m_{MS}(t,r)/r$. In Figs. 2.7 and 2.8, we show the whole evolution of this function for two simulations: two different values of the initial amplitude of the scalar field.

In Fig. 2.7 we see that after some time of the evolution, the amplitude of the mass function starts to grow near the origin but rapidly decays to small values. At the end of the simulation, the mass function is almost zero. This evolution is an example that the scalar field is dispersed to infinity at the end of the collapse. Instead, in Fig. 2.8, we can see that the mass function starts to grow, reaching the limiting value of 1 near the origin, a signal that a black hole is formed.

To reproduce Choptuik's conclusions, we take these two different values of the initial scalar field and perform bisection of this range. This fine-tuning procedure gives the critical

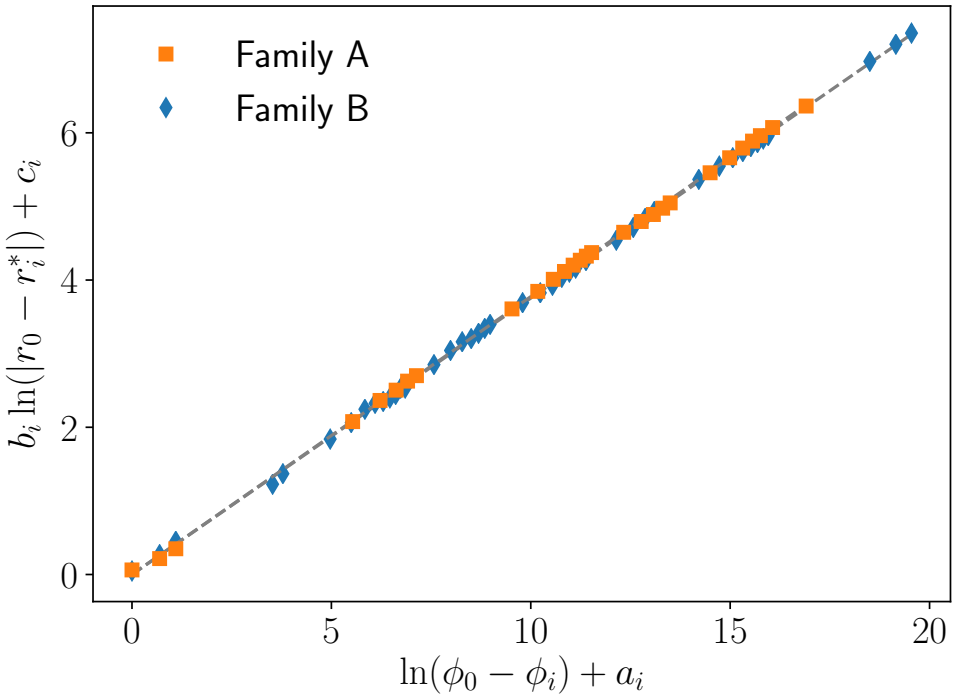

Figure 2.9: *Illustration of the conjectured mass-scaling relation (2.31). Data from two different one-parameter families.*

value, p^*, that separates the phase space of the solution. In the upper limit, when the amplitude of the scalar field is greater than p^* but near it, we obtain that the mass of the black hole that is formed satisfies the scaling relation

$$M_{BH} \propto (p - p^*)^\gamma \tag{2.31}$$

where $\gamma = 0.376$. This scaling relation is shown in Fig. 2.9 for the two families we are studying. Since this exponent is the same for both families and many others analyzed in [34], it has the character of a universal parameter. However, after many studies, it has been found that this parameter depends on the type of matter that is chosen and the dimensions of the spacetime. For example, we have generalized our code to perform gravitational collapse of a massless scalar field in d dimensions. For $d = 6$, we have obtained $\gamma = 0.42$, reproducing the well-known results of [70]. For dimension $d = 5$ to $d = 8$, we recover the results of [39].

The pioneering work of Choptuik on the spherical massless scalar field opened a new line of investigation to study the gravitational collapse of other fields. For example, the previous work has been extended to massive scalar fields [36], the gravitational collapse of radiation [38] and perfect fluid [71], a complex scalar field with angular momentum [72], the

Einstein-Massless-Dirac system [73], massive vector field [74].

As shown in [59], the gravitational collapse of various types of matter/fields has been studied in the literature because it could have an impact on understanding astrophysical phenomena. Other examples have been analyzed as toy models to get a deep insight into the gravitational field in $(3+1)-$dimensions, and others for purely mathematical interest. In particular, we will extend these studies by investigating the gravitational collapse of the *k-essence* model, which can be thought of as the generalization of the Choptuik problem.

Chapter 3

Numerical Techniques

As we mentioned in the previous chapter, we solve the equations that govern the evolution of gravitational collapse using numerical techniques, e.g., the *Runge-Kutta method*. In order to gain confidence that the numerical evolution works appropriately, we also solve the constraint equations using the *Newton solver approximation*, also known as the relaxation method. In this way, we ensure that any error in the evolution of the system is given by physical properties rather than a numerical instability associated with a particular discretization scheme. This chapter explains these numerical approximations and gives some stability conditions that guarantee that our numerical evolution converges to the analytical/real solution. For this section, we follow the standard textbooks [75, 76, 77].

Before describing any numerical solution of partial differential equations, we need to discretize the spacetime in a discrete grid. Instead of evaluating any function $f(t, x)$ at all values of x and t, we will only consider discrete values. The distance between spacial points in the grid (Δx) is called *grid spacing*, which in principle could depend on the position, but to simplify the numerical scheme, it is chosen to be constant. Thus, given an initial point on the grid (x_0), any further point is obtained by

$$x_i = x_0 + i\Delta x \qquad (i \in \mathbb{N}). \tag{3.1}$$

In the same manner, we discretize the time coordinate as

$$t^n = t^0 + n\Delta t \qquad (n \in \mathbb{N}), \tag{3.2}$$

where Δt is the spacing in the time coordinate. If our problem depends on more spatial dimensions, they are discretized in a similar way.

3.1 Finite Difference Methods

The result of the discretization is a spacetime lattice/grid in which all functions have to be evaluated. The purpose of a finite-difference approximation, when applied to a PDE, is to replace the continuum function by its discrete values in this grid and the replacement of derivatives/differential operators by its finite-difference expressions. In this process, any continuum function is replaced by

$$f(t,x) \longrightarrow f_i^n = f(t^n, x_i) + \text{truncation error}$$

where f_i^n represents the value of the function at the discrete point (t^n, x_i) on the grid. In the above expression, we have explicitly added the "truncation error" as a warning that f_i^n only approaches the correct value of $f(t,x)$ as the finite difference solution converges to the correct solution. To discretize derivatives on the grid, consider that function $f(x)$ depends only on one coordinate (the generalization with a dependency of two or more variables is performed in the same way) and assume that $f(x)$ can be differentiated to sufficiently high order. Using a Taylor expansion, we get

$$f_{i+1} = f(x+\Delta x) = f(x) + \Delta x f'(x) + \frac{1}{2}(\Delta x)^2 f''(x) + \mathcal{O}(\Delta x^3) \tag{3.3}$$

from which we obtain

$$[\partial_x f(x)]_i = \frac{f_{i+1} - f_i}{\Delta x} + \mathcal{O}(\Delta x)\,. \tag{3.4}$$

In the computational language, this expression is known as *the forward finite-differencing stencil*, which is first order in Δx. As we see, if we take the limit $\Delta x \to 0$, we recover the standard definition of the partial derivative. Another option is to perform the Taylor expansion using the x_{i-1} point, in this case

$$f_{i-1} = f(x-\Delta x) = f(x) - \Delta x f'(x) + \frac{1}{2}(\Delta x)^2 f''(x) + \mathcal{O}(\Delta x^3) \tag{3.5}$$

from which we obtain

$$[\partial_x f(x)]_i = \frac{f_i - f_{i-1}}{\Delta x} + \mathcal{O}(\Delta x) \tag{3.6}$$

which is known as *the backward finite-differencing stencil*. Combining (3.3) and (3.5) we get

$$[\partial_x f(x)]_i = \frac{f_{i+1} - f_{i-1}}{2\Delta x} + \mathcal{O}(\Delta x^2) \tag{3.7}$$

which is second order in Δx, meaning that the truncation error drops by a factor of four

when we reduce in half the grid spacing. The main conclusion is: we can combine two (or more) Taylor expansions so that the leading order error term cancels out, leaving us with a higher-order representation of the derivative. The cost required to achieve better truncation error is introducing more grid points in the differential stencil. Equation (3.7) is known as *centered finite-differencing stencil.*

Higher-order derivatives can be constructed in a similar way. Using the Taylor expansions shown above, we can obtain an expression for the second derivative

$$\left[\partial_x^2 f(x)\right]_i = \frac{f_{i+1} - 2f_i + f_{i-1}}{\Delta x^2} + \mathcal{O}(\Delta x^2) \tag{3.8}$$

which is a centered derivative and second-order in Δx.

Example: Discretization of equation (2.18)

To illustrate how the discretization of an equation works in a grid, we discretized the Hamiltonian equation (2.18). Since this equation has only one spatial derivative, the discretization is simple

$$\frac{a_{i+1}^n - a_{i-1}^n}{2\Delta r} + a_i^n \left[\frac{(a_i^n)^2 - 1}{2r_i} - 2\pi r_i\big((\Phi_i^n)^2 + (\Pi_i^n)^2\big)\right] = 0\,. \tag{3.9}$$

We have used the centered finite-differencing stencil to keep the truncation error at second order. From the above discretization, we can solve for the variable a_{i+1}^n. This means we can compute the value of the function $a(t, r)$ at any subsequent step $(i + 1)$ if we know the values of the function at a previous step. This is known as an explicit method. The above discretization scheme can be applied to field equations (2.13) and (2.14). For example, in addition to discretizing the radial coordinates as in the previous case, we can use a first- or second-order scheme to discretize the time derivative. However, in general, equations with time derivatives and small order truncation error give instabilities at a later time because errors accumulate during the evolution and break the convergence of the solution. For this reason, to solve equations (2.13) and (2.14), we used the Runge–Kutta method. It is an explicit and a higher-order scheme.

3.2 Runge-Kutta Method

As we stated before, the difference between the numerical and real solution of a partial differential equation resides in the truncation error. We have to apply a numerical scheme with many grid points in the finite difference method to minimize this error. When applied to time evolution, the disadvantage of this scheme relies on the fact that we have to store

a large amount of data for previous time steps. Instead, another technique widely used in numerical relativity codes that achieves higher-order solutions taking few points on the grid is the Runge-Kutta Method. These methods use the information on the slope at more than one point to extrapolate the solution to the future time/spatial step. The most widely known method of the Runge–Kutta family is generally referred to as "RK4" — a fourth-order scheme. It consists in the following. Let an initial value problem be

$$\dot{y} = f(t, y), \qquad y(t_0) = y_0.$$

Given the initial condition at time t_0, the solution in the future time step can be computed as

$$\begin{aligned} y_{n+1} &= y_n + \tfrac{1}{6}\left(k_1 + 2k_2 + 2k_3 + k_4\right), \\ t_{n+1} &= t_n + h \end{aligned} \tag{3.10}$$

where

$$\begin{aligned} k_1 &= h\ f(t_n, y_n)\,, & k_3 &= h\ f\left(t_n + \frac{h}{2}, y_n + \frac{k_2}{2}\right) \\ k_2 &= h\ f\left(t_n + \frac{h}{2}, y_n + \frac{k_1}{2}\right), & k_4 &= h\ f\left(t_n + h, y_n + k_3\right) \end{aligned} \tag{3.11}$$

and h is the grid spacing in the coordinate, in this case, time. The above discretization scheme for the RK4 method is known as the "classic Runge–Kutta method"[1]. RK4 is an excellent method to solve a numerical equation with time derivatives since we do not have to store large amounts of data for previous time steps. This approach is much easier than implementing a fourth-order time differencing scheme from scratch.

A simpler numerical scheme is obtained by applying a second-order Runge-Kutta method (RK2), but it is unconditionally unstable for the linear wave equation.

3.3 Method of lines

The method of lines (MoL) is a numerical technique to solve partial differential equations in which one of the variables (typically a spatial component) is replaced by algebraic approximations using Finite Difference Methods and leaving the other coordinate (time variable, in our case) as continuous. This formalism leads to a system of ordinary differential equations that can be solved using a numerical method with initial conditions, like the Runge-Kutta Method.

[1] There are infinite variants of the fourth-order Runge–Kutta scheme and the other well-known variant is the Runge–Kutta 3/8 scheme, see [77].

To illustrate this procedure, we consider the MoL in evolution equations, (2.13) and (2.14). As we pointed out, we replace the spatial derivative using the centered finite-differencing stencil (3.7)

$$\begin{aligned}\partial_t \Phi_i &= \frac{1}{2\Delta x}\left(\frac{\alpha_{i+1}}{a_{i+1}}\Pi_{i+1} - \frac{\alpha_{i-1}}{a_{i-1}}\Pi_{i-1}\right)\\ \partial_t \Pi_i &= \frac{1}{2r_i^2\Delta x}\left(r_{i+1}^2\frac{\alpha_{i+1}}{a_{i+1}}\Phi_{i+1} - r_{i-1}^2\frac{\alpha_{i-1}}{a_{i-1}}\Phi_{i-1}\right)\end{aligned} \tag{3.12}$$

where i is an index designating the position along the grid. Equations (3.12) have to be integrated at all grid points, using boundary conditions that may either result in ordinary differential equations or algebraic equations. Since equations (3.12) are first order in time, we used the initial form of the auxiliary fields, equation (2.21), as initial conditions to solve the system of equations using the RK4 method. This is the numerical technique that we used to solve partial equations with time derivatives.

3.4 Newton solver method

The Hamiltonian and Momentum constraint equations can be solved using the RK4 method. In fact, these equations can be written in the form

$$\partial_r f = S(a, \alpha, \Phi, \Pi)$$

where f can be any of the metric functions, and S is a general function. Thus, given initial conditions, the scheme (3.10) can be applied.

As a further check, we solve these constraint equations using Newton's solver method. The purpose of implementing this extra calculation is to ensure that any error in the evolution of the system is given by physical properties rather than a numerical instability associated with a particular discretization scheme. Since the equation for $a(t, r)$ is nonlinear, solving the Hamiltonian constraint requires an extra step. The ODE for the metric function a can be written as

$$E^{(a)} \equiv \partial_r a + \mathcal{F}_{(a)} = 0 \tag{3.13}$$

where $\mathcal{F}_{(a)}$ is a nonlinear function in a that depends on the variables Φ and Π. The Newton method consists in discretizing the above equation by means of a finite difference approximation and defining the vector $\mathcal{R}_j \equiv (E^{(a)})_j$ which is the residual of equation (3.13). We

iteratively find a_j by solving the linear correction δa_j

$$\mathcal{J}_{ij}\delta a_j + \mathcal{R}_i = 0 \tag{3.14}$$

where $\mathcal{J}_{ij} \equiv \delta\mathcal{R}_i/\delta a_j$ (see Section 10 in [78]). To solve the above equations, we inverted the matrix $\mathcal{J}_{ij}$ using the Gauss-Seidel method. The Newton iteration was then repeated until the residual $\mathcal{R}_j$ was below some tolerance, smaller than the truncation error.

On the other hand, the ODE for the function $\alpha(t, r)$ can be written in the form

$$\partial_r\alpha + \mathcal{H}_{(\alpha)} = 0\,. \tag{3.15}$$

Since $\mathcal{H}_{(\alpha)}$ does not depend on α, from the discretization of this equation, it follows

$$\alpha_{i+1} = \alpha_i - \Delta r[\mathcal{H}_{(\alpha)}]_{i+1/2} \tag{3.16}$$

where $[f]_{i+1/2} = (f_{i+1} + f_i)/2$ is the average value of the function between two grid points. From the numerical point of view, Newton's method is more time-consuming due to the iterative process and the inversion of the equation (3.14).

3.5 Courant–Friedrichs–Lewy condition

To ensure convergence of our numerical solutions, we have to choose the correct value for the time-step interval, Δt. For the $(1 + 1)-$dimensional case, our continuous-time model equations have the general form

$$\partial_t f + v\partial_r f = 0\,,$$

which is sometimes referred to as the model advective equation, where v is the magnitude of the velocity. Performing a von Neumann stability analysis (as shown in section 6.2.3 of [76]), the stability for the scheme is obtained if the condition $\lambda := v\Delta t/\Delta x \leq 1$ is satisfied. Such constraint is called the *Courant–Friedrichs–Lewy (CFL) condition*, and λ is referred to as the *Courant number*. Physically, the CFL condition states that the grid point for f_j^{n+1} at the new time level $n + 1$ has to reside inside the domain of determinacy of the interval spanned by the finite-difference stencil at the time level n; if f_j^{n+1} were outside this domain, its physical specification would require more information about the past than we are providing numerically, which may trigger an instability.

3.6 Testing the numerical evolution

3.6.1 Convergence Test

Once developed the numerical scheme that solves the system of equations, the next important step is to check the numerical solution. One obvious test to the code is to treat a case in which an analytical solution, or at least some very accurate numerical solution, is available for comparison. In our case, we have compared our numerical solutions with the well-known results obtained by Choptuik [34]; we reproduced the scaling relation for the mass of the black hole near the critical solution.

However, comparing a single simulation with an "analytical" solution is not the most desirable way because it would not be possible to distinguish a deviation caused by a coding error from a truncation error. A more meaningful test, common in the numerical relativity community, is to perform a sequence of simulations. Since the truncation error decrease in a predictable way with increasing numerical resources, we used this fact to detect the loss of convergence due to an error/typo in the code.

In order to get this analysis, we compute three distinct finite-difference solutions χ^h, χ^{2h}, χ^{4h} at resolutions h, $2h$ and $4h$, respectively, using the same initial data. We also assume that the finite difference meshes coincide, i.e., the $h-$grid is contained in the $2h-$grid, and this one is inside the $4h-$grid. Let us denote a numerical solution for any of the evolving fields by $\chi^h(t,r)$, with a corresponding exact (continuum) solution, $\chi^c(t,r)$. Making a Taylor expansion, we get

$$\chi^h(t,r) = \chi^c(t,r) + h^2 E_2 + \mathcal{O}(h^3) \tag{3.17}$$

where the error terms E_i are independent of the grid spacing h. We now define the *convergence factor*, $Q[\chi](t)$, associated with χ by

$$Q[\chi](t) = \frac{||\chi^{4h} - \chi^{2h}||_2}{||\chi^{2h} - \chi^{h}||_2} \tag{3.18}$$

where $||\cdot||$ is any suitable discrete norm, such as the l_2 norm, $||\cdot||_2$, defined for any grid function, f_i, by

$$||f_i||_2 = \sqrt{\frac{\Sigma_{i=1}^{N} f_i^2}{N}} \tag{3.19}$$

where N is the total number of spatial grid points. It should be noted that the subtractions in (3.18) can be taken to involve the sets of points that are common between the grids. Using

(3.17), we obtain that the convergence factor should asymptote to 4 in the continuum limit:

$$\lim_{h\to 0} Q[\chi](t) = 4\,. \tag{3.20}$$

When this condition is satisfied for any variable/field evolving in the grid, we say that the finite-difference approximation is converging.

3.6.2 Redundant Equation Test

To obtain the full constrained evolution scheme that describes the gravitational collapse of a massless scalar field (see Chapter 2), we employed only the $tt-$ and $rr-$components of Einstein's equations. Hence, we have two remaining equations that we can use to check the evolution of our numerical code. These equations are the $tr-$ and $\theta\theta-$components of Einstein's equations. Notice that this particular test is only present in spherically symmetric scenarios, in which the Einstein equations are over-determined, i.e., not independent.

Therefore, we define the following quantities

$$R_{tr} \equiv G_{tr} - 8\pi T_{tr}\,, \qquad\qquad R_{\theta\theta} \equiv G_{\theta\theta} - 8\pi T_{\theta\theta} \tag{3.21}$$

which, for a numerical solution, should be the residuals. Replacing the right-hand side of the above equations with the finite-difference approximations, which are second-order in the grid spacing, and taking the continuum limit, we should find $||R_{tr}||_2 = \mathcal{O}(h^2)$ and $||R_{\theta\theta}||_2 = \mathcal{O}(h^2)$.

3.6.3 Conservation of Energy

During the evolution of our simulation, it is necessary to make tests that validate that the numerical solutions are physically correct. One of these tests is monitoring the energy contained in the spacetime. When all the scalar field is inside our domain, energy can not be created or destroyed, so the energy has to be constant at infinity.

In general relativity it is no so easy to define mass/energy. However, it is still possible to define a global mass in an asymptotically flat spacetime. As mentioned before, in numerical relativity with spherical symmetry problems, the most usual definition of mass is the *Misner-Sharp mass* [69] (see Appendix C), which is defined as

$$m_{MS}(t,r) = \frac{r}{2}\big(1 - (\nabla r)^2\big) = \frac{r}{2}\left(1 - \frac{1}{a^2(t,r)}\right). \tag{3.22}$$

Also, we can derive this expression by comparing the form of the metric in polar-areal coordinates (2.10) with the usual Schwarzschild metric. The Misner-Sharp mass, in asymptotically flat spacetime, approaches the Arnowitt-Deser-Misner (ADM) mass

$$M_{ADM} = \lim_{r\to\infty} m_{MS}(t, r) \tag{3.23}$$

which is a conserved quantity. Physically, $m_{MS}(t, r)$ measures the amount of mass inside a sphere with radius r at time t: in vacuum regions it is thus (locally) conserved and this fact can be used to advantage in the testing of a spherically symmetric code.

3.7 FMR: Fixed Mesh Refinement

In order to get a numerical solution, we have bounded and discretized the spacetime to a domain where all functions must be evaluated. As we described earlier, the standard method introduces a grid with fixed spacing, Δx, which determines the local errors and the solution's accuracy. Through the CFL condition, this spacing also determines the number of evolution steps that we need to perform to cover the time domain of the problem and thus the cost of the computation.

The disadvantage of working with a grid whose spacing is constant comes from the required computational cost. To analyze the global picture, let us focus on our problem: we solve the evolution equations in a grid whose spatial component ranges from $r = 0$ to $r_{max} = 50$. With this range, we ensure that matter/energy is contained inside the integration domain for most of the simulation. When a black hole is produced, to identify a scaling relation, it is necessary to determine the radius of the black hole that is formed with considerable precision, typically $\Delta x = 10^{-5}$. If we take a fixed grid, we will need $\approx 10^5$ points for each iteration of time. Computational resources scale, in our case, as quadratic with the number of grid-points processed during an evolution. Obtaining results with this type of grid requires a lot of computing time (weeks!). One obvious solution is to use non-uniform grids; however, this complicates the finite difference stencil.

Instead, considering that the event horizon occurs near the origin, one strategy to circumvent this problem is to apply Fixed Mesh Refinement (FMR). It consists in taking several grids, each with a fixed grid spacing, with the particularity that the first grid (Grid 1: main grid) has a spacing Δx, the subsequent grid (Grid 2) has $\Delta x/2$, and the next one (Grid 3) has $\Delta x/4$, and so on. To respect the CFL condition, it is necessary to emphasize that the temporal spacing must also be adapted (Δt, $\Delta t/2$, $\Delta t/4$ for each grid), see Fig. 3.1.

In general, solving evolution equations with multiple grids is not too difficult, except

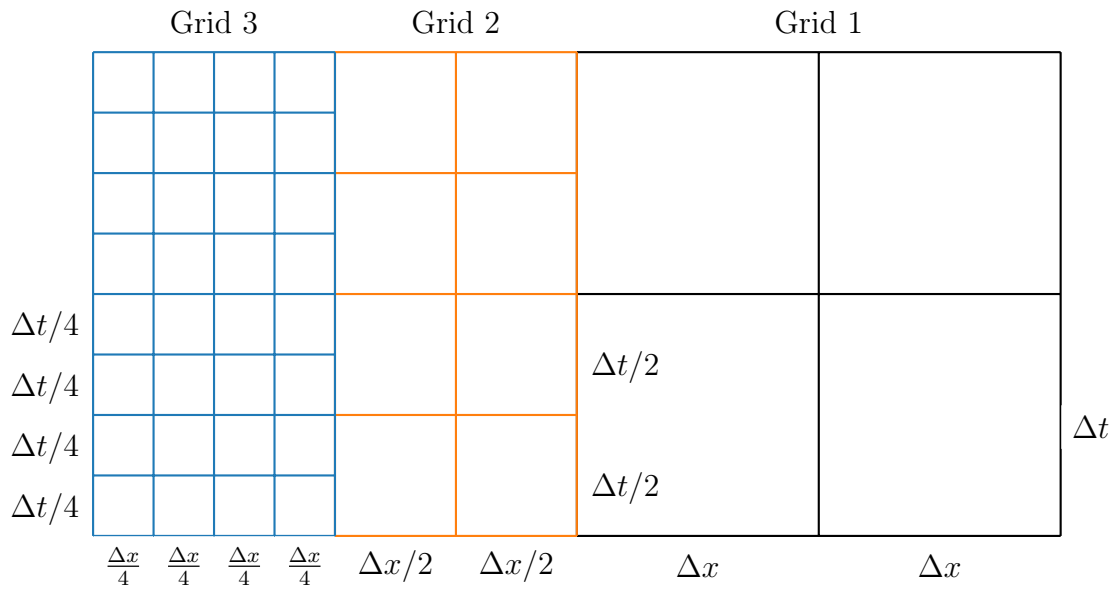

Figure 3.1: *Schematic figure of computational domains in an FMR scheme. In this example, the total computational domain is composed of three subdomains Grid 1, Grid 2, and Grid 3. Each subdomain is supposed to be covered by the same grid number, N, and thus, the grid spacing is* $\Delta x = L/N$, $\Delta x/2$, *and* $\Delta x/4$, *respectively.*

when we have to evaluate derivatives of functions in the vicinity of outer-boundary regions of each subdomain. This is the most crucial process for implementing an FMR algorithm. We have followed the process described in [77], and we will review it in the following.

A good implementation of a FMR technique has to consider two crucial points:

- **Spatial interpolation:** To compute derivatives at the edges of each inner grid, we have to extend each sub-grid with the necessary number of points. Such regions are knowns as refinement boundaries or buffer zones. The data in these zones must be supplied from their "parent" subdomain by an interpolation procedure. Therefore, it is crucial that the parent subdomain completely encloses its "child" subdomain, including the buffer zone.

- **Time integration scheme:** Since we deal with different time spacing, we have to assign the data in the buffer zone for intermediate time steps by an interpolation scheme in time. Furthermore, we need interpolation procedures in time for several substep levels because we employ a higher-order time integration scheme in which one time-step integration is composed of multi-substep procedures, like the Runge–Kutta scheme.

The question is, how many points are required in the buffer zones? It depends on the differential stencil that we use to solve the numerical equations. In our case, since we use the

RK4 scheme combined with a finite-difference of second- and fourth-order, the buffer zone must have 12 points at least.

Chapter 4

k-*essence* field

4.1 Introduction

General relativity (GR) has been our best classical theory to describe gravity. All direct experimental tests are consistent with the theory [9]. However, there are pieces of evidence that tell us that GR is not a complete theory. To begin with, GR is a purely classical theory; it is valid up to some energy scale. We can find many/infinite arguments that indicate that GR is not renormalizable in the standard quantum field theory sense. In the high energy limit, it is geodesically incomplete for most of its solutions, like black holes that contain spacetime singularity.

In addition, cosmological observations of the large-scale structure of the universe, the cosmic microwave background anisotropy, and Type IA supernovae at deep redshift suggest that our Universe is expanding at an accelerating rate [14, 15, 79]. The most straightforward solution to this acceleration based on GR is adding a cosmological constant [80]. However, this explanation introduces other conceptual issues that need to be addressed. For example, astronomical observations indicate that the cosmological constant is many orders of magnitude smaller than estimated in modern theories of elementary particles [81]. Also, recently, a lot of attention has focused on String Swampland conjectures [82, 83], which reject any de Sitter solution [84] and therefore the existence of the cosmological constant. Therefore, no dynamic solution to the expansion of our Universe is possible within GR and the standard model of particle physics.

The above arguments suggest that GR should be modified. But, there are countless unequal ways to modify this theory. Nevertheless, Lovelock's theorem serves as a guide to classify modified theories of gravity [18]. The most conservative and trodden path is to introduce new degrees of freedom. In this context, the most promising way to explain the

origin of the recent acceleration of the Universe could be due to a scalar field. This would be an exciting promotion of the relevance of scalar fields in the dynamics of the Universe. The simplest modification is obtained by adding a canonical massive scalar field described by the Lagrangian

$$\mathcal{L} = -\frac{1}{2}(\partial\phi)^2 - \frac{1}{2}m\phi^2 \,. \tag{4.1}$$

However, a simple generalization of the above Lagrangian is obtained by replacing the standard mass term by an arbitrary potential; namely

$$\mathcal{L} = -\frac{1}{2}(\partial\phi)^2 - V(\phi) \equiv X - V(\phi) \tag{4.2}$$

where X is the standard kinetic energy term and $V(\phi)$ is the potential energy that takes into account the interaction. This type of Lagrangian has been popular in the literature for some time by the name *Quintessence* as a model to explain Dark energy [85]. Depending on the ratio of its kinetic and potential energy, quintessence can be either attractive or repulsive.

When applied to the late time evolution of the Universe, the accelerated expansion is due to the potential energy of the scalar field; a similar mechanism as in slow-roll inflation. Also, the aim of considering quintessence models is to address the cosmic coincidence problem, the issue of explaining the initial conditions of the Universe necessary to yield the densities of dark energy and dark matter with the same order of magnitude that we observe today. However, to explain this coincidence, we need to fine-tune the potential energy density. In fact, the mass of the quintessence field (defined by $m_\phi^2 = d^2V(\phi)/d\phi^2$) needs to be small enough, i.e., $|m_\phi| \approx 10^{-33}\,\text{eV}$, in order to realize the cosmic acceleration. In general, there is a difficulty to reconcile such an ultra-light mass with the energy scales appearing in particle physics [86]. Even though quintessence theory has been discarded, it provided a way to construct more general theories using scalar fields.

A more recent model is to go further than the quintessence model and promote the scalar field Lagrangian density to be an arbitrary function of the standard kinetic term as

$$\mathcal{L} = K(X, \phi)\,, \tag{4.3}$$

this type of model is known as *k-essence*. It was introduced by Armendariz-Picon, Mukhanov and Steinhardt [31] following the earlier application of similar models to the very early Universe under the name *k-inflation* [30]. *K-essence* model is a scalar-tensor theory that considers gravity and a scalar field ϕ with the non-standard (non-canonical) kinetic sector in the action. The advantage of introducing *k-essence* is that we avoid the fine-tuning problem of initial conditions since *k-essence* model has a dynamical attractor behavior as a solution,

so cosmic evolution is insensitive to initial conditions [87].

In the literature, the inclusion of non-linear terms in the action has been considered in previous theories. For example, in 1934, Born and Infeld [88] used a non-linear electromagnetic field to avoid the infinite self-energy of the electron in classical electrodynamics. The proposal of scalar fields with nonminimal couplings to gravity appears in several contexts, such as in string theory [89], in Kaluza-Klein-like theories [90] or in braneworld scenarios [91, 92]. They also have important applications in cosmology [93]. Usually, non-linear terms are neglected because they are supposed to be small and irrelevant since the Hubble expansion dilutes the kinetic energy density over time.

Since scalar fields have played an important role in the development of the fundamental theories of physics, more complex Lagrangian and generalized extensions have been constructed. For example, *Galileons theory* [42] try to produce an accelerated expansion of the Universe without introducing any dark energy nor cosmological constant. *Horndeski theory* [21] is the most general theory of gravity in four dimensions whose Lagrangian is constructed out of the metric tensor and a scalar field and leads to second order equations of motion. Even if these models seem to have been finely constructed, they appear to be viable models in high symmetrical backgrounds such as homogeneous and isotropic or spherically symmetric spacetimes. But, they suffer from a major problem [94]. The equations of motion are not strongly hyperbolic for most Horndeski models except *k-essence* which arise as the most legitimate sub-class of scalar-tensor theories. At the same time, many studies try to see if scalar fields could be locally observed and what are their effects around black holes. For example, we can ask if we could observe any deviation from Kerr black hole by measuring quasi-normal modes. Even if the answer is, at present time, negative, quintessence and their extensions with non-standard kinetic terms, attracted considerable interest.

Much of the effort to understand k-essence theory has focused on the cosmological scenario [95, 96, 97], through this way, *k-essence* enter to modify GR at large scales. However, we also have to understand the effects that this field causes at high energies. We have seen that black holes serve as the ideal laboratory to detect intrinsic properties of spacetime. Thus, what are the new features that arise when this field is coupled to gravity? If any, what are the characteristics of a black hole formed through the gravitational collapse of this scalar field? In Chapter 2, we saw that the numerical study of gravitational collapse has a long history with a significant impact on understanding astronomical phenomena.

At the moment, few previous investigations explored this issue. For example, numerical simulations of various *k-essence*-type scalar fields under spherically symmetric gravitational collapse are studied in [98, 99]; they focused on the superluminality and Cauchy breakdown

present in those models. On the other hand, the intention of [100] is to identify conditions for achieving global solutions in Horndeski's theory, giving as a numerical example a model of *k-essence*. However, not much has been investigated in the local properties at the threshold of black hole formation. Choptuik's results have inspired us to analyze the scaling relation when a non-canonical scalar field is coupled to gravity. In such a way, we generalize the pioneering work done by Choptuik and complement the study of gravitational collapse of scalar fields.

For this purpose, in section 4.2, we describe the dynamics of a general *k-essence* field and review the exciting properties that arise when a non-canonical scalar field is coupled to gravity. Next, we describe some physical conditions that constrain the Lagrangian (4.3) in order to describe physical situations. As in chapter 2, the main goal of this section is to find a set of equations that forms a fully constrained evolution scheme. Using the numerical techniques described in the last chapter, these equations will enter into the numerical code to solve the gravitational collapse. The main results of these evolutions are given in the next chapter.

4.2 Dynamics for k-*essence* field

We study *k-essence* as a real scalar field ϕ, minimally coupled to gravity with a non-canonical kinetic energy term. In general, the action is of the form

$$\mathcal{S} = \int d^4x\sqrt{-g}\left[\frac{1}{2\kappa}R + \mathcal{L}(\phi, X)\right], \tag{4.4}$$

where $X := -\frac{1}{2}\partial_\mu\phi\,\partial^\mu\phi$ is the kinetic term and $\mathcal{L}$ is the Lagrangian for the *k-essence* field. In particular, we will consider models where the action is a function of X only, i.e., $\mathcal{L} = K(X)$. For example, considering small values of[1] X, we have $K(X) = const + X + \mathcal{O}(X^2)$; ignoring quadratic and higher-order terms, we recover the Lagrangian with the usual canonical scalar field with some potential. For this choice of the Lagrangian, we have a new global symmetry: our theory is invariant under constant translation in field space, $\phi \to \phi + const$. This symmetry should either be manifest in the original field variables or reveal itself after an appropriate field redefinition. As described in [101], this is the only possible solution for stationary configurations of the scalar field.

Variation of the action with respect to the metric gives us the Einstein field equations,

[1] An requiring K to be regular when $X = 0$

$G_{\mu\nu} = 8\pi T_{\mu\nu}$, where the energy-momentum tensor for the *k-essence* scalar field has the form

$$T_{\mu\nu} = K_{,X}\,\partial_\mu\phi\partial_\nu\phi + K g_{\mu\nu}\,. \tag{4.5}$$

For convenience, we have introduce the notation $K_{,X} = \partial K/\partial X$. On the other hand, the equation of motion for the scalar field is obtained by variation of (4.4) with respect to ϕ

$$g^{\mu\nu}\nabla_\nu(K_{,X}\,\nabla_\mu\phi) = \tilde{g}^{\mu\nu}\nabla_\mu\nabla_\nu\phi = 0 \tag{4.6}$$

where, in order to rewrite it as a generalized Klein-Gordon equation, we have defined

$$\tilde{g}^{\mu\nu} \equiv g^{\mu\nu}K_{,X} - K_{,XX}\,\nabla^\mu\phi\nabla^\nu\phi \tag{4.7}$$

which is the *inverse effective metric* governing propagations of perturbations of the *k-essence* scalar field[2]. As usual, this effective metric must satisfy $\tilde{g}^{\mu\nu}\tilde{g}_{\nu\alpha} = \delta^\mu_\alpha$, thus we can propose that effective metric has the form

$$\tilde{g}_{\mu\nu} = \frac{1}{K_{,X}}g_{\mu\nu} + F\nabla_\mu\phi\nabla_\mu\phi$$

where F is a function to be determined by the previous condition. Evaluating

$$\begin{aligned}\delta^\mu_\alpha &= (g^{\mu\nu}K_{,X} - K_{,XX}\,\nabla^\mu\phi\nabla^\nu\phi)\left(\frac{1}{K_{,X}}g_{\nu\alpha} + F\nabla_\nu\phi\nabla_\alpha\phi\right)\\ &= \delta^\mu_\alpha + FK_{,X}\,\nabla^\mu\phi\nabla_\alpha\phi - \frac{K_{,XX}}{K_{,X}}\nabla^\mu\phi\nabla_\alpha\phi + 2FXK_{,XX}\,\nabla^\mu\phi\nabla_\alpha\phi\end{aligned}$$

so, we finally conclude that

$$\tilde{g}_{\mu\nu} = \frac{1}{K_{,X}}g_{\mu\nu} + c_s^2\frac{K_{,XX}}{K_{,X}^2}\nabla_\mu\phi\nabla_\nu\phi\,, \qquad c_s^2 = \frac{K_{,X}}{K_{,X} + 2XK_{,XX}} \tag{4.8}$$

where c_s^2 is defined as the effective "speed of sound", which determines the propagation of perturbations of *k-essence* field. We can see that this velocity is always equal to one for models with the canonical kinetic energy term. The metric $\tilde{g}_{\mu\nu}$ describes the *emergent spacetime* and determines the cone of influence for *k-essence*. We observed from (4.8) that the effective metric $\tilde{g}_{\mu\nu}$ is not conformally equivalent to $g_{\mu\nu}$.[3] Therefore, its features (cone of influence) are not the same as the ones of the standard canonical scalar field Lagrangians.

[2]In this definition, it is assumed that the metric is invertible. It is an additional condition that physically means the scalar field is a propagating degree of freedom.

[3]Except for the trivial configuration $\partial_\mu\phi = 0$.

Since we are working with a coupled system of equations of motion, the gravitational and *k-essence* field equations, a key aspect that we need to take care of is the breakdown of the Cauchy problem. As explained in Chapter 2, to study the evolution in time of the gravitational collapse, we foliated the spacetime with spacelike hypersurfaces orthogonal to a timelike vector. Therefore, the Cauchy problem is well-posed if the condition $g^{tt} < 0$ is satisfied at each time. In this manner, we ensure that all evolution of the system is determined uniquely from the initial data. In *k-essence* theory, we have to check that our hypersurface is also spacelike to the effective metric. A breakdown of the Cauchy problem happens when the time-constant hypersurface becomes null concerning any metric. If this happens, the Cauchy problem ceases to be well-posed, and our simulations must end. Clearly, for some Lagrangians, $\tilde{g}^{tt}$ can go to zero independently of g^{tt}.

In the literature, the spacetime described by the metric (4.8) is also known as acoustic spacetime. We can find singularities that occur when the effective metric collapse, forming a trapped surface known as the *sonic horizon*. GR tells us that the luminal apparent horizon forms when surfaces of constant r become null; if we consider a coordinate basis where r is the only spatial coordinate, this happens when

$$g^{\mu\nu}\nabla_\mu r \nabla_\nu r = 0 \qquad \longrightarrow \qquad g^{rr} = 0\,.$$

Similarly, as described in [98], a sonic horizon requires the same condition as before but in the effective metric, so

$$\tilde{g}^{\mu\nu}\nabla_\mu r \nabla_\nu r = 0 \qquad \longrightarrow \qquad \tilde{g}^{rr} = 0$$

is the condition to detect a surface trapped in the emergent spacetime.

4.3 Analogy with a perfect fluid

One of the remarkable properties of the *k-essence* theory is its versatility. Although this theory was inspired by studying models with non-canonical scalar fields, using Lagrangian (4.4), we can model other types of matter characterized by a particular equation of state. This relations is revealed when we closely analyze the energy–momentum tensor of the *k-essence* field. If the gradient of the scalar field is timelike, $X > 0$, we can define a four-velocity as $u_\mu = \partial_\mu\phi/\sqrt{2X}$. So, the energy-momentum tensor (4.5) is written as

$$T_{\mu\nu} = 2XK_{,X}\,u_\mu u_\nu + K g_{\mu\nu}\,. \tag{4.9}$$

It implies that, the energy density measured by an observer with this four-velocity reads

$$\rho_c = T_{\mu\nu}u^\mu u^\nu = 2XK_{,X} - K \tag{4.10}$$

while the pressure is

$$P_c = T_{\mu\nu}n^\mu n^\nu = K \tag{4.11}$$

where n^μ is a space-like unit vector, perpendicular to u^μ. These are the usual definitions for pressure and energy density for a "cosmological" fluid; for this reason, in the previous equations, we added the subscript c. Based on this, we can rewrite the energy-momentum tensor as

$$T_{\mu\nu} = (\rho_c + P_c)u_\mu u_\nu + P_c g_{\mu\nu} \tag{4.12}$$

which has the same form as the energy-momentum tensor of a perfect fluid. In this case, the equation of state (EoS) is

$$\omega_c = \frac{P_c}{\rho_c} = \frac{K}{2XK_{,X} - K}\,. \tag{4.13}$$

On the other hand, when the gradient of the *k-essence* field is spacelike, $X < 0$, we can also define an energy-momentum tensor similar (in form, but not physically equivalent) to the perfect fluid. Defining a spacelike unit vector $n_\mu = \partial_\mu\phi/\sqrt{-2X}$, the relation (4.5) is written as

$$T_{\mu\nu} = -2XK_{,X}\, n_\mu n_\nu + K g_{\mu\nu}\,. \tag{4.14}$$

In this case, an observer with four-velocity u^μ —perpendicular to n_μ— measures an energy density ρ, and a pressure in the direction perpendicular to n_μ given by

$$\begin{aligned} \rho &= T_{\mu\nu}u^\mu u^\nu = -K \\ P &= T_{\mu\nu}n^\mu n^\nu = K - 2XK_{,X}\ . \end{aligned}$$

From these equations, it is easy to check that the EoS is the inverse of the equation defined for the timelike gradient of the scalar field. Finally, we can rewrite the energy-momentum tensor as

$$T_{\mu\nu} = (\rho + P)n_\mu n_\nu - \rho g_{\mu\nu}\,. \tag{4.15}$$

Note that the last term is different from (4.12), thus the pressure of the fluid is no longer isotropic.

In any case, we can see that for a purely $X-$dependent Lagrangian, the pressure is a function of the energy density only, $P = P(\rho)$. Therefore, choosing an action is equivalent to specifying an EoS for the equivalent hydrodynamical model. For a standard kinetic term,

$K(X) = X$, the EoS is $w_k = 1$. However, for a general choice of $K(X)$, it is easy to get any value of w_k. For example, considering $K = (\alpha X^{1/2\beta} - A)^\beta$, the EoS is $P = A\rho^{(\beta-1)/\beta}$, a polytropic law similar to various models describing neutron stars (without the anisotropic stress tensor). In many cases, the EoS can be written as $P \propto \rho^\kappa$, where κ is a constant. When $\kappa = 1$, the theory is known as Barotropic Lagrangian; on the other hand, when $\kappa > 0$ or $\kappa < 0$, we have Polytropic or Born-Infeld Lagrangian, respectively. From this analysis, we notice that we can work in the opposite direction, i.e., given the form of the EoS, we can derive the *k-essence* Lagrangian needed to describe such fluid, see [95] for various examples.

Notice also that $K(X)$ models can be related to canonical complex scalar field theories [102], where the potential of the complex scalar field is defined by $K(X)$. More than an equivalence between these theories, this is an extension which eliminates the caustics of $K(X)$ models. In fact, the complex scalar field can be seen as a theory with 2 real scalar fields with an $O(2)$ symmetry. It's only when one of these fields is frozen, that the model reduces to *k-essence*.

4.4 Constraining the Lagrangian

4.4.1 Null Energy Condition

Since the action (4.4) is general, the possible Lagrangians that we can consider are almost infinite. In order to describe physical situations, there are several conditions on the energy-momentum tensor, consequently on the Lagrangian, which are essential for crucial results in General Relativity as singularity theorems, vacuum conservation theorem, and black hole area theorem [103]. One of these restrictions is imposed by the Null Energy Condition (NEC)

$$T_{\mu\nu} n^\mu n^\nu \geq 0 \tag{4.16}$$

where n^μ in any null vector, $n^\mu n_\mu = 0$. Using the energy-momentum tensor for the *k-essence* field (4.5), we obtain

$$(K_{,X}\, \nabla_\mu\phi\nabla_\nu\phi + K g_{\mu\nu}) n^\mu n^\nu = K_{,X}\, (n^\mu \partial_\mu \phi)^2 \geq 0 \qquad \longrightarrow \qquad \boxed{K_{,X} \geq 0} \tag{4.17}$$

Physically, this requirement guarantees that perturbations of the scalar field carry positive kinetic energy density. Violation of this condition would imply that Hamiltonian is unbounded from below, leading to the inherent instability of the system [104, 105, 106].

4.4.2 Hyperbolicity Condition

To ensure that field equation (4.6) describes the dynamics of the system, we need to check that this equation is globally hyperbolic; it means that the effective metric has a Lorentzian signature. As proved in Theorem 10.1.3. of Ref. [64], if a metric has a Lorentzian signature, the field equation admits a well-posed initial value-formulation. Therefore, we have to prove that $\tilde{g}^{\mu\nu}$ has a negative determinant.

We review the procedure presented in [95]. Let us take the determinant of equation (4.7)

$$\det \tilde{\mathbf{g}} = \det \left(K_{,X}\, \mathbf{g} + K_{,XX}\, \mathbf{n} \right) = K_{,X}^{4} \cdot \det \mathbf{g} \cdot \det \left(\mathbf{1} + \frac{K_{,XX}}{K_{,X}} \mathbf{g}^{-1} \mathbf{n} \right), \tag{4.18}$$

where $\tilde{\mathbf{g}}$, $\mathbf{g}$ and $\mathbf{n}$ denote the matrices with elements $\tilde{g}^{\mu\nu}$, $g^{\mu\nu}$ and $\nabla^{\mu}\phi\nabla^{\nu}\phi$, respectively, and we have assumed $K_{,X} \neq 0$. Using the identity $\det e^{\mathbf{A}} = e^{\mathrm{tr}\mathbf{A}}$, we get

$$\det \left(\mathbf{1} + \frac{K_{,XX}}{K_{,X}} \mathbf{g}^{-1} \mathbf{n} \right) = \exp \left[\mathrm{tr} \ln \left(\mathbf{1} + \frac{K_{,XX}}{K_{,X}} \mathbf{g}^{-1} \mathbf{n} \right) \right]. \tag{4.19}$$

Furthermore, expanding the logarithm in a Taylor series around the identity, we obtain

$$\mathrm{tr}\, \ln \left(\mathbf{1} + \frac{K_{,XX}}{K_{,X}} \mathbf{g}^{-1} \mathbf{n} \right) = \sum_{k} \frac{(-1)^{k+1}}{k} \left(\frac{K_{,XX}}{K_{,X}} \right)^{k} \mathrm{tr} \left(\mathbf{g}^{-1} \mathbf{n} \right)^{k} = \ln \left(1 + 2X \frac{K_{,XX}}{K_{,X}} \right), \tag{4.20}$$

where we have used $\mathrm{tr} \left(\mathbf{g}^{-1} \mathbf{n} \right)^{k} = (2X)^{k}$. Finally, substituting equation (4.20) back into equation (4.19) we arrive at our desired result

$$\det \tilde{\mathbf{g}} = K_{,X}^{4} \cdot \det \mathbf{g} \cdot \frac{K_{,X} + 2X K_{,XX}}{K_{,X}}. \tag{4.21}$$

We know that the metric of spacetime is Lorentzian, so $\det \mathbf{g} < 0$. Therefore, $\tilde{\mathbf{g}}$ is Lorentzian if and only if

$$1 + 2X \frac{K_{,XX}}{K_{,X}} > 0. \tag{4.22}$$

This is the condition obtained in [107] and [108]. If equation (4.22) is satisfied, the generalized Klein-Gordon equation for the *k-essence* scalar field has a well-posed initial value formulation, at least locally. We can use the sign of $K_{,X} + 2X K_{,XX}$ to monitor the character of the equation of motion for the scalar field: if positive, it is hyperbolic; when negative, it is elliptic and when null it is parabolic.

A similar approach is taken in [100]. In that paper, the character of the equation is given by the sign of $\det(\tilde{g}^{\mu\nu})$ —which is the same condition as (4.22)— and the sign of the

eigenvalues of the effective metric

$$\lambda_{\pm} = \frac{\tilde{g}^{tt}+\tilde{g}^{rr}}{2} \pm \sqrt{\left(\frac{\tilde{g}^{tt}+\tilde{g}^{rr}}{2}\right)^2 - \tilde{g}^{tt}\tilde{g}^{rr} + (\tilde{g}^{tr})^2}$$
$$= \frac{\tilde{g}^{tt}+\tilde{g}^{rr}}{2} \pm \sqrt{\left(\frac{\tilde{g}^{tt}+\tilde{g}^{rr}}{2}\right)^2 - \det(\tilde{g}^{\mu\nu})}\,. \tag{4.23}$$

4.4.3 Superluminality Condition

Theories that minimally couple fields to the metric tensor have a unique cone of influence. All connected causal events of any field are inside this region. Therefore, the gravitational metric $g_{\mu\nu}$ defines global chronology of the spacetime. When we consider theories in which at least two fields are coupled to different metric tensors that are not equivalent, these conditions break down[4], and we obtain solutions in which perturbations of the matter field propagate faster than light, so we get superluminal signals. This property has been debated for a long time in different contexts in the literature, see for example Ref. [108] and the references therein.

To further illustrate the causal structure tied to the propagation of a *k-essence* field and determine a condition for a superluminal signal, let us consider the cone of influence of the effective metric $\tilde{g}_{\mu\nu}$ (portion of the emergent spacetime causally connected) defined by the condition $\tilde{g}_{\mu\nu}N^\mu N^\nu = 0$. Then it follows from equation (4.8) that

$$g_{\mu\nu}N^\mu N^\nu = -c_s^2\frac{K_{,XX}}{K_{,X}}(N^\mu\nabla_\mu\phi)^2\,. \tag{4.24}$$

Thus, N^μ is not a null vector for the metric $g_{\mu\nu}$, unless $K_{,XX}=0$. Going further, taking into account (4.17), we have that N^μ is a spacelike vector with respect to $g_{\mu\nu}$ ($g_{\mu\nu}N^\mu N^\nu > 0$) if and only if $K_{,XX} < 0$. Therefore, to avoid superluminal signals, we require

$$K_{,XX} > 0\,. \tag{4.25}$$

This condition is also obtained in [109] considering the tree-level scattering amplitude between two massive particles on a flat background and applying cosmological parameter estimation analysis. Also, this condition is related to the Positivity bounds of Scalar-Tensor theories [110, 111, 112], meaning that it is a consequence of requiring a unitary, causal, local UV completion of the theory.

[4]For example, Galileon models and Horndeski theories naturally predict that the spin-2 and scalar degrees of freedom propagate in different effective metrics, which depend on the background solution.

4.5 k-*essence* in polar-areal coordinates

We study gravitational collapse of *k-essence* scalar field in the simplest geometry, a spherically symmetry spacetime. We choose polar-areal coordinates where the line element is given by

$$\mathrm{d}s^2 = -\alpha^2(t,r)\mathrm{d}t^2 + a^2(t,r)\mathrm{d}r^2 + r^2(\mathrm{d}\theta^2 + \sin^2\theta\mathrm{d}\varphi^2). \tag{4.26}$$

We have to mention that these coordinates are not the best suitable ones to describe the *k-essence* model because these coordinates are only valid until the first horizon forms. However, as we will see later, when we apply it to our particular model, the sonic horizon is produced before or at the same time as the luminal horizon. Thus, these coordinates are valid to study gravitational collapse and the dynamics of the horizons.

Following a similar procedure as the one used for the massless canonical scalar field, we introduce the same two auxiliary fields defined in (2.12). Then, the generalized Klein-Gordon equation for the scalar field (4.6) can be rewritten as a set of two partial differential equations

$$\partial_t\Phi = \partial_r\Big(\frac{\alpha}{a}\Pi\Big) \tag{4.27}$$

$$\mathcal{A}\,\partial_t\Pi = \frac{1}{r^2}\partial_r\Big(r^2\frac{\alpha}{a}\Phi K_{,X}\Big) + \mathcal{B}\,, \tag{4.28}$$

where we have defined

$$\mathcal{A} = K_{,X} + K_{,XX}\frac{\Pi^2}{a^2}\,, \qquad \mathcal{B} = K_{,XX}\left[8\pi r\frac{\alpha}{a}\Phi\Pi^2 X K_{,X} + \frac{\Phi\Pi}{a^2}\partial_r\Big(\frac{\alpha}{a}\Pi\Big)\right]. \tag{4.29}$$

In the case of a canonical scalar field, the above equations reduce to the Choptuik problem. On the other hand, the $tt-$ and $rr-$component of Einstein equations become

$$\frac{a'}{a} + \frac{a^2-1}{2r} = 4\pi r\big(K_X\Pi^2 - a^2K\big)\,, \tag{4.30}$$

$$\frac{\alpha'}{\alpha} + \frac{1-a^2}{2r} = 4\pi r\big(K_X\Phi^2 + a^2K\big)\,, \tag{4.31}$$

and the other components are zero or not independent of these ones. As in the massless scalar field case, the previous equations contain no time derivatives, so they are constraint equations that must be satisfied at all times. The equations (4.27)–(4.31) form a fully constrained evolution scheme that describes the gravitational collapse of a *k-essence* field. Since the above equations require initial conditions to determine an exact evolution scheme, we use a 1-parameter family as initial data. See sec. 2.2.1 and Appendix B for more details.

4.6 Characteristics

The inclusion of non-canonical terms in the action makes that perturbations of the *k-essence* field propagate in the emergent spacetime. Thus, we have to analyze the causal structure defined by the effective metric $\tilde{g}_{\mu\nu}$.

This analysis is performed using the *characteristic curves*, which describe the "light-cone" where perturbations of the field propagate. In the case of a canonical scalar field in a Minkowski spacetime, the characteristic curves are parallel straight lines. It is well known that in GR, the cone of influence is not the same in all spacetimes; namely, the light–cones may differ from one point to another. As noted in [113], in a non–canonical field theory, characteristic curves can intersect, leading to caustic singularities (see also [114]). This is a severe problem because, when a caustic forms, the system of equations becomes singular and the theory loses predictability. Additionally, the method of characteristic curves is commonly used to study the hyperbolicity of a system of partial differential equations.

We follow the standard textbooks [115] to compute the characteristic structure of our system of PDEs (see also [116]). Since metric functions a and α are fully constrained, it is sufficient to analyze the evolution equations of $(\Phi,\ \Pi)$ defined in eqs.(4.27, 4.28) in which we replace $(\alpha',\ a')$ from the constraint equations to reach a system of 2 equations of the following form

$$E^{(i)}[\alpha, a, w^{(j)}, \partial_r w^{(j)}, \partial_t w^{(j)}] = 0,$$

where $w^{(1)} = \Phi$ and $w^{(2)} = \Pi$. We introduce the principal symbol

$$P^i_j(\xi_a) \equiv \frac{\delta E^{(i)}}{\delta(\partial_a w^{(j)})}\xi_a \tag{4.32}$$

where $(\xi_t,\ \xi_r)$ define the characteristic covector. This definition does not assume any properties of the system of partial differential equations, except that we can take functional derivatives of them. By solving the characteristic equation defined by

$$\det\left[P^i_j(\xi_a)\right] = 0$$

we deduce the characteristic speed as $c = -\xi_t/\xi_r$. Taking our system of PDEs, we obtain the speed for a *k-essence* field in the form

$$c_\pm = \frac{-K_{,XX}a\alpha\Pi\Phi \pm a^3\alpha\sqrt{K_{,X}(K_{,X} + 2XK_{,XX})}}{K_{,X}a^4 + K_{,XX}a^2\Pi^2}\,. \tag{4.33}$$

In the case of a canonical scalar field, $K = X$, we get $c_{\pm} = \pm\alpha/a$, which reduce to the characteristic speeds of GR, and the equation is always hyperbolic. For a *k-essence* field, to keep the hyperbolicity character of the system of equations, the discriminant must be positive; thus, relation (4.22) has to be satisfied.

Chapter 5

Gravitational Collapse of k-*essence* model: Numerical results

In the last chapter, we described the *k-essence* model from a general point of view and showed its main properties. Despite being a fairly flexible theory, in section 4.4, we showed various conditions which constrain the Lagrangian such that its corresponding dynamics describe physical processes. For numerical purposes, we have to define a particular model. We choose the simplest extension of quintessence, which fulfills all previously required conditions, given by a quadratic correction to the canonical kinetic energy term,

$$K = X + \beta X^2 \,. \tag{5.1}$$

The constant β could take any real value but, as previously mentioned, we have to impose $K_{,XX} > 0$ (4.25) which implies $\beta > 0$. As mentioned before, this condition, which leads to a standard UV completion of the theory, turns out to be also related to the hyperbolicity of the equations and therefore causality.

Performing the numerical evolution of the gravitational collapse of this model, we found that there are two regimes. Similarly as in the Choptuik case, depending on the amplitude of the initial scalar field, we obtain either a dispersion of the *k-essence* field, or the formation of a trapped surface. As we will see later, the big difference concerning the canonical case resides in the second regime, which becomes more complicated. In what follows, we give our numerical results in both cases separately.

To ensure that our results are family independent, we run simulations using two different families. The *Family A*: describes a Gaussian pulse (2.20); whereas the *Family B*: presents a step function (2.22). For each family of initial conditions, we keep only ϕ_0 as a free parameter,

the other parameters are fixed to $r_0 = 20$, $q = 2$, and $d = 3$. The system evolves between $r = 10^{-50}$ and $r = 50$ from $t = 0$ until it forms an apparent horizon (r_H) featuring fixed mesh refinement (see section 3.7). The grid spacing Δr varies from the finest value near the origin to larger values of r in 5 different sectors. Near the origin and up to r_H (which is approximately determined in a first run) the resolution is $\Delta r = 10^{-4}$. The time resolution is also fixed, but it satisfies the Courant-Friedrichs-Lewy condition $\Delta t = \Delta r/5$. It means that, we have considered 1/5 as a Courant number. All results are verified by modifying the resolution in space and time and for most of them we checked with a fixed grid spacing of $\Delta r = 10^{-4}$ in all space.

5.1 Weak field regime

This regime is obtained when the amplitude of the initial scalar field is small, $\phi_0 \ll 1$. In this case, the scalar field bounces at the origin ($r = 0$) and then disperses to infinity. We see in Fig. 5.1 this behavior for three different time[1] and for three different values of $\beta = \{0, 5, 10\}$ for the two families of initial conditions that we are considering, (2.20) and (2.22). For $t = 4000$ for family A and $t = 1000$ for family B, the field is yet collapsing. Around $t = 9500$ for Gaussian initial conditions and $t = 10000$ for the second family of initial conditions the field bounces at $r = 0$ and finally at a later time, the field disperses to infinity. We see that the parameter gives a small variation to the dynamics of the scalar field because of the weak regime studied in this section. However, we can notice that, for larger values of β, the field takes more time to bounce and therefore it reaches infinity a bit later compared to $\beta = 0$. Notice that taking larger values of the constant β increases the mass of the spacetime and therefore we get closer to the threshold of black hole formation.

For *k-essence* model, instead of studying the scalar field, it is better to monitor the $rr-$component of the gravitational metric (g^{rr}) and the effective metric ($\tilde{g}^{rr}$). A complete evolution is shown in Fig. 5.2, where we can notice that after some time, the minimum value of both metric components are near the origin but are far from collapsing ($\min[g^{rr}(t, r)] \sim 1$, $\min[\tilde{g}^{rr}(t, r)] \sim 1$). It means, when ϕ_0 is far from the critical point, both metrics remain closer to one in all the evolution. Instead, as we will see, when ϕ_0 approaches the critical point, the minimum value of both metrics approaches zero, indicating a formation of a horizon. This figure was done for an arbitrary value of the initial scalar field.

[1] Time is the iteration step and not proper time at $r = 0$.

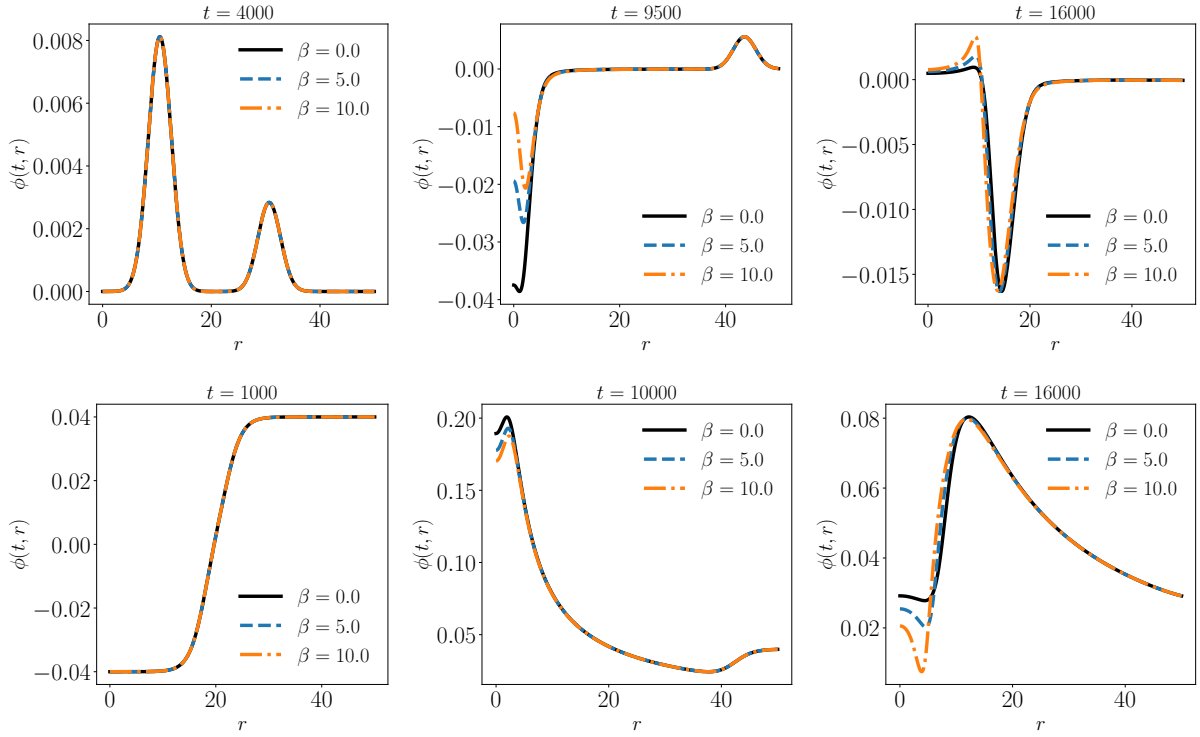

Figure 5.1: *Scalar field profile ϕ in the weak field regime, for $\beta = 0.0$ (solid line) which is the canonical case, $\beta = 5.0$ (dashed line) and $\beta = 10.0$ (dash-dotted line). Upper panel is for Gaussian family type of initial conditions (Family A) while the bottom panel represents family B.*

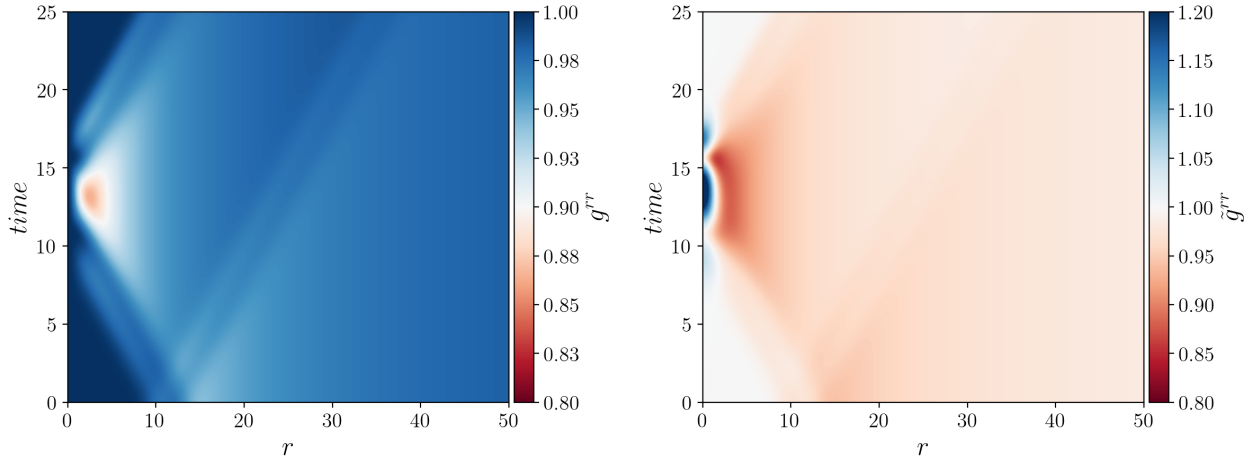

Figure 5.2: *Complete evolution of the $rr-$component of the metric (left) and the effective metric (right) for a value of the initial scalar field in the weak field regime. Both metric components remain closer to one; they are far to collapse.*

5.1.1 Convergence and consistency checks

In this section, we applied the numerical tests presented in section 3.6 to check the design and implementation of our numerical solver for the system of equations (4.27)–(4.31).

Our first check is monitoring the Misner-Sharp or ADM mass. As mentioned in section 3.6.3, this has to be a conserved quantity. Fig. 5.3 shows a plot of M_{ADM} as a function of time during a period when there is no scalar field leaving the computational domain. We observe that the value of M_{ADM} is roughly conserved. More importantly, as the resolution increases, we have convergence to the conservation: the deviation of M_{ADM} from its time-averaged value decreases as the resolution increases.

Our second check is the convergence test described in section 3.6.1 that we applied to the metric functions and the auxiliary scalar fields. To perform a basic convergence test, we had to run the code with the same initial data using three different mesh spacings. Fig. 5.4 plots the value of the convergence factor (3.18) as a function of time for the metric functions $a(t,r)$ and $\alpha(t,r)$, as well as for the scalar fields $(\Phi(t,r),\ \Pi(t,r))$. The displayed results suggest that our numerical method is second-order convergent for all of the variables. In Fig. 5.5, we show the same convergence test. In this case, for the Ricci scalar, the left hand side of the Hyperbolicity condition (4.22), and the Null Energy Condition (4.16). It is shown that any function computed from the fundamental variables (a, α, Φ, Π) also must satisfy the convergence inside the grid.

Our final check is the Redundant Equation, section 3.6.2. Since we are working in a spherical symmetry scenario, the $tr-$component of the Einstein equations serves to test our numerical scheme. In Fig. 5.6, we plot the residual of this equation for three different grids. Convergence of the residual is evident, and closer examination reveals that the convergence is also second-order, as expected. Also, from this figure, we observe that the residual norm shows more variation around the time $t = 15$, which corresponds to the time in which most of the scalar field is concentrated near the origin. Around this time, the evolution of the system is more dynamica and the scalar fields have more significant gradients, which results in relatively large fluctuations.

5.2 Strong field regime

We expect that, when the mass of the scalar field is sufficiently large, it would collapse and produce a black hole. We run simulations varying the amplitude of the *k-essence* scalar field ϕ_0 from a value in the weak limit regime to a value where the final result of the evolution is the creation of an event horizon (collapse of the metric) or a sonic horizon (collapse of the

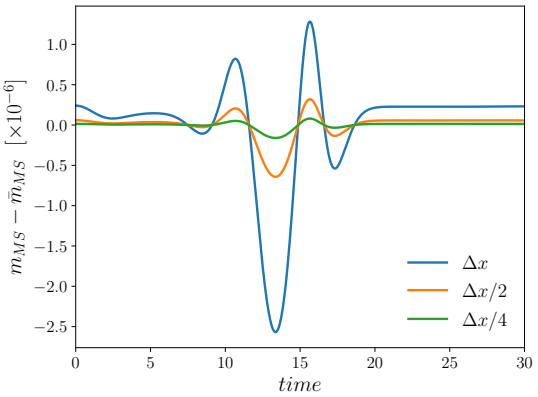

Figure 5.3: *Value the deviation of $M(t,r)$ at $r = r_{max}$ as a function of time for three different resolutions.*

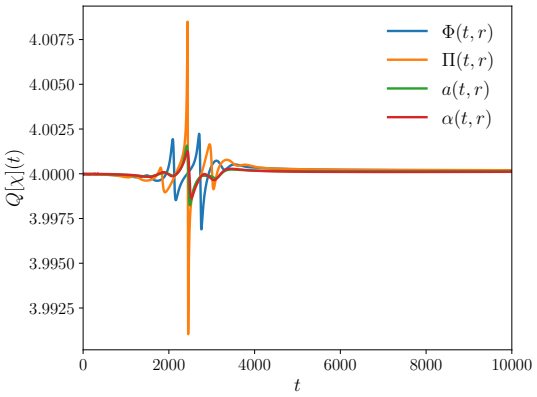

Figure 5.4: *Value of the convergence factor, $Q(t)$, for the fundamental variables, a, α, Φ, Π, as a function of time.*

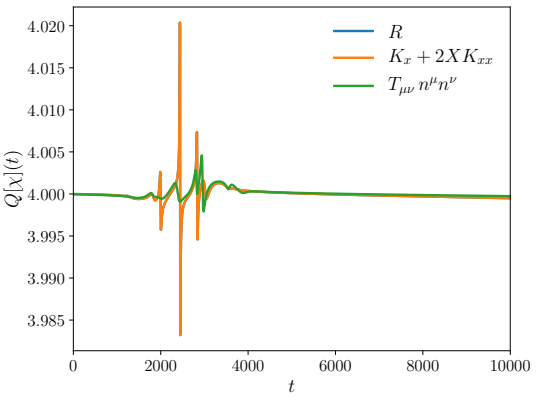

Figure 5.5: *Convergence factor, $Q(t)$, for the Ricci scalar (R), the Hyperbolicity condition (4.22) and the Null Energy Condition (4.16).*

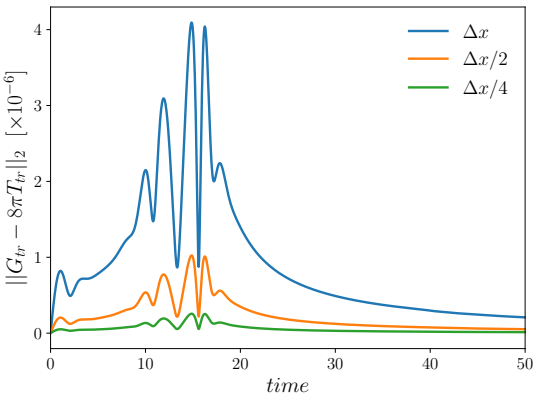

Figure 5.6: *l_2 norm of the residuals $\mathcal{R}_{tr}$ as a function of time, from a sequence of calculations using the same initial data, and grid spacings Δx, $\Delta x/2$ and $\Delta x/4$.*

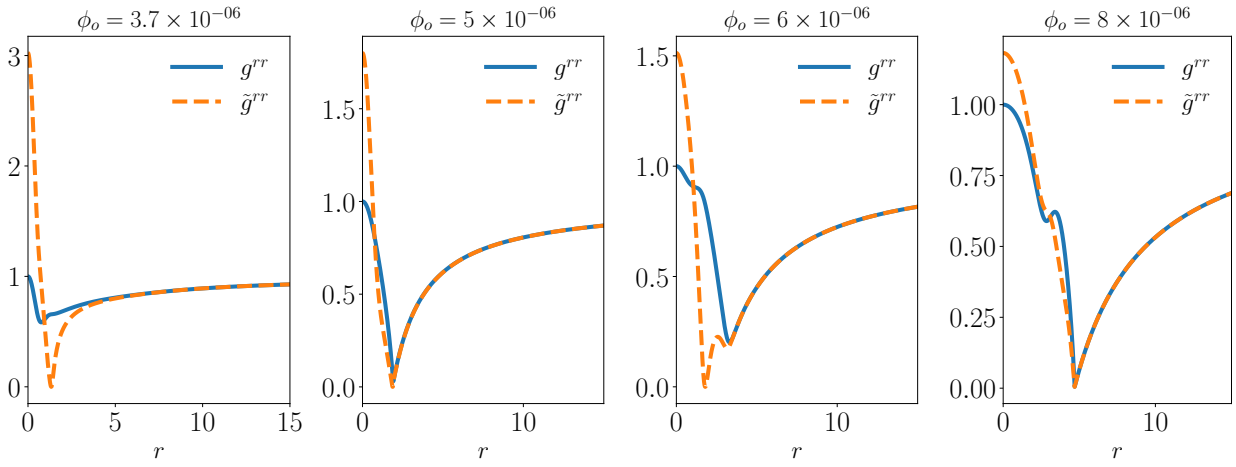

Figure 5.7: *Last time evolution before formation of a horizon. The event horizon forms when* $g^{rr} = 0$ *and the sonic horizon when* $\tilde{g}^{rr} = 0$*. For* $\phi_0 = 3.7\ 10^{-6}$ *and* $\phi_0 = 6\ 10^{-6}$ *a sonic horizon forms while the event horizon is not yet formed, while for* $\phi_0 = 5\ 10^{-6}$ *and* $\phi_0 = 8\ 10^{-6}$ *both horizons form at the same time within our numerical precision.*

effective metric). As we described previously, since our metric is not horizon penetrating, we cannot evolve the spacetime beyond the formation of any horizon. The main difference with respect to the Choptuik case is that we found four different regimes, depending on the value of ϕ_0. For $\beta = 5$, we found situations described in Fig.(5.7) but which are generic for any value of $\beta \neq 0$.

Explicitly, we obtained the following results:

- For a small amplitude of the scalar field, $\phi_0 = 3.7 \times 10^{-6}$ for $\beta = 5$, we observe the formation of a sonic horizon without being able to continue the simulation to know if a black hole (event horizon) forms. However, it is interesting to notice that during a very short period of time, the simulation continues and this regime shows a loss of hyperbolicity, namely, the condition (4.22) breaks down. This result is similar to [100].

- Increasing the amplitude of the initial field, the sonic horizon is still present, but now the metric also tends to collapse forming an event horizon with the same radius than the sonic horizon (within the accuracy of our simulation). This behavior is observed when the β parameter is not too strong. We do not observe any loss of hyperbolicity.

- Increasing the amplitude of the scalar field, the evolution ends because of the formation of a sonic horizon, similarly as in the previous case, but this time the dynamics of the metric seems clearly to indicate that a black hole would form in the future and it seems that hyperbolicity will not be lost, the function $K_{,X} + 2XK_{,XX}$ is far from vanishing.

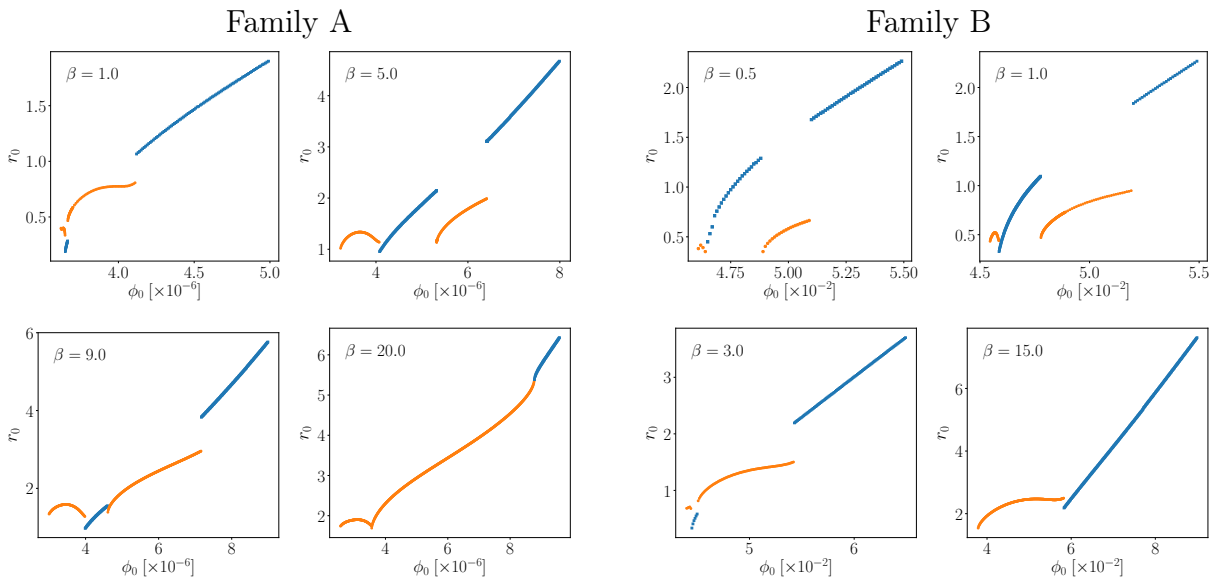

Figure 5.8: *Radius of the first horizon formed as a function of the amplitude of the initial scalar field, ϕ_0, for various values of β. The blue-branch represents the formation of both horizons at the same time while the orange-branch describes formation of a sonic horizon only. Results are shown for the Gaussian family (first two columns) and the Family B initial conditions (last two columns).*

- For strong values of ϕ_0, both metrics collapse at the same radius (within the accuracy of the numerical evolution). This behavior has been observed for all values of β. The larger the value of β, the larger the value of ϕ_0 is, producing this behavior. In this case, a BH forms and hyperbolicity is maintained until the end of the simulation.

In general, the formation of a sonic horizon indicates the formation of an event horizon in the future, except in the first regime described earlier, where the hyperbolicity is lost and therefore the BH never forms.

As shown in Fig. 5.7, depending on the initial value of the amplitude of the scalar field, we have either the formation of a sonic horizon without the existence yet of an event horizon, or both horizons (sonic and luminal) form and are indistinguishable. To illustrate these behaviors in a better way, in Fig. 5.8 we show the variation of the apparent radius defined either by the sonic horizon or by both horizons when formed simultaneously. We see, e.g., for $\beta = 5$ and for the Family A of initial conditions, that we have four different regimes corresponding to the cases described in Fig. 5.7. The first and the third regimes (in orange) correspond to the formation of the sonic horizon, while the second and the last ones (in blue) correspond to the simultaneous formation of both horizons. For larger values of β, some regimes disappear since the non-linear term are predominant; in contrast, for small values, the range of the first regime tends to be very small. In the case of Family A and

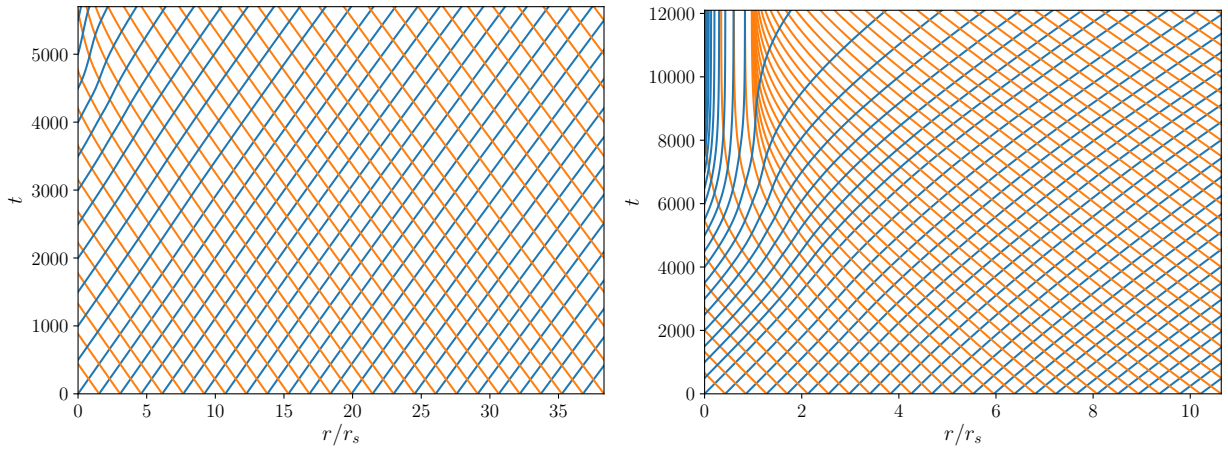

Figure 5.9: *Integral curves of the ingoing (orange) and outgoing (blue) characteristic speed $c_\pm$ defined by eq. (4.33) for $\beta = 5$ and Gaussian initial conditions. In the left panel, $\phi_0 = 3.5\ 10^{-6}$ and therefore the solution belongs to the first branch, where we have formation of the sonic horizon only. In the right panel, $\phi_0 = 8\ 10^{-6}$ and therefore it belongs to the last branch where a black hole forms.*

$\beta = 5$, the blue lines seem to form only one line if extended. In fact, we expect, in this case, the third regime where only a sonic horizon forms to evolve in time with an increasing sonic horizon until it forms the link between the second regime and the last one. This behavior can be observed in all cases like, e.g., $\beta = 1$ for Family B, where the two blue lines seem clearly to be extended and joined.

Therefore, we expect the sonic horizon to be dynamical and evolve in time until the formation of the event horizon if hyperbolicity is not lost. Because in all our simulations, the spacetime seems to converge to the Schwarzschild solution, we expect both horizons to join in the future. Therefore, we presume that for longer time evolution, the radius of the black hole formed should describe a continuous function of the initial condition ϕ_0 except if hyperbolicity is lost as shown in the first branch. Surprisingly, the first branch which does not represent a BH because hyperbolicity is lost, and therefore an event horizon will never form, shows a universal behavior as if it represents the threshold of black hole formation.

We can see from Fig. 5.9 the evolution of the characteristic line defined from equation (4.33) in (t, r) coordinates. In the first case, a sonic horizon is formed but we do not expect a black hole to form as explained previously, while in the second case, an event horizon forms at normalized radius $r = 1$. Recently, it has been shown that, in the flat spacetime, these models could produce caustics [113]. But as it can be seen from Fig. 5.9, the characteristic lines do not intersect. We have not found any formation of caustics in our simulations. In the second case, where the event horizon forms, indicated by the lines converging to $r = r_s$

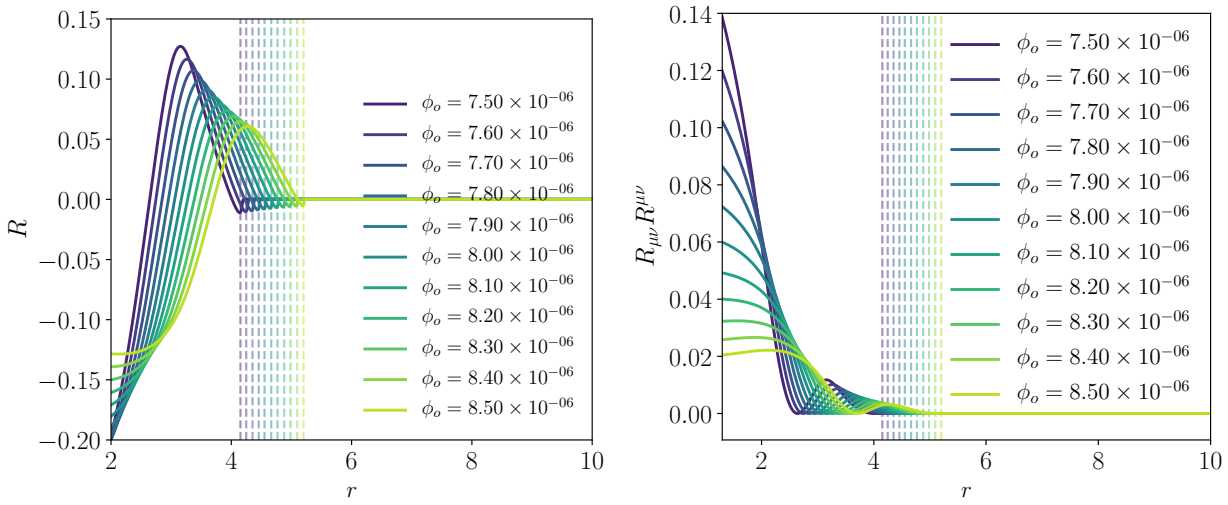

Figure 5.10: *Curvature scalar R and Ricci tensor squared $R_{\mu\nu}R^{\mu\nu}$ as a function of the radial radius r at last time t before formation of the event horizon for $\beta = 10$ and ϕ_0 corresponding to the last branch. The vertical line represents the position of the event horizon for each initial condition ϕ_0.*

of the characteristic lines, the BH is Schwarzschild.

In fact, every time a black hole forms, the exterior solution is the Schwarzschild one as we can see in Fig. 5.10. Considering, e.g., the Family A of initial conditions and for various values of ϕ_0 which all correspond to the fourth branch where the event horizon forms at the same time as the sonic horizon (blue-branch in Fig. 5.8), we have represented the curvature scalar R and the Ricci tensor squared $R_{\mu\nu}R^{\mu\nu}$ during the last moment of evolution before a black hole formation. We see that, for all values of ϕ_0, the curvature scalar and the Ricci tensor squared vanish for r larger than the event horizon, indicating the formation of the Schwarzschild solution, which has also been checked directly from the metric. This behavior has been observed for both families of initial conditions and for all values of β. The end state of the evolution when the event horizon is formed is the Schwarzschild spacetime. Notice also that the event horizon increases with increasing ϕ_0, as expected.

On the other hand, when the sonic horizon forms first, the metric is not Schwarzschild as seen in Fig. 5.11. In this case, we expect the system to continue to evolve until the formation of the Schwarzschild spacetime or a loss of hyperbolicity. This behavior should be checked with coordinates such as Gullstrand-Painlevé.

For a given family of initial conditions and for a given β, values of ϕ_0 lower than the first branch produce dispersion and therefore flat spacetime, while values taken within this branch produce a sonic horizon and later a loss of hyperbolicity. It is interesting to see from the curvature in Fig. 5.11 that we are still far from the Schwarzschild solution and therefore the formation of the event horizon but, very surprisingly, considering the sonic horizon we

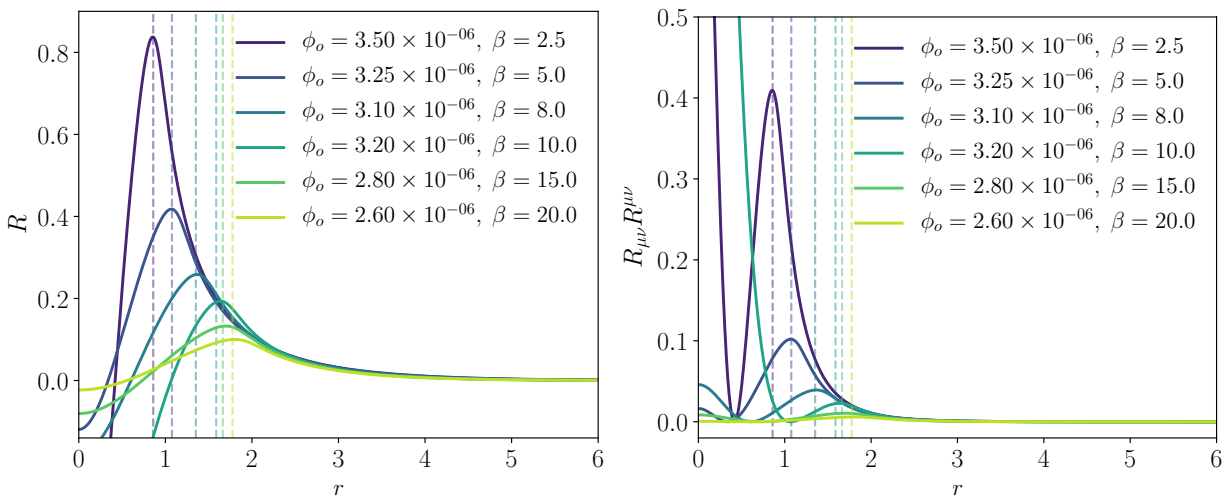

Figure 5.11: *Curvature scalar R and Ricci tensor squared $R_{\mu\nu}R^{\mu\nu}$ as a function of the radial radius r at last moment t before the formation of the sonic horizon for various values of β and ϕ_0 corresponding to the first branch. The vertical line represents the position of the sonic horizon.*

found a universal behavior. For any family of initial conditions and for any β, there exists a critical value of ϕ_0 named ϕ_i in Fig. 5.12 around which the radius of the sonic horizon follows a universal behavior given by

$$r = r_0 + (\phi_0 - \phi_i)^\gamma \ , \quad \gamma \simeq 0.51 \tag{5.2}$$

This is very similar to the scaling relation that Choptuik found for the massless scalar field, relation (2.31). In the *k-essence* case, because of the existence of an additional scale in our system (β), we have a non-vanishing minimum radius of the black hole corresponding therefore to the Type I critical phenomena [59].

5.3 Discussions

In this chapter, we presented studies of numerical solutions of *k-essence* models in spherically symmetric case, in gravitational collapse scenarios with additional shift symmetry. We have presented the various constraints for a well-defined problem at classical level and for its quantum completion which reduces to $K_{,X} > 0$, $K_{,XX} > 0$ and $K_{,X} + 2XK_{,XX} > 0$. For these theories, we generically have the formation of two horizons, an event horizon and a sonic horizon, which define a limit for the propagation of the perturbations of the scalar field. For numerical purposes, we focused on a particular model defined by $K = X + \beta X^2$. We found that in the weak field regime, the scalar field disperses and spacetime is flat, while in

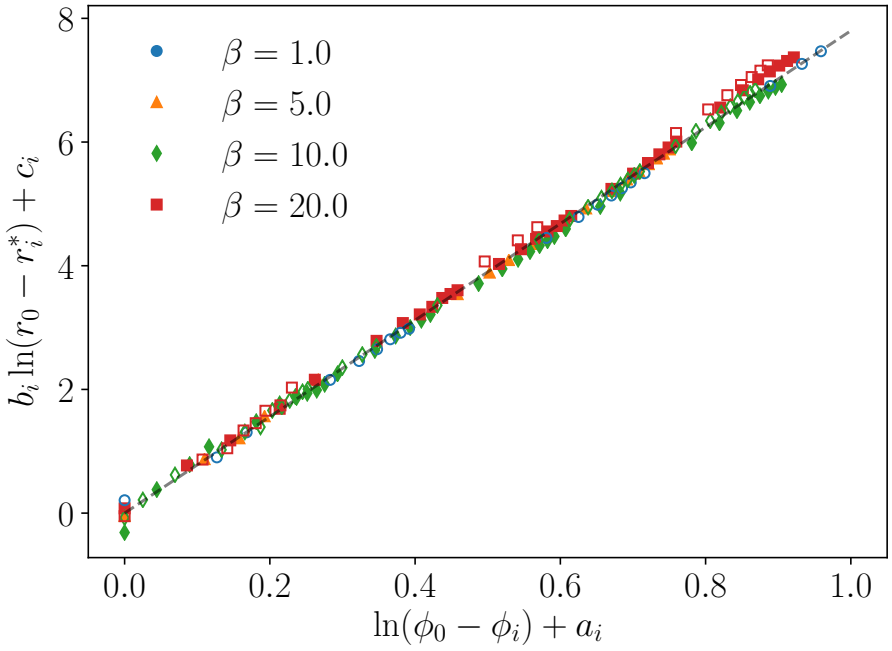

Figure 5.12: *Radius scaling relation of the sonic horizon for the two families of initial conditions and for various values of β. Data with filled markers correspond to Family A. Data with empty markers correspond to Family B.*

the strong field regime, we have the formation of a horizon. Two situations occur, either only a sonic horizon forms or both horizons form at the same time. In this last case, the exterior solution is always Schwarzschild and we never observed formation of caustics. In the cases where the sonic horizon formed first, we could have either a dynamics of the field showing the possible formation of a BH in the future or a loss of hyperbolicity of the equations. Very surprisingly, the lowest regime, corresponding to a situation were the field does not disperse to infinity, and which corresponds to the formation of a sonic horizon, reveals a universal behavior even if the hyperbolicity is rapidly lost after the formation of the sonic horizon. We found that in the critical limit of the formation of the sonic horizon r_S, a universal power-law scaling of r_S appears with a critical exponent of order 0.51 for any parameter $\beta \neq 0$. This result seems to indicate that the universal behavior is also encoded in the sonic horizon.

Chapter 6

Stability of generalized Einstein-Maxwell-Scalar black holes

Dropping the assumption of Lovelock theorem that "*a theory of gravity must be constructed only from the metric tensor*" opens the window to include extra fundamentals fields. As we mentioned in the previous chapters, the simplest modification is obtained by adding a scalar field ϕ in the action. In this context, and assuming a second-order equation of motion, Horndeski theory [21] is the most general covariant scalar-tensor theory that introduces one scalar degree of freedom. Similarly, we can introduce a vector field into the gravity sector. This gives the generalized Proca theories [43], the most general vector-tensor theory. Both theories can be unified in the framework of Scalar-Vector-Tensor (SVT) theories [44].

The simplest example of a SVT theory is the Einstein-Maxwell action plus a scalar field in which we add its respective kinetic energy term and consider a general coupling to the Maxwell field. If the coupling is minimal, we obtain the Reissner-Nordström spacetime; no new charged BH solutions are possible. If we relax this condition and consider a non-minimal coupling between the scalar and Maxwell field, hairy BH solutions can be obtained.

In the literature, it is common to find that the coupling between such fields is in an exponential form. This type of coupling arises in the low-energy limit of Kaluza-Klein models [45, 46] and supergravity/string theories [117], in which the scalar field describes how the extra dimensions dilate along the four-dimensional spacetime; consequently, the scalar field is referred to as *the dilaton*. The first black hole solution in the Einstein-Maxwell-dilaton (EMD) theory was presented in 1982 by Gary Gibbons and Kei-ichi Maeda [118, 119]. This is a BH with electric and magnetic charges that contains a scalar (dilaton) hair. The magnetically charged solution was later reobtained by Garfinkle, Horowitz and Strominger [120] in the context of string theory, giving a more profound discussion about this solution.

Instead of studying a particular model, we will focus on the classical stability of black holes in the generalized Einstein-Maxwell-Scalar (EMS) theory in which the scalar field is nonminimally coupled to gravity and, with an arbitrary coupling between the scalar and Maxwell field. Stability is one of the most important areas in physics. It distinguishes cosmological solutions from transient situations. Also, this analysis is used to constrain the space of solution of any theory of gravity. On the other hand, thermodynamic stability is also widely studied. But, it is important to mention that (mechanical) stability should be a condition before any thermodynamical analysis. Indeed, if the black hole is mechanically unstable, any Hawking radiation would destabilize it and therefore render any thermodynamic analysis impossible.

The formalism of BH stability was developed by Regge and Wheeler [47], where they proved partially the stability of the Schwarzschild black hole. This analysis was completed by Zerilli [48], who provided the stability equations for the even-parity perturbations. They showed that after separating the angular part of the equations through an expansion in tensor spherical harmonics, the formalism reduces the problem to a master linear differential equation similar to the Schrödinger equation. Since this formalism is based on the geometrical properties of spacetime, it has been applied and extended to other solutions. For example, following the same approach, Moncrief [121, 122] derived the stability of the Reissner-Nordstrom black hole.

Since in the EMS theory, we add a scalar and vector field into the action, in this chapter we will extend the Regge–Wheeler formalism to include perturbations of the new degrees of freedom. It is expected that linearized field equations in the EMS theory reduce to coupled differential equations describing the propagation of the gravitational, scalar and vector modes. As we mentioned, the generalized EMS theory allows for black holes with mass, rotation, electric charge and scalar hair; thus, this theory offers an attractive theoretical and computational playground to explore possible deviations from GR predictions.

The inclusion of new degrees of freedom would leave an imprint in the gravitational radiation. Since typical gravitational waves come from strong gravity regions such as the vicinity of a BH, the detection of GWs enables us to test general relativity and alternative theories of gravity in the strong-field regime. However, to distinguish GR from other theories of gravity, a theoretical understanding of the fundamental properties of modified gravity is crucial. Any deviation from GR can be measured via the frequency emitted during the last moments of BH mergers, the so-called quasinormal modes (QNMs). Any hairy BH could be discriminated through these modes. QNMs are easily computed if their equation is known. The analysis performed in this chapter will provide these equations.

We begin this chapter with section 6.1, by introducing the action for the generalized EMS theory that we are interested in. Next, we derive the dynamics of the model, considering the particular case of a spherically symmetric and static background, to then discuss the separation of perturbations into odd- and even-parity modes in section 6.2. Since we focus on a theory that is invariant under parity transformation, perturbation modes are decoupled from each other. Therefore, in section 6.3, the action is expanded up to second order in odd-parity perturbations; we analyze the stability of the solution and determine conditions to avoid ghost instabilities. The analysis of even-parity perturbations is made in section 6.4, where we derive the stability conditions as well as the propagation speeds for the available degrees of freedom in this sector. Finally, in Sec. 6.5, we apply our results to some well-known examples.

6.1 Background equations of motion

We are interested in generalized Einstein-Maxwell-Scalar theories described by the following action

$$S = \int \mathrm{d}^4x\sqrt{-g}\left[f_1(\phi)\frac{R}{2} + f_2(\phi, X, F)\right] \tag{6.1}$$

where R is the Ricci scalar, $f_1(\phi)$ is a function of the real scalar field ϕ, representing the non-minimal coupling to gravity, and $f_2(\phi, X, F)$ is a function of the scalar field and its kinetic energy X, and the kinetic energy of the vector field F. In particular, we use the notation

$$X = -\frac{1}{2}\partial_\mu\phi\partial^\mu\phi\,, \qquad F = -\frac{1}{4}F_{\mu\nu}F^{\mu\nu}\,, \qquad F_{\mu\nu} = \partial_\mu A_\nu - \partial_\nu A_\mu \tag{6.2}$$

where $F_{\mu\nu}$ is the field strength. We can see from the action that our theory respects the $U(1)$ gauge symmetry. We do not consider any mass term à la Proca $A_\mu A^\mu$, therefore, we have five propagating degrees of freedom —one scalar, two vectors, and two tensors. We will study the linear stability of static spherically symmetric spacetimes. To begin with, we will consider a background spacetime described by the following general line element[1]

$$\mathrm{d}s^2 = \bar{g}_{\mu\nu}\mathrm{d}x^\mu\mathrm{d}x^\nu = -A(r)\mathrm{d}t^2 + \frac{\mathrm{d}r^2}{B(r)} + C(r)\left(\mathrm{d}\theta^2 + \sin^2\theta\mathrm{d}\varphi^2\right) \tag{6.3}$$

where the metric functions $A(r)$, $B(r)$ and $C(r)$ depend on the radial coordinate r. It is common to fix $C = r^2$, but we will work as general as possible because various solutions in the literature cannot be written in a coordinate system with that choice for the metric

[1] We will use the notation $\bar{X}$ to refer to quantities evaluated at the background level.

function $C(r)$.

To satisfy the background symmetries, the scalar field only depends on the radial coordinate, $\bar{\phi} = \phi(r)$, and the vector field takes the form

$$\bar{A}_\mu = (\bar{A}_0(r), \bar{A}_1(r), 0, 0) \tag{6.4}$$

where $\bar{A}_1$ is the only possible non-zero spatial component. Using the Helmholtz's theorem, we get that $\bar{A}_1$ is a longitudinal mode since the transverse part is eliminated by regularity condition at $r = 0$, see [123]. The background (6.4) is not the most generic spherically symmetric spacetime[2]. In fact, we should only impose that the energy-momentum tensor $T_{\mu\nu}$ is invariant under the lie derivative along the generators of the group SO(3), or we could consider a less restrictive situation where the electromagnetic part of the energy-momentum tensor is spherically symmetric. Therefore we could consider $\bar{A} = \bar{A}_0(r)dt + \bar{P}\cos\theta d\varphi$ where $\bar{P}$ is the magnetic charge. We will consider in this chapter only electric charge.

On the background, the kinetic terms for the fields takes the simple form

$$\bar{X} = -\frac{1}{2}B\phi'^2\,, \qquad\qquad \bar{F} = \frac{B\bar{A}_0'^2}{2A} \tag{6.5}$$

where here, and in the rest of the chapter, a prime denotes derivative with respect to the radial coordinate r. Replacing the metric (6.3), the scalar and vector field in (6.1) and varying the action with respect to the functions $\{A,\, B,\, C,\, \phi,\, \bar{A}_0\}$ we get the equations of motion shown in Box 6.1. As we can see from these equations, the longitudinal mode $\bar{A}_1(r)$ does not contribute to the vector-field dynamics since our action is invariant under $U(1)$ gauge symmetry. Also, from equation (6.10), it follows that $\mathcal{G}(r) = constant$; this expresses the existence of a conserved charged current (related to the electric charge) arising from this symmetry.

It is useful to introduce the following variables to simplify the notation

$$\mathcal{J}(r) = \sqrt{AB}Cf_{2,X}\,\phi'(r)\,, \qquad\qquad \mathcal{S}(r) = \sqrt{\frac{A}{B}}C\left(f_{2,\phi} + \frac{1}{2}f_{1,\phi}\,R\right). \tag{6.11}$$

Hence, the equation of motion for the scalar field (6.9) is written as $\mathcal{E}_\phi = \mathcal{J}' + \mathcal{S}$.

6.2 Perturbation formalism

[2]We are thankful to Julio Oliva for mentioning to us this point.

$$\mathcal{E}_A := \frac{1}{C}\left[f_1\left(1+\frac{BC'^2}{4C}\right) - BCf_1'' - \frac{1}{2}B'(Cf_1)' - B(C'f_1)'\right] + f_2 - 2Ff_{2,F} \tag{6.6}$$

$$\mathcal{E}_B := \frac{1}{C}\left[f_1\left(1-\frac{BC'^2}{4C}\right) - \frac{BA'}{2A}(Cf_1)' - BC'f_1'\right] + f_2 - 2\bar{F}f_{2,F} - 2Xf_{2,X} \tag{6.7}$$

$$\mathcal{E}_C := 2f_2 - f_1\left[\sqrt{\frac{B}{A}}\left(\sqrt{\frac{B}{A}}A'\right)' + \sqrt{\frac{B}{C}}\left(\sqrt{\frac{B}{C}}C'\right)' + \frac{BA'C'}{2AC}\right] - \frac{f_1'}{AC}(ABC)' - 2B\,f_1'' \tag{6.8}$$

$$\mathcal{E}_\phi := \partial_r\left[\sqrt{AB}C\,f_{2,X}\,\phi'(r)\right] + \sqrt{\frac{A}{B}}C\left(f_{2,\phi} + \frac{1}{2}f_{1,\phi}\,R\right) \tag{6.9}$$

$$\mathcal{E}_{\bar{A}_0} := \mathcal{G}'(r) = \partial_r\left(\sqrt{\frac{B}{A}}C\,\bar{A}_0'\,f_{2,F}\right) \tag{6.10}$$

Table 6.1: *Background equations of motion for the SVT theory*

We can find exact solutions by solving the background equations shown in Box 6.1, but not all of them describe a gravitating system. The stability of an exact solution is the first step that we have to examine to ensure a good description of a physical phenomenon. Showing stability is an essential issue for any theory of gravity. If we prove the stability of the solution, we can guarantee that it will be the final state of a gravitating system. On the contrary, the solution will decay in a different branch of solutions. This analysis can be done by applying linear perturbation theory.

In this section, we will briefly summarize the formalism for perturbations around a spherically symmetric spacetime. Let us consider small perturbations $h_{\mu\nu}$ on top of the static and spherically symmetric background (6.3)

$$g_{\mu\nu} = \bar{g}_{\mu\nu} + h_{\mu\nu} \tag{6.12}$$

where $|h_{\mu\nu}| \ll |\bar{g}_{\mu\nu}|$. The previously studied problem of how a perturbation propagates through a BH spacetime changes to finding an evolution equation for $h_{\mu\nu}$. The starting point of the mathematical analysis is to take advantage of the spacetime symmetries.

To begin with, notice that under two-dimensional rotations on a sphere, the ten components of the metric perturbations $h_{\mu\nu}$ transform in different ways:[3]

[3]In the rest of the chapter, the indices $i, j, \ldots$ refer to $v^i = (t, r)$, while $a, b, \ldots$ to the spherical angular coordinates $x^a = (\theta, \varphi)$.

- h_{ij} transform as scalar,
- h_{ia} transform as vector, while
- h_{ab} transform as tensor quantities.

In fact, under a reparametrization of the angles x^a into $x^a \to R^a(\theta, \varphi)$ we get

$$h_{ia}\mathrm{d}x^i\mathrm{d}x^a \to h_{ia}\partial_b R^a \mathrm{d}x^i\mathrm{d}x^b\,,$$

meaning that h_{ia} indeed transform as a vector.

Thus, we have classified perturbations into three types. We have three scalars, two vectors of dimension two and a rank two tensor. Since we are considering a spherically symmetric background, we follow a standard decomposition of these components into a basis of (scalar/vector) spherical harmonics to derive perturbation equations.

Each scalar function S can be decomposed as

$$S(t, r, \theta, \varphi) = \sum_{\ell,m} s_{\ell m}(t, r) Y_{\ell m}(\theta, \varphi). \tag{6.13}$$

On the other hand, any vector V_a can be decomposed using an orthogonal decomposition

$$V_a(t, r, \theta, \varphi) = \nabla_a \Phi_1 + w_a \tag{6.14}$$

where Φ_1 is a scalar function and w_a is a divergence-free vector. As we know $(\vec{\nabla} \times \vec{A})^a = \epsilon^{abc}\nabla_b A_c$, which in two dimensions gives $w^a = \epsilon^{ab}\nabla_b \Phi_2$, where Φ_2 is another scalar function, and $\epsilon^{ab} = \{0, +1, -1\}$ is the Levi-Civita symbol, normalized as $\epsilon^{\theta\varphi} = 1$. Substituting in the above expression, we get

$$V_a(t, r, \theta, \varphi) = \nabla_a \Phi_1 + E_a^b \nabla_b \Phi_2, \tag{6.15}$$

where $E_{ab} \equiv \sqrt{\det \gamma}\ \epsilon_{ab}$ is the covariant Levi-Civita symbol such that the indices are raised and lowered by the two-dimensional metric on the sphere γ_{ab} and its inverse. Also, ∇_a represents the covariant derivative with respect to the metric γ_{ab}. Since V_a is a two-component vector, it is completely specified by the potentials Φ_1 and Φ_2. It can be checked that the first and second terms of Eq. (6.15) transform as scalar and vector modes, respectively. Applying the scalar decomposition (6.13), we get

$$V_a = \sum_{\ell,m} w_{\ell m}(t, r)\, \nabla_a\, Y_\ell^m(\theta, \varphi) + \sum_{\ell,m} \omega_{\ell m}(t, r) E_{ab} \nabla^b\, Y_\ell^m(\theta, \varphi)\,. \tag{6.16}$$

From this relation we recognize $E_a^{\ell m} \equiv \nabla_a Y_\ell^m(\theta,\varphi)$ and $S_a^{\ell m} \equiv E_{ab}\nabla^b Y_\ell^m(\theta,\varphi)$ as the *electric and magnetic vector spherical harmonics*, respectively.

Finally, any symmetric tensor T_{ab} can be decomposed as

$$T_{ab}(t,r,\theta,\varphi) = \nabla_a\nabla_b\Psi_1 + \gamma_{ab}\Psi_2 + \frac{1}{2}\left(E_a{}^c\nabla_c\nabla_b\Psi_3 + E_b{}^c\nabla_c\nabla_a\Psi_3\right) + t_{ab}, \tag{6.17}$$

where Ψ_1, Ψ_2 and Ψ_3 are scalar functions, and t_{ab} is a transverse-traceless tensor. Since we are interested in studying gravitational perturbation in four dimensions (4D), any symmetric tensor, such as t_{ab}, has only three independent components. However, none of them is a degree of freedom since the conditions $\nabla^a t_{ab} = 0$ (transverse) and $t^a{}_a = 0$ (traceless) impose three relations or constraints that determine them completely. So, in 4D there are no tensor perturbations. Thus, (Ψ_1, Ψ_2, Ψ_3) completely specify T_{ab}. As before, we can apply the scalar decomposition (6.13) to these functions to decompose the tensor quantity into spherical harmonics. As we have seen, in 4D we only have two types of perturbations, whereas in higher dimensions, we have an additional tensor mode. We will give a more in-depth detail of this type of perturbations in Chapter 7.

It is also common in the literature to label perturbations depending on how they transform under parity transformation. In fact, changing $(\theta,\varphi) \to (\pi-\theta,\ \pi+\varphi)$, we get that any scalar perturbation picks a factor $(-)^\ell$, which is thus said to be polar or even. In contrast, a vector perturbation picks a factor $(-)^{\ell+1}$, it is said to be axial or odd.

At the end, decomposition of the perturbed metric into spherical harmonics leaves us with ten functions representing the ten components of the metric. With the above analysis, it can be checked that seven of them behave as scalar quantities and the rest as vectors. Because of general covariance, not all metric perturbations are physical, because some of them can be set to zero by means of the gauge transformation

$$x^\mu \longrightarrow x'^\mu = x^\mu + \xi^\mu\,. \tag{6.18}$$

Choosing ξ_μ so that $\bar{\nabla}_\mu\xi_\nu$ is of the same order as $h_{\mu\nu}$, under this transformation the background metric $\bar{g}_{\mu\nu}$ becomes invariant while, to linear order in $\bar{\nabla}_\mu\xi_\nu$, the perturbation metric $h_{\mu\nu}$ transforms as

$$h_{\mu\nu} \longrightarrow h'_{\mu\nu} = h_{\mu\nu} - \bar{\nabla}_\mu\xi_\nu - \bar{\nabla}_\nu\xi_\mu\,. \tag{6.19}$$

Since ξ_μ is a generic four-vector field, using the above arguments, we get that the $t-$ and $r-$component transform as scalars, while the $\theta-$ and $\varphi-$component transform as vector

quantities. Thus, they can be expanded in scalar and vector spherical harmonics as follows:

$$\begin{aligned}\xi_t &= \sum_{\ell,m} T_{(\ell m)}(t,r)Y_\ell^m(\theta,\phi)\\ \xi_r &= \sum_{\ell,m} R_{(\ell m)}(t,r)Y_\ell^m(\theta,\phi)\\ \xi_a &= \sum_{\ell,m} \Theta_{(\ell m)}(t,r)\nabla_a Y_\ell^m(\theta,\phi) + \sum_{\ell,m}\Lambda_{(\ell m)}(t,r)E_{ab}\nabla^b Y_\ell^m(\theta,\phi)\,.\end{aligned} \tag{6.20}$$

Clearly, the coefficient proportional to $\Lambda_{(\ell m)}(t,r)$ generates a contribution to the vector sector, while the other terms contribute to the scalar perturbations.

What makes these decompositions useful is that in the linearized equations of motion —or equivalently, in the second-order action for $h_{\mu\nu}$— scalar/even-parity and vector/odd-parity perturbations completely decouple from each other, reflecting the invariance of the background spacetime under a parity transformation. Clearly, this is not the case in a Lagrangian containing parity-violating terms, which leads to an analysis of coupled equations [124, 125]. Based on these properties, we can analyze each type of perturbations separately.

6.3 Odd-parity perturbations

In this section, we will study the odd-parity perturbations of generalized Einstein-Maxwell-Scalar theories given by the action (6.1) around the spherically symmetric spacetime (6.3). This type of perturbation is also known in the literature as axial or vector perturbation. Since the scalar field does not contribute, we will consider only perturbations of the metric and the vector field

$$g_{\mu\nu} = \bar{g}_{\mu\nu} + h^{odd}_{\mu\nu}\,, \qquad A_\mu = \bar{A}_\mu + \delta A^{odd}_\mu\,. \tag{6.21}$$

As we mentioned earlier, only three components of the metric perturbations belong to this sector. Thus, decomposition of the odd-type metric perturbations can be written as

$$h_{tt} = 0, \quad h_{tr} = 0, \quad h_{rr} = 0, \tag{6.22}$$

$$h_{ta} = \sum_{\ell,m} h^{(0)}_{\ell m}(t,r)E_{ab}\nabla^b Y_{\ell m}(\theta,\varphi), \tag{6.23}$$

$$h_{ra} = \sum_{\ell,m} h^{(1)}_{\ell m}(t,r)E_{ab}\nabla^b Y_{\ell m}(\theta,\varphi), \tag{6.24}$$

$$h_{ab} = \frac{1}{2}\sum_{\ell,m} h^{(2)}_{\ell m}(t,r)\left[E_a{}^c\nabla_c\nabla_b Y_{\ell m}(\theta,\varphi) + E_b{}^c\nabla_c\nabla_a Y_{\ell m}(\theta,\varphi)\right]. \tag{6.25}$$

The expansion coefficients $h^{(0)}_{\ell m}$, $h^{(1)}_{\ell m}$ and $h^{(2)}_{\ell m}$ are not independent. We can set to zero some of them using the gauge transformation (6.18). For odd-parity perturbations, transformation (6.20) is simplified to:

$$\xi_t = \xi_r = 0, \quad \xi_a = \sum_{\ell m} \Lambda_{\ell m}(t,r) E_a{}^b \nabla_b Y_{\ell m}. \tag{6.26}$$

Under this gauge transformation, the expansion coefficients transform as

$$h^{(0)}_{\ell m} \to h^{(0)}_{\ell m} - \dot{\Lambda}_{lm} \tag{6.27}$$

$$h^{(1)}_{\ell m} \to h^{(1)}_{\ell m} - \Lambda'_{lm} + \frac{C'}{C}\Lambda_{lm} \tag{6.28}$$

$$h^{(2)}_{\ell m} \to h^{(2)}_{\ell m} - 2\Lambda_{lm} \tag{6.29}$$

thus, we can choose $\Lambda_{\ell m}$ such that $h^{(2)}_{\ell m} = 0$. This choice is known as the *Regge-Wheeler gauge*. It is valid for higher multipoles ($\ell \geq 2$), since the odd-parity perturbations do not have the monopole term ($\ell = 0$), and $h^{(2)}_{\ell m}$ coefficient is vanishing for the dipole term ($\ell = 1$). We can also use other gauges to simplify the problem. Notice that $\Lambda_{\ell m}$ is completely fixed and there are no remaining arbitrary gauge functions.

On the other hand, the perturbation for the vector field is given by

$$\delta A_t = \delta A_r = 0\,, \qquad \delta A_a = \sum_{\ell m} A^{(v)}_{\ell m}(t,r) E_{ab} \nabla^b Y^m_\ell(\theta,\varphi)\,. \tag{6.30}$$

As explained in [49], when studying perturbations of any spherically symmetric system, without any loss of generality, we can restrict oneself to axisymmetric modes of perturbations, we will assume $m = 0$. With this simplification, we can rewrite spherical harmonics in terms of Legendre Polynomials. Also, since modes with different ℓ evolve independently, we focus on a specific mode and omit the indices.

In what follows, we investigate $\ell \geq 2$ and $\ell = 1$ modes separately and discuss the stability of BH solutions.

6.3.1 Second order action for higher multipoles, $\ell \geq 2$

In this section we will focus on higher multipoles since dipole modes $\ell = 1$ require a special treatment. To obtain linear equations for h_0, h_1 and A_v,[4] we expand the action (6.1) to

[4] We have renamed for simplicity of notations $h^{(0)}_{\ell m} \to h_0$, $h^{(1)}_{\ell m} \to h_1$, $A^{(v)}_{\ell m} \to A_v$.

second order in perturbation coefficients. We obtain the following action

$$S^{(2)}_{\rm odd} = \frac{2\ell+1}{4\pi}\int \mathrm{d}t\,\mathrm{d}r\,\mathcal{L}^{(2)}_{\rm odd}\,, \tag{6.31}$$

where we performed an integration over angular variables (θ,φ) by using the standard relations of Legendre Polynomials (see Appendix D) and multiple integration by parts. The second-order Lagrangian is of the form

$$\begin{aligned}\mathcal{L}^{(2)}_{\rm odd} = a_1 h_0^2 + a_2 h_1^2 + a_3\Big[\dot{h}_1^2 + h_0'^2 + 2\frac{C'}{C}h_0\dot{h}_1 - 2h_0'\dot{h}_1 + 2a_4\Big(h_0' - \dot{h}_1\Big)A_v\Big] + \\ a_5 h_0 A_v + a_6 A_v^2 + a_7\dot{A}_v^2 + a_8 A_v'^2\,,\end{aligned} \tag{6.32}$$

where the coefficients a_i are given in Box 6.2. Here, a dot denotes differentiation with respect to t, and a prime is a differentiation with respect to the radial coordinate r. We have defined $\lambda = \ell(\ell+1)$ to simplify the expressions. On-shell, $\mathcal{E}_A = \mathcal{E}_B = \mathcal{E}_{\bar{A}_0} = 0$, thus, background equations allow us to rewrite these coefficients in a simpler form. Performing a few integrations by parts, the term inside square brackets in (6.32) can be rewritten in a more convenient way such that the Lagrangian is simplified to

$$\begin{aligned}\mathcal{L}^{(2)}_{\rm odd} = b_1 h_0^2 + a_2 h_1^2 + a_3\Big[\dot{h}_1 - h_0' + \frac{C'}{C}h_0 - a_4 h_2\Big]^2 \\ + \big(a_6 - a_3 a_4^2\big)h_2^2 + a_7\dot{h_2}^2 + a_8 h_2'^2 + b_2 h_0 h_2\,,\end{aligned} \tag{6.33}$$

where we have defined

$$b_1 = a_1 - (C'a_3)'/C\,, \qquad b_2 = a_5 + 2a_3a_4C'/C = \lambda\mathcal{E}_{\bar{A}_0}/C\,.$$

$$\begin{aligned}
a_1 &= \frac{\lambda}{4C}\Big[\frac{\mathrm{d}}{\mathrm{d}r}\left(C'\sqrt{\frac{B}{A}}f_1\right) + \frac{(\lambda-2)f_1}{\sqrt{AB}} + \frac{2C}{\sqrt{AB}}\mathcal{E}_A\Big]\,, & a_5 &= \frac{\lambda}{C}\left(\mathcal{E}_{\bar{A}_0} - \frac{C'}{C}\mathcal{G}\right)\\
a_2 &= -\frac{\lambda}{2}\sqrt{AB}\left[\frac{(\lambda-2)f_1}{2C} + \mathcal{E}_B\right]\,, & a_6 &= -\frac{\lambda^2\bar{A}_0'}{4C^2}\frac{\mathcal{G}}{\bar{F}}\\
a_3 &= \frac{\lambda}{4}\sqrt{\frac{B}{A}}f_1\,, & a_7 &= \frac{\lambda}{2BC\bar{A}_0'}\mathcal{G}\\
a_4 &= 2\sqrt{\frac{A}{B}}\frac{\mathcal{G}}{Cf_1}\,, & a_8 &= -\frac{\lambda A}{2C\bar{A}_0'}\mathcal{G}
\end{aligned}$$

Table 6.2: *Coefficients of the second-order Lagrangian (6.32)*

On-shell, the last coefficient vanishes, $b_2 = 0$. We can see from the above Lagrangian that h_0 is an auxiliary field since it does not contain time derivatives; consequently, variation with respect to h_0 yields a constraint equation. However, because of the presence of h_0' in the action, this constraint results in a second-order ordinary differential equation which cannot be immediately solved for h_0. To overcome this obstacle, we follow the procedure described in [124, 126]. We introduce an auxiliary field $q(t, r)$ and define the following Lagrangian

$$\begin{aligned}\mathcal{L}^{(2)}_{\text{odd}} = b_1 h_0^2 + a_2 h_1^2 + a_3 \left[2q\left(\dot{h}_1 - h_0' + \frac{C'}{C}h_0 - a_4 A_v\right) - q^2\right] \\ + \left(a_6 - a_3 a_4^2\right) A_v^2 + a_7 \dot{A}_2^2 + a_8 A_v'^2 \,.\end{aligned} \tag{6.34}$$

We can easily check that, by substituting the equation of motion for $q(t, r)$ into Eq. (6.34), we recover the original Lagrangian. This trick enables us to put all derivatives on q using integration by parts, transforming both h_0 and h_1 to removable auxiliary fields. Variation of the Lagrangian (6.34) with respect to h_0 and h_1 leads to

$$b_1 h_0 + \left[(a_3 q)' + a_3 q \frac{C'}{C}\right] = 0 \qquad \longrightarrow \qquad h_0 = -\frac{(a_3 q C)'}{C b_1} \tag{6.35}$$

$$a_2 h_1 - a_3 \dot{q} = 0 \qquad \longrightarrow \qquad h_1 = \frac{a_3}{a_2}\dot{q} \,. \tag{6.36}$$

These relations explicitly link the physical modes h_0 and h_1 to the auxiliary field q. Once $q(t, r)$ is known, also h_0 and h_1 are, and thus all perturbation variables in the Regge-Wheeler gauge are fixed. Notice that one cannot rewrite the previous Lagrangian for $\ell = 1$ since $a_2 = b_1 = 0$, thus the redefinition of the variables h_0 and h_1 are not well defined. This is why this mode has to be studied separately.

Substituting these expressions into the Lagrangian and performing integration by parts, we get

$$\mathcal{L}^{(2)}_{\text{odd}} = \alpha_1 \dot{q}^2 + \beta_1 q'^2 + \gamma_1 q^2 + \alpha_2 \dot{A}_v^2 + \beta_2 A_v'^2 + \gamma_2 A_v^2 + \sigma A_v q \tag{6.37}$$

which explicitly shows that we only have two degrees of freedom, one associated with the gravitational perturbation and another related to vector perturbation of the electromagnetic field. The coefficients of the above Lagrangian, in terms of the variables defined in Box 6.2, are

$$\begin{aligned}
\alpha_1 &= -\frac{a_3^2}{a_2}\,, & \alpha_2 &= a_7\,, & \sigma &= -2a_3 a_4 \\
\beta_1 &= -\frac{a_3^2}{b_1}\,, & \beta_2 &= a_8\,, & \gamma_2 &= a_6 - a_3 a_4^2 \\
\gamma_1 &= \frac{a_3}{b_1^2 C^2}\left[-C b_1'(a_3 C)' + b_1\left[C(a_3 C)'' - 2C'(a_3 C)'\right] - b_1^2 C^2\right] \,.
\end{aligned} \tag{6.38}$$

We see that, in the absence of electromagnetic perturbations, the Lagrangian (6.37) becomes $\mathcal{L}^{(2)}_{\rm odd} = \alpha_1\dot{q}^2 + \beta_1 q'^2 + \gamma_1 q^2$, from which we should at least impose the no-ghost condition $\alpha_1 > 0$ translating into $a_2 < 0$ and therefore $f_1 > 0$. Similarly, in the absence of the gravitational perturbations, we have $\mathcal{L}^{(2)}_{\rm odd} = \alpha_2\dot{A}_v^2 + \beta_2 A_v'^2 + \gamma_2 A_v^2$, from which we impose the condition $\alpha_2 > 0$ which means $Q/\bar{A}_0' > 0$ and using Eq. (6.10) gives $f_{2,F} > 0$.

Thus, from the odd-parity sector we obtain the conditions

$$f_1(\phi) > 0 \qquad \text{and} \qquad f_{2,F}(\phi, X, F) > 0\,. \tag{6.39}$$

■ Master equation

To arrive at our final result, it is convenient to rescale variables in (6.37) as

$$q(t,r) = \sqrt{\frac{A}{f_1 BC}}\, V_g(t,r)\,, \qquad A_v(t,r) = \frac{V_e(t,r)}{\sqrt{2(\lambda-2)f_{2,F}}}\,, \tag{6.40}$$

where (V_g, V_e) represent, respectively, the vector perturbations associated to the gravitational and electromagnetic sector. Notice that we have assumed the previous conditions (6.39). Finally, introducing the tortoise coordinate, $\mathrm{d}r = \sqrt{AB}\,\mathrm{d}r_*$, we get that the action (6.31) can be written in the simple form

$$S^{(2)}_{\rm odd} = \frac{\ell(\ell+1)(2\ell+1)}{16\pi(\ell+2)(\ell-1)} \int \mathrm{d}t\mathrm{d}r_* \left[\dot{\Psi}_i^2 - \left(\frac{\partial\Psi_i}{\partial r_*}\right)^2 - \mathcal{V}_{ij}\Psi_i\Psi_j\right], \tag{6.41}$$

where $\vec{\Psi} = (V_g, V_e)^t$ encloses the two degrees of freedom, and $\mathcal{V}_{ij}$ are the components of a 2×2 symmetric potential energy matrix whose components are given, after substituting relations of Box 6.2, by

$$\mathcal{V}_{11} = (\lambda-2)\frac{A}{C} - \partial_{r_*}S_1 + S_1^2\,, \qquad S_1(r) = \frac{\sqrt{AB}}{2}\left(\frac{C'}{C} + \frac{f_1'}{f_1}\right) \tag{6.42}$$

$$\mathcal{V}_{22} = \frac{\lambda A}{C} + G(r) - \partial_{r_*}S_2 + S_2^2\,, \qquad S_2(r) = -\frac{\sqrt{AB}}{2}\frac{f_{2,F}'}{f_{2,F}} \tag{6.43}$$

$$\mathcal{V}_{12} = \sqrt{(\lambda-2)\frac{A}{C}G(r)}\,, \qquad G(r) = 2\sqrt{AB}\frac{\bar{A}_0'}{Cf_1}\mathcal{G}\,. \tag{6.44}$$

The introduction of the functions (S_1, S_2) will be clearer in the stability analysis section. Variation of the action (6.41) with respect to $\vec{\Psi}$ leads to a wave-like equation

$$-\frac{\partial^2\vec{\Psi}}{\partial t^2}+\frac{\partial^2\vec{\Psi}}{\partial r_*^2}-\mathbf{V}\vec{\Psi}=0 \tag{6.45}$$

from which we conclude that odd-parity modes propagate at the speed of light, independently of the choice of functions $f_1(\phi)$ and $f_2(\phi, X, F)$. Since matrix $\mathbf{V}$ is not diagonal, the previous equation is a set of two coupled differential equations.

6.3.2 Stability Analysis

Equation (6.45) tells us that a BH reacts to a perturbation emitting a signal in the form of waves, the gravitational radiation. Detection of gravitational waves [127] opened the possibility of testing GR in the strong-field regime of gravity. It is well known that the signal of a GW can be divided into three stages:

1. An early response which depends strongly on the initial conditions, the merger.
2. An exponentially decaying phase known as the ringdown.
3. A late tail.

The linear theory of perturbations tackles the last two stages of this process. The waveform of the ringdown is accurately described by a superposition of damped oscillations, called the quasi-normal modes (QNMs) of the BH. Thus we can write

$$\Psi(t,r)=\sum_n e^{-i\omega_n t}\phi_n(r)\,. \tag{6.46}$$

Replacing into (6.45), we found that the problem is reduced to an eigenvalue equation

$$\hat{H}\vec{\Psi}=\omega^2\vec{\Psi}\,,\qquad\qquad \hat{H}\equiv-\frac{d^2}{dr_*^2}+V(r)\,, \tag{6.47}$$

where $\vec{\Psi}$ are the eigenvectors and ω^2 the eigenvalues of the operator $\hat{H}$. We can find stable solutions to this equation if all the eigenvalues of the differential operator $\hat{H}$ are positive. Therefore, the stability of the spacetime is related to the positivity of $\hat{H}$; it must have no negative spectra. To prove the stability, let us define the inner product

$$(\vec{\psi},\vec{\xi})=\int \mathrm{d}r_*\Big[\bar{\psi}_1\xi_1+\bar{\psi}_2\xi_2\Big] \tag{6.48}$$

where $\vec{\psi} = (\psi_1, \psi_2)^T$ and $\vec{\xi} = (\xi_1, \xi_2)^T$. Stability means that the operator $\hat{H}$ is a positive self-adjoint operator in $L^2(r_*)$ —the Hilbert space of square integrable functions of r_*. Therefore, we need to prove the positivity defined as

$$\forall \chi\,, \quad (\vec{\chi}, \hat{H}\vec{\chi}) > 0\,. \tag{6.49}$$

This condition will imply that, given a well-behaved initial data, of compact support, χ remains bounded at all times. This is a sufficient condition. The rigorous and complete proof of the stability related to equations of the form (6.45) can be found in [52, 128] using spectral theory.

When the potential in (6.47) is non-negative everywhere, it can be checked that condition (6.49) is automatically satisfied. However, even if the potential contains a small negative region, the spacetime is still stable against linear perturbations. In this case, and when the potential is not positively defined at first glance, to prove (6.49), it is common to apply the *S-deformation* approach [55, 54]: If there exists a function S such that it is continuous everywhere and satisfies $V + dS/dr_* - S^2 \geq 0$, then the solution of (6.47) remains stable.

In what follows, we apply a similar procedure to deduce the stability of Eq. (6.45). From (6.41) we have

$$\begin{aligned}
(\vec{\chi}, \hat{H}\vec{\chi}) &= \int \mathrm{d}r_* \Big[\bar{\chi}_1\Big(-\partial_{r_*}^2\chi_1 + \mathcal{V}_{11}\chi_1 + \mathcal{V}_{12}\chi_2\Big) + \bar{\chi}_2\Big(-\partial_{r_*}^2\chi_2 + \mathcal{V}_{22}\chi_2 + \mathcal{V}_{12}\chi_1\Big)\Big] \\
&= \int \mathrm{d}r_* \Big[\Big|\frac{\mathrm{d}\chi_1}{\mathrm{d}r_*}\Big|^2 + \Big|\frac{\mathrm{d}\chi_2}{\mathrm{d}r_*}\Big|^2 + \mathcal{V}_{12}\Big(\bar{\chi}_1\chi_2 + \chi_1\bar{\chi}_2\Big) + \mathcal{V}_{11}|\chi_1|^2 + \mathcal{V}_{22}|\chi_2|^2\Big] \\
&= \int \mathrm{d}r_* \Big[\Big|\frac{\mathrm{d}\chi_1}{\mathrm{d}r_*} + S_1\chi_1\Big|^2 + \Big|\frac{\mathrm{d}\chi_2}{\mathrm{d}r_*} + S_2\chi_2\Big|^2 + (\lambda-2)\frac{A}{C}|\chi_1|^2 + (\lambda\frac{A}{C} + G)|\chi_2|^2 \\
&\qquad + \sqrt{(\lambda-2)\frac{A}{C}G}\Big(\bar{\chi}_1\chi_2 + \chi_1\bar{\chi}_2\Big)\Big] \\
&= \int \mathrm{d}r_* \Big[\Big|\frac{\mathrm{d}\chi_1}{\mathrm{d}r_*} + S_1\chi_1\Big|^2 + \Big|\frac{\mathrm{d}\chi_2}{\mathrm{d}r_*} + S_2\chi_2\Big|^2 + \Big|\sqrt{(\lambda-2)\frac{A}{C}}\chi_1 + \sqrt{G}\chi_2\Big|^2 + \lambda\frac{A}{C}|\chi_2|^2\Big] \\
&\geq 0\,.
\end{aligned}$$

In the second line, we have neglected the boundary term $\bar{\chi}_1\partial_{r_*}\chi_1 + \bar{\chi}_2\partial_{r_*}\chi_2$ coming from the integration by parts, because we assumed χ_1 and χ_2 to be smooth functions of compact support, while in the third line we have neglected the boundary term $S_1|\chi_1|^2 + S_2|\chi_2|^2$.

Therefore, we conclude that the black hole is stable under vector perturbations for $\ell \geq 2$ if the no-ghost conditions (6.39) are satisfied[5].

[5]It was also noticed that, in Horndeski theory, the black hole is stable if the no-ghost and hyperbolicity conditions are satisfied [126]. Notice that, for Lovelock black holes, the no-ghost and hyperbolicity conditions

6.3.3 Second order action for $\ell = 1$

We should first mention that, for $\ell = 0$, spherical harmonics are constant and therefore the three vector perturbations of the metric and the vector perturbation of the electromagnetic field are identically zero, as we can see from their definition (6.23, 6.24, 6.25, 6.30).

For the dipole mode, $\ell = 1$, the perturbation h_{ab} (6.25) vanishes identically by properties of the spherical harmonics. In fact, assuming $m = 0$ because the final result is independent of the azimuthal angle, we have $Y_1^0 \propto \cos\theta$, and substituting in (6.25) we get $h_{ab} = 0$. Consequently, it does not make sense to apply the Regge-Wheeler gauge. Instead, we can use the gauge degree of freedom to vanish h_1. However, we can see from the transformation (6.28) that the gauge is not entirely fixed. We have a residual gauge degree of freedom, defined as $\Lambda \to \Lambda + f(t)C(r)$. For this reason, we will fix the gauge after finding the equations of motion.

We start from the Lagrangian (6.33) with $\ell = 1$. After imposing background equations, we get $a_2 = b_1 = 0$; thus, the Lagrangian simplifies a bit

$$\mathcal{L}^{(2)}_{\text{odd},\,\ell=1} = a_3\left[\dot{h}_1 - h_0' + \frac{C'}{C}h_0 - a_4 A_v\right]^2 + \left(a_6 - a_3 a_4^2\right)A_v^2 + a_7\dot{A}_v^2 + a_8 A_v'^2\,. \tag{6.50}$$

Variation of this action with respect to h_0 and h_1 gives

$$\dot{\mathcal{E}} = 0\,, \qquad\qquad (C\mathcal{E})' = 0 \tag{6.51}$$

where we have defined

$$\mathcal{E} = a_3\left(\dot{h}_1 - h_0' + \frac{C'}{C}h_0 - a_4 A_v\right). \tag{6.52}$$

The solution to equations (6.51) is given by $\mathcal{E} = \mathcal{J}/C(r)$, where $\mathcal{J}$ is an integration constant. Fixing the gauge and integrating this solution with (6.52) to solve for h_0, it follows that

$$h_0(t,r) = -\mathcal{J}C(r)\int\frac{\mathrm{d}r}{C(r)^2 a_3} - C(r)\int\frac{a_4}{C(r)}A_v\mathrm{d}r + F(t)C(r) \tag{6.53}$$

where $F(t)$ is a constant of integration. This last term can be eliminated using the residual gauge function, giving finally

$$h_0(t,r) = -2\mathcal{J}C(r)\int\frac{1}{C^2(r)f_1}\sqrt{\frac{A}{B}}\mathrm{d}r - 2QC(r)\int\frac{A_v}{C(r)^2 f_1}\sqrt{\frac{A}{B}}\mathrm{d}r\,. \tag{6.54}$$

---

could be satisfied while the black hole is unstable [129].

Variation of the action (6.50) wrt A_v gives

$$a_7\ddot{A}_v + (a_8 A_v')' - \left(a_6 - a_3 a_4^2\right)A_v + a_4\frac{\mathcal{J}}{C(r)} = 0\,. \tag{6.55}$$

Defining a new variable $a_v = \sqrt{f_{2,F}}A_v$ and using the tortoise coordinate, we find

$$-\frac{\partial^2 a_v}{\partial t^2} + \frac{\partial^2 a_v}{\partial r_*^2} - \mathcal{V}_{22}a_v - \frac{2Q\mathcal{J}A}{C^2 f_1\sqrt{f_{2,F}}} = 0 \tag{6.56}$$

where $\mathcal{V}_{22}$ is the coefficient defined in Eq.(6.43) for $\ell = 1$, i.e. $\lambda = 2$.

The solution of Eq.(6.56) is the sum of a particular solution that we can consider as a function of r only and a homogeneous solution. In order to understand this solution, let us consider the simple case where we have perturbed Reissner-Nordström BH in general relativity. For that we take $f_1 = 2$, $f_2 = 4F$ and $Q = 4q$, from which we get

$$A(r) = B(r) = 1 - \frac{2M}{r} + \frac{q^2}{r^2}\,, \qquad C(r) = r^2\,. \tag{6.57}$$

For this spacetime, a particular solution of Eq. (6.56) is

$$a_v = -Jq/6Mr \qquad \longrightarrow \qquad A_v = -Jq/12Mr\,. \tag{6.58}$$

Therefore, integrating (6.54), we have

$$h_0 = -\frac{\mathcal{J}}{6M}\left(\frac{-2M}{r} + \frac{q^2}{r^2}\right). \tag{6.59}$$

which means that the metric perturbation is

$$h_{t\varphi} = -\frac{\mathcal{J}}{6M}\left(\frac{-2M}{r} + \frac{q^2}{r^2}\right)\sin^2\theta \tag{6.60}$$

This is the Kerr-Newman solution at the first order in J if we define $\mathcal{J} = -12J$. Therefore, the particular solution of Eq.(6.56) describes a slow rotating black hole, while the homogeneous solution describes the propagation of the electromagnetic field in our spacetime [130]. This propagation is stable because the potential $\mathcal{V}_{22}$ can be easily deformed to a positive potential using the function $S_2(r)$. In fact, as we have shown in Sec. 6.3.2, the associated operator is positive definite.

In conclusion, we have shown that for any theory described by the action (6.1) and

satisfying the conditions $f_1 > 0$ and $f_{2,F} > 0$, the static spherically symmetric spacetime described by a generic metric (6.3) is stable under vector perturbations.

6.4 Even-partiry perturbations

In this section we analyze even-parity perturbations, also referred as polar or scalar perturbations, since under parity transformations $(\theta \to \pi - \theta, \phi \to \phi + \pi)$ they are multiplied by a factor $(-1)^\ell$. In contrast with the odd-parity modes, here we have to include perturbations of the scalar field. Using the harmonic decomposition (6.13), it is introduced as

$$\phi(t, r, \theta, \varphi) = \bar{\phi}(r) + \sum_{\ell m} \delta\phi_{\ell m}(t, r) Y_\ell^m(\theta, \varphi) \tag{6.61}$$

where $\bar{\phi}(r)$ is the background value, and $\delta\phi_{\ell m}$ is the perturbed part being a function of t and r. As we mentioned in section 6.2, seven components of the perturbed metric belong to this sector. Therefore, the mathematical analysis is more involved. The first three scalar functions come from the components h_{tt}, h_{tr} and h_{rr} and we write them as

$$\begin{aligned} h_{tt} &= \sum_{\ell,m} A(r) H_{\ell m}^{(0)}(t, r)\, Y_\ell^m(\theta, \varphi) \\ h_{tr} &= \sum_{\ell,m} H_{\ell m}^{(1)}(t, r)\, Y_\ell^m(\theta, \varphi) \\ h_{rr} &= \sum_{\ell,m} \frac{1}{B(r)} H_{\ell m}^{(2)}(t, r)\, Y_\ell^m(\theta, \varphi) \end{aligned} \tag{6.62}$$

where we have factorized the functions $A(r)$ and $B(r)$ for convenience. The second set of scalar functions come from the vector decompostion of the componets h_{ta} and h_{ra}

$$h_{ta} = \sum_{\ell,m} \beta_{\ell m}(t, r)\, \nabla_a Y_\ell^m(\theta, \varphi) \tag{6.63}$$

$$h_{ra} = \sum_{\ell,m} \alpha_{\ell m}(t, r)\, \nabla_a Y_\ell^m(\theta, \varphi)\,. \tag{6.64}$$

Finally, the last scalar component comes from the tensor decomposition (6.17)

$$h_{ab} = \sum_{\ell,m} \left[K_{\ell m}(t, r)\, \gamma_{ab}\, Y_\ell^m(\theta, \varphi) + G_{\ell m}(t, r)\, \nabla_a \nabla_b Y_\ell^m(\theta, \varphi) \right]. \tag{6.65}$$

As we mentioned before, we can set to zero some of these functions using the gauge fixing.

Applying the infinitesimal transformation (6.18), the components of (6.20) that contribute to the scalar sector are

$$\begin{aligned}\xi_t &= \sum_{l,m} T_{\ell m}(t,r)Y^m_\ell(\theta,\varphi)\\ \xi_r &= \sum_{l,m} R_{\ell m}(t,r)Y^m_\ell(\theta,\varphi)\\ \xi_a &= \sum_{l,m} \Theta_{\ell m}(t,r)\nabla_a Y^m_\ell(\theta,\varphi)\,.\end{aligned} \tag{6.66}$$

Then, the perturbation functions transform as

$$H^{(0)}_{\ell m} \to H^{(0)}_{\ell m} - 2\frac{\dot{T}_{\ell m}}{A} + \frac{BA'}{A}R_{\ell m} \tag{6.67}$$

$$H^{(1)}_{\ell m} \to H^{(1)}_{\ell m} - \dot{R}_{\ell m} - T'_{\ell m} + \frac{A'}{A}T_{\ell m} \tag{6.68}$$

$$H^{(2)}_{\ell m} \to H^{(2)}_{\ell m} - 2BR'_{\ell m} - B'R_{\ell m} \tag{6.69}$$

$$\beta^{(0)}_{\ell m} \to \beta^{(0)}_{\ell m} - \dot{\Theta}_{\ell m} - T_{\ell m} \tag{6.70}$$

$$\alpha^{(0)}_{\ell m} \to \alpha^{(0)}_{\ell m} - \Theta'_{\ell m} - R_{\ell m} + \frac{C'}{C}\Theta_{\ell m} \tag{6.71}$$

$$K^{(0)}_{\ell m} \to K^{(0)}_{\ell m} - \frac{BC'}{C}R_{\ell m} \tag{6.72}$$

$$G^{(0)}_{\ell m} \to G^{(0)}_{\ell m} - 2\Theta_{\ell m} \tag{6.73}$$

For lower multipoles $\ell = \{0,1\}$, some perturbations are identically zero; thus, we have to analyze each case separately. For multipoles $l \geq 2$, the scalar transformation functions $T_{\ell m}$ and $\Theta_{\ell m}$ can be fixed by choosing the gauge in which

$$\beta_{\ell m} = 0\,, \qquad G_{\ell m} = 0\,. \tag{6.74}$$

At this point, we have a remaining gauge freedom associated with the function $R_{\ell m}(t,r)$. Depending on its values, different gauge choices can be found in the literature.

$$\text{(i) Uniform curvature gauge}: \;\; K_{\ell m} = 0\,, \tag{6.75}$$

$$\text{(ii) Unitary gauge}: \;\; \delta\phi_{\ell m} = 0\,, \tag{6.76}$$

$$\text{(iii) Spatially diagonal gauge}: \;\; \alpha_{\ell m} = 0\,. \tag{6.77}$$

The results are independent of the choice of the gauge. The pioneering work made by Zerilli [48] that computes the perturbation of Schwarzschild black hole was done using the spatial diagonal gauge. However, the Uniform curvature gauge has recently been applied in the

study of perturbations since the equations appear to be more manipulable, see for example [124, 125, 131, 132]. Following this line of work, we will choose the uniform curvature gauge (6.75) to compute the second-order action of even-parity perturbations.

On the other hand, we introduced even-parity perturbation of the vector field as $A_\mu = \bar{A}_\mu + \delta A_\mu$, where the components of the perturbation are decomposed as

$$\delta A_t = \sum_{\ell m} A^{(0)}_{\ell m}(t,r) Y^m_\ell(\theta,\varphi)\,, \tag{6.78}$$

$$\delta A_r = \sum_{\ell m} A^{(1)}_{\ell m}(t,r) Y^m_\ell(\theta,\varphi)\,, \tag{6.79}$$

$$\delta A_a = \sum_{\ell m} A^{(2)}_{\ell m}(t,r) \nabla_a Y^m_\ell(\theta,\varphi)\,. \tag{6.80}$$

In addition, we have a gauge freedom associated to the vector field, which can be used to set $A^{(2)}_{\ell m} = 0$. In fact, computing the field strength $F_{\mu\nu}$, we get that the components are proportional to the combination, $(A^{(0)}_{\ell m} - \dot{A}^{(2)}_{\ell m})$, $(A'^{(0)}_{\ell m} - \dot{A}^{(1)}_{\ell m})$ or $(A^{(1)}_{\ell m} - A'^{(2)}_{\ell m})$. Therefore, we can define the transformation

$$A_t \to A_t - \sum_{\ell m} \dot{A}^{(2)}_{\ell m} Y^m_\ell\,, \quad A_r \to A_r - \sum_{\ell m} A'^{(2)}_{\ell m} Y^m_\ell\,, \quad A_a \to A_a - \sum_{\ell m} A^{(2)}_{\ell m} \nabla_a Y^m_\ell$$

to simplify the expressions. It is important to notice that scalar perturbations remain scalar after this redefinition. Since we choose the Uniform curvature gauge, which is valid for higher multipoles, we study this case separately from $\ell = \{0, 1\}$.

6.4.1 Second order Lagrangian for $\ell \geq 2$

Substituting the above relations into the action (6.1), after integrating the angular coordinates and many integrations by parts, the second-order action is expressed in the form

$$S^{(2)}_{\text{even}} = \frac{2\ell+1}{2\pi} \int \mathrm{d}t\, \mathrm{d}r\, \mathcal{L}^{(2)}_{\text{even}}\,, \tag{6.81}$$

where the second-order Lagrangian is

$$\begin{aligned}\mathcal{L}^{(2)}_{\text{even}} &= a_1 H_0^2 + H_0\left[a_2 H_2' + \lambda a_3\alpha' + (a_4+\lambda a_5)H_2 + \lambda a_6\alpha + (a_7+\lambda a_8)\delta\phi + a_9\delta\phi'\right.\\ &\left.+a_{10}\delta\phi'' + a_{11}(A_0' - \dot{A}_1)\right] + (b_1+\lambda b_2)H_1^2 + H_1\left[b_3\dot{H}_2 + \lambda b_4\dot{\alpha} + b_5\dot{\delta\phi} + b_6\dot{\delta\phi}'\right]\\ &+ c_1 H_2^2 + \lambda c_2\alpha^2 + \lambda c_3 H_2\alpha + \lambda c_4\dot{\alpha}^2 + (c_5+\lambda c_6)H_2\delta\phi + c_7 H_2\delta\phi' + c_8\dot{H}_2\dot{\delta\phi}\\ &+ \lambda c_9\alpha\delta\phi + \lambda c_{10}\alpha\delta\phi' + c_{11}H_2(A_0' - \dot{A}_1) + \lambda c_{12}\alpha A_0 + e_1\dot{\delta\phi}^2 + e_2\delta\phi'^2\\ &+ (e_3+\lambda e_4)\delta\phi^2 + e_5\delta\phi(A_0' - \dot{A}_1) + e_6\delta\phi'(A_0' - \dot{A}_1)\\ &+ d_1(A_0' - \dot{A}_1)^2 + \lambda d_2 A_0^2 + \lambda d_3 A_1^2\,.\end{aligned} \tag{6.82}$$

Here a_i, b_i, c_i, d_i and e_i are all functions of r only and their expressions are given in Box 6.3.

In what follows, we will reduce this Lagrangian and rewrite it in terms of three variables, representing the remaining three degrees of freedom of the theory. Variation of the action (6.81) with respect to A_0 and A_1 leads to

$$\lambda c_{12}\alpha + 2\lambda d_2 A_0 - \partial_r\left[a_{11}H_0 + c_{11}H_2 + e_5\delta\phi + e_6\delta\phi' + 2d_1(A_0{}' - \dot{A}_1)\right] = 0 \tag{6.83}$$

$$2\lambda d_3 A_1 + \partial_t\left[a_{11}H_0 + c_{11}H_2 + e_5\delta\phi + e_6\delta\phi' + 2d_1(A_0{}' - \dot{A}_1)\right] = 0 \tag{6.84}$$

which inspired us to introduce a new variable

$$S_e(t,r) = a_{11}H_0 + c_{11}H_2 + e_5\delta\phi + e_6\delta\phi' + 2d_1(A_0{}' - \dot{A}_1) \tag{6.85}$$

which will be associated to the scalar perturbation of the electromagnetic field. Thus, we can rewrite

$$A_0 = \frac{1}{2\lambda d_2}(S_e' - \lambda c_{12}\alpha)\,, \qquad A_1 = -\frac{\dot{S}_e}{2\lambda d_3}\,. \tag{6.86}$$

We can see from Lagrangian (6.82) that H_1 is an auxiliary field, because it has no derivatives. Thus, we can integrate out this non-propagating field by using its own equation of motion

$$H_1 = -\frac{1}{2\lambda b_2}\partial_t[b_3 H_2 + \lambda b_4\alpha + b_5\delta\phi + b_6\delta\phi']\,. \tag{6.87}$$

Notice that the coefficient b_1 is zero on-shell, so we have dropped this term in the previous equation. At this point, the Lagrangian (6.82) only depends on the variables H_0, H_2, α, S_e

$$
\begin{aligned}
a_1 &= -\frac{C}{4}\sqrt{\frac{A}{B}}(\mathcal{F}+\mathcal{E}_A)\\
a_2 &= -\frac{1}{2}\sqrt{AB}\Xi\\
a_3 &= \sqrt{AB}f_1\\
a_4 &= a_2' + \frac{C}{2}\sqrt{\frac{A}{B}}(\mathcal{F}+\mathcal{M}-\mathcal{E}_B)\\
a_5 &= -\frac{1}{2}\sqrt{\frac{A}{B}}f_1\\
a_6 &= a_3' + \left(\frac{C'}{2C}-\frac{A'}{2A}\right)a_3\\
a_7 &= -C\sqrt{\frac{A}{B}}\frac{\partial\mathcal{E}_A}{\partial\phi}\\
a_8 &= -\sqrt{\frac{A}{B}}\frac{\mathcal{Z}}{C}\\
a_9 &= \frac{\sqrt{A}C}{\mathcal{Z}}\left[\frac{\sqrt{B}}{C}\mathcal{Z}^2\right]' + \mathcal{J} - \sqrt{\frac{A}{B}}\frac{C}{\phi'}\mathcal{M}\\
a_{10} &= \sqrt{AB}\mathcal{Z}\\
a_{11} &= -\sqrt{\frac{A}{B}}\frac{C}{\bar{A}_0'}\mathcal{F}\\
b_1 &= \sqrt{\frac{B}{A}}C\mathcal{E}_B\\
b_2 &= \frac{1}{2}\sqrt{\frac{B}{A}}f_1\\
b_3 &= \sqrt{\frac{B}{A}}\Xi\\
b_4 &= -2b_2\\
b_5 &= \frac{2}{A}(a_{10}'-a_9) - \frac{2C\mathcal{M}}{\sqrt{AB}\phi'}\\
b_6 &= -2\sqrt{\frac{B}{A}}\mathcal{Z}\\
c_1 &= \frac{C}{4}\sqrt{\frac{A}{B}}\left[2\Sigma + 2B\left(\frac{A'}{2A}+\frac{C'}{C}\right)f_1' - \mathcal{E}_B\right.\\
&\qquad \left. + \left(\frac{A'}{A}+\frac{C'}{2C}\right)\frac{BC'}{C}f_1 - \mathcal{F} - 2\mathcal{M}\right]\\
c_2 &= \sqrt{AB}(f_1 - C\mathcal{E}_B)/C\\
c_3 &= -\frac{1}{2}\sqrt{AB}\left[f_1\left(\frac{A'}{A}+\frac{C'}{C}\right)+2f_1'\right]\\
c_4 &= \frac{1}{2}\sqrt{\frac{B}{A}}f_1\\
c_5 &= C\sqrt{\frac{A}{B}}\frac{\partial\mathcal{E}_B}{\partial\phi}\\
c_6 &= -a_8\\
c_7 &= -\sqrt{AB}\left[\left(\frac{A'}{2A}+\frac{C'}{C}\right)\mathcal{Z} + \frac{C}{B\phi'}(2\Sigma-\mathcal{M})\right]\\
c_8 &= -\frac{\mathcal{Z}}{\sqrt{AB}}\\
c_9 &= \frac{2\mathcal{J}}{C} + 2\sqrt{ABC}\left(\frac{\mathcal{Z}}{C^{3/2}}\right)'\\
c_{10} &= \frac{2\sqrt{AB}}{C}\mathcal{Z}\\
c_{11} &= \sqrt{\frac{A}{B}}\frac{C}{\bar{A}_0'}(\mathcal{F}+\mathcal{M})\\
c_{12} &= -2\mathcal{G}/C\\
d_1 &= -\sqrt{\frac{A}{B}}\frac{C}{\bar{A}_0'^2}\mathcal{F}\\
d_2 &= \frac{\mathcal{G}}{BC\bar{A}_0'}\\
d_3 &= -AB\,d_2\\
e_1 &= \frac{\mathcal{J}}{AB\phi'}\\
e_2 &= -\sqrt{AB}C\frac{\Sigma}{\bar{X}}\\
e_3 &= \frac{\partial\mathcal{E}_\phi}{\partial\phi}\\
e_4 &= -\frac{\mathcal{J}}{BC\phi'}\\
e_5 &= 2C\bar{A}_0'\sqrt{\frac{B}{A}}f_{2,\phi F}\\
e_6 &= -\frac{2C}{\bar{A}_0'\phi'}\sqrt{\frac{A}{B}}\mathcal{M}
\end{aligned}
$$

Table 6.3: *Coefficients of the second-order Lagrangian (6.82). A prime denotes derivative wrt r. $\mathcal{Z} = Cf_{1,\phi}$. The other functions are given in the text.*

and $\delta\phi$. Variation of the action with respect to H_0 leads to

$$\begin{aligned}\mathcal{E}_1 \equiv 2a_1H_0 + a_2H_2' + \lambda a_3\alpha' + (a_4+\lambda a_5)h_2 + \lambda a_6\alpha + \\ (a_7+\lambda a_8)\delta\phi + a_9\delta\phi' + a_{10}\delta\phi'' + a_{11}(A_0' - \dot{A}_1) = 0\end{aligned} \tag{6.88}$$

Taking the combination $\mathcal{E}_1 - a_{11}/(2d_1)S_e(t,r)$, and using the fact that $2a_1 - a_8^2/2d_1 = 0$, we obtain a relation that sets a constraint for the other fields, but this is not an algebraic constraint. In order to resolve this issue, we perform a field redefinition introducing a new variable $S_q(t,r)$ defined by

$$H_2 = \frac{1}{a_2}[S_q(t,r) - a_{10}\delta\phi' - \lambda a_3\alpha] \tag{6.89}$$

which will be associated to the scalar perturbation of the gravitational field. Using this relation, the constraint becomes an algebraic equation for $\alpha(t,r)$, which can be solved to give

$$\alpha = \frac{a_3}{\lambda b_4}T(r)\left[S_q' + \lambda\frac{a_5}{a_2}S_q + \left(P(r) - \lambda\frac{a_{10}a_5}{a_2}\right)\delta\phi' + \frac{a_{11}S_e}{2d_1} + (P'(r)+\lambda a_8)\delta\phi\right] \tag{6.90}$$

where we have defined

$$\begin{aligned}T(r) &= \frac{2}{Af_1\sqrt{AB}}\left(\frac{C'}{C} - \frac{A'}{A} - \frac{2\lambda f_1}{B(Cf_1)'}\right)^{-1}, \\ P(r) &= \sqrt{B}C\left[A\left(\frac{f_{1,\phi}}{\sqrt{A}}\right)' + \sqrt{A}\phi' f_{2,X}\right].\end{aligned} \tag{6.91}$$

Replacing this definition into $\mathcal{E}_1$, we can rewrite H_0 in terms of the other variables and their derivatives (this is a large expression and, at this point, it is not necessary to write it). Substituting this relations into (6.82) we obtain a Lagrangian that only depends on variables $S_q(t,r)$, $S_e(t,r)$ and $\delta\phi(t,r)$ given by

$$\begin{aligned}\mathcal{L}^{(2)}_{\text{even}} = {}& \alpha_1\dot{S}_g^{\,2} + \beta_1 S_g'^{\,2} + \gamma_1 S_g^2 + \alpha_2\dot{S}_e^{\,2} + \beta_2 S_e'^{\,2} + \gamma_2 S_e^2 + \alpha_3\dot{\delta\phi}^{\,2} + \beta_3\delta\phi'^2 + \gamma_3\delta\phi^2 \\ &+ \sigma_1 S_g S_e + \sigma_2 S_g' S_e + \sigma_3 S_g' S_e' + \sigma_4\dot{S}_g\dot{S}_e + \eta_1 S_g\delta\phi + \eta_2 S_g'\delta\phi + \eta_3 S_g'\delta\phi' + \eta_4\dot{S}_g\dot{\delta\phi} \\ &+ \nu_1 S_e\delta\phi + \nu_2 S_e\delta\phi' + \nu_3 S_e'\delta\phi' + \nu_4\dot{S}_e\dot{\delta\phi}\,.\end{aligned} \tag{6.92}$$

Since the coefficients are long expressions, we give their definition in the MATHEMATICA®

notebook [133]. The above Lagrangian can be rewritten in matrix form[6]

$$\mathcal{L}^{(2)}_{even} = K_{ij}\dot{\chi}_i\dot{\chi}_j - L_{ij}\chi'_i\chi'_j + D_{ij}\chi'_i\chi_j + M_{ij}\chi_i\chi_j \tag{6.93}$$

where $\vec{\chi} = (S_q,\ S_e,\ \delta\phi)^T$ encloses the three degrees of freedom and (K_{ij}, L_{ij}, M_{ij}) are symmetric matrices while D_{ij} is anti-symmetric. Studying the stability of this Lagrangian is more complicated than the odd-parity sector, and the reduction to a wave-like equation is more involved. However, from the Lagrangian (6.93), we can derive some conditions which have to be fulfilled in order to describe physical processes.

■ No-ghost condition

The no-ghost condition requires the matrix $\mathbf{K}$ to be positive definite; for this purpose, we employ the Sylvester's criterion[7], which is

$$K_{11} > 0\,, \qquad K_{11}K_{22} - K_{12}^2 > 0 \qquad \det(K_{ij}) > 0\,. \tag{6.94}$$

Substituting all previous expressions, we obtain that the first two conditions correspond to

$$K_{11} = \frac{AT^2}{\lambda C}\sqrt{\frac{A}{B}}\left(\lambda P_1 - f_1 + \frac{BC}{A}\bar{A}_0'^2 f_{2,F}\right) > 0 \tag{6.95}$$

$$K_{11}K_{22} - K_{12}^2 = \frac{A}{BC}\left(\frac{T}{2\lambda}\right)^2 \frac{\lambda P_1 - f_1}{f_{2,F}} > 0\,, \tag{6.96}$$

where we have defined

$$P_1 = \frac{B\Xi}{2ACf_1^2}\left[\frac{AC^2 f_1^4}{\Xi^2 B}\right]', \qquad \text{and} \qquad \Xi = (Cf_1)'\,. \tag{6.97}$$

Imposing the conditions that we obtained in the odd-parity sector (6.39), i.e. $f_1 > 0$ and $f_{2,F} > 0$, we get that the last term in (6.95) is always positive, so the previous two relations are reduced to a single constraint: $\lambda P_1 - f_1 > 0$. Finally, the third condition is given by

$$\det(K_{ij}) = \sqrt{\frac{A}{B}}\left(\frac{TC'}{4\lambda C\phi'}\right)^2 \frac{(\lambda-2)f_1}{B\, f_{2,F}}(2P_1 - f_1) > 0 \tag{6.98}$$

which is satisfied if and only if

$$2P_1 - f_1 > 0\,. \tag{6.99}$$

[6] Definitions of these matrices are given in the MATHEMATICA® file [133]
[7] See Theorem 7.2.5 of Ref. [134]

Clearly, if Eq. (6.99) is satisfied then conditions (6.95) and (6.96) are satisfied automatically, given that $\ell \geq 2$. This no-ghost condition is the same that was computed in [131] for a general scalar-tensor theory. Using the background equations, we find

$$2P_1 - f_1 = \frac{C^2 f_1 \phi'^2}{\Xi^2}\left(3f_{1,\phi}^{\,2} + 2f_1 f_{2,X}\right) \tag{6.100}$$

and assuming stability of odd-parity perturbations, namely $f_1 > 0$, we obtain

$$3f_{1,\phi}^{\,2} + 2f_1 f_{2,X} > 0\,. \tag{6.101}$$

■ Speed of propagation of scalar perturbations

We know that our model contains five degrees of freedom. They are decomposed around a spherically symmetric spacetime as two vector perturbations and three scalar perturbations. As we have seen, vector perturbations propagate at the speed of light. From the Lagrangian (6.93), it is not possible to get the propagation speed of scalar modes at first glance. In that direction, to compute the propagation of perturbations (along the radial direction), let us consider that the solution of the EOM obtained from this Lagrangian is of the form $\chi \propto e^{i(\omega t - kr)}$. Considering the small scale limit, the dispersion relation obtained from (6.93) can be expressed as

$$\det\left(\omega^2 K_{ij} - k^2 L_{ij}\right) = 0.$$

The propagation speed c_r along the radial direction in proper time outside the horizon is given by $c_r = dr_*/d\tau$, where we have defined $d\tau = \sqrt{A}dt$ and $dr_* = dr/\sqrt{B}$. Since this is related to the propagation speed $\hat{c}_r$ in the coordinates (t, r) as $\hat{c}_r = \sqrt{AB}c_r$, by substituting $\omega = \sqrt{AB}c_r k$ into the dispersion relation and solving for c_r, we get

$$c_{r1}^2 = c_{r2}^2 = 1\,, \qquad c_{r3}^2 = \frac{C^2 f_1\left(3Bf_1'^2 - 2P_3 f_1\right)}{B\Xi^2(2P_1 - f_1)} \tag{6.102}$$

where we have defined

$$P_3 = 2\Sigma + \frac{\mathcal{M}^2}{\mathcal{F}} \tag{6.103}$$

with

$$\Sigma = \bar{X}\left(f_{2,X} + 2\bar{X}f_{2,XX}\right), \tag{6.104}$$

$$\mathcal{M} = -4\bar{X}\bar{F}f_{2,FX}\,, \tag{6.105}$$

$$\mathcal{F} = -2\bar{F}\left(f_{2,F} + 2\bar{F}f_{2,FF}\right). \tag{6.106}$$

The propagating mode different than the speed of light is related to the scalar field perturbation. Indeed, in the case where the vector field is absent, we have that $P_3 = 2\Sigma$, and c_{r3}^2 reduces to the propagation speed of the scalar field given in [131] (Eq. (41)). As we will see, this conclusion is also supported by the propagation speeds of the monopole and dipole perturbations. Using previous relations, we get

$$c_{r3}^2 = 1 + 4\bar{X} f_1 \frac{f_{2,XX}(f_{2,F} + 2\bar{F} f_{2,FF}) - 2\bar{F} f_{2,XF}^2}{(f_{2,F} + 2\bar{F} f_{2,FF})(3f_{1,\phi}^2 + 2f_1 f_{2,X})} \,. \tag{6.107}$$

Notice that if we consider a theory for which $f_{2,F} + 2F f_{2,FF} = 0$, that is,

$$S = \int \mathrm{d}^4x\sqrt{-g}\Big[F(\phi)R + K(\phi, X) + G(\phi, X)\sqrt{F}\Big], \tag{6.108}$$

one of the degrees of freedom propagates at infinite speed, which could be similar to the Cuscuton [135], for which this perturbation does not carry any microscopic information.

It is important to emphasize that these velocities are very weakly constrained by gravitational waves. Certainly, between the merger of two compact objects and an observer, the wave propagates mostly over a FLRW spacetime and not on a static spherically symmetric background. However, we should also take into account that a model described by our action is just an effective low energy description of some more fundamental theory. For that reason, we should also impose standard conditions such as Lorentz invariance, unitarity, analyticity. Even if not proved generically, it has been shown in various situations and around different backgrounds that these conditions imply nonsuperluminal propagation (see e.g. [110, 42, 109]). Hereafter, we will not consider this condition but the much more restrictive, possibly more interesting, condition $c_{r_3}^2 = 1$, which translates from Eq.(6.107) into

$$f_{2,XX} = \frac{2\bar{F}(f_{2,XF})^2}{f_{2,F} + 2\bar{F} f_{2,FF}} \,. \tag{6.109}$$

We conclude that any action given by the form below would propagate at the speed of light and contain five degrees of freedom

$$S = \int \mathrm{d}^4x\sqrt{-g}\Big[f_1(\phi)R + f_2(\phi, F) + X f_3(\phi)\Big] \,, \tag{6.110}$$

where (f_1, f_2, f_3) are generic functions.

■ Master equation

Varying the action (6.93) with respect to the fields χ_i, we obtain the equations of motion

$$L_{ij}\chi_j'' + (L_{ij}' - D_{ij})\chi_j' + (M_{ij} + \omega^2 K_{ij} - \frac{1}{2}D_{ij}')\chi_j = 0 \tag{6.111}$$

where we have performed a Fourier transform with respect to the time variable, i.e., we have employed $\vec{\chi}(t,r) \to e^{-i\omega t}\vec{\chi}(r)$.

Making a change of variable $\chi_i \to \Phi_j$ given by $\chi_i(r) = S_{ij}(r)\Phi_j(r)$, and changing to tortoise coordinates $dr = \sqrt{AB}dr_*$, we get

$$\frac{d^2\Phi_q}{dr_*^2} + \omega^2\big(ABS_{qp}^{-1}L_{pi}^{-1}K_{in}S_{nk}\big)\Phi_k + ABS_{qp}^{-1}L_{pi}^{-1}B_{in}S_{nk}\Phi_k = 0 \tag{6.112}$$

where the matrix $\mathbf{S}$ is a solution of

$$S_{ij}' + C_{ik}S_{kj} = 0\,. \tag{6.113}$$

This set of four first-order differential equation will have four integration constants which can be left arbitrary, as long as $\mathbf{S}$ is invertible. In Eq. (6.112), we have defined

$$C_{mj} = \frac{1}{2}L_{mi}^{-1}\left[L_{ij}' - D_{ij} - \frac{1}{2}\left(\frac{A'}{A} + \frac{B'}{B}L_{ij}\right)\right]S_{jk} \tag{6.114}$$

$$B_{in} = L_{ij}(C_{jm}C_{mn} - C_{jn}') - L_{ij}'C_{jn} + D_{ij}C_{jn} + M_{in} - \frac{1}{2}D_{in}'\,. \tag{6.115}$$

When the condition (6.109) is taken into account, the matrix of the second term in (6.112) is the identity matrix (we have $\mathbf{L} = AB\mathbf{K}$); thus, the equation of motion is simplified to:

$$\frac{d^2\vec{\Phi}}{dr_*^2} + \omega^2\vec{\Phi} - \mathbf{V}\vec{\Phi} = 0 \tag{6.116}$$

where $\mathbf{V}$ is the matrix potential, whose expression can be read off directly from (6.112)

$$\mathbf{V} = -\mathbf{S}^{-1}\mathbf{K}^{-1}\mathbf{B}\mathbf{S}\,. \tag{6.117}$$

Given the matrix $\mathbf{S}$, the potential $\mathbf{V}$ can be easily derived and the stability of a solution studied. Unfortunately, in the generic case, we were not able to obtain the matrix $\mathbf{S}$, but we will see in the following sections a number of examples where these calculations can be performed easily.

As already mentioned, generic conditions of stability are difficult to obtain. Proceeding as in the vector case, let us define the operator $\mathcal{H}_{ij} = -\delta_{ij}\frac{\mathrm{d}^2}{\mathrm{d}r_*} + V_{ij}$. We have

$$\begin{aligned}(\Phi, \mathcal{H}\Phi) &= \int \mathrm{d}r_* \bar{\Phi}_i \mathcal{H}_{ij} \Phi_j \\ &= \int \mathrm{d}r_* \Big[\Big| \frac{d\Phi_i}{dr_*} \Big|^2 + V_{ij} \bar{\Phi}_i \Phi_j \Big] \end{aligned} \tag{6.118}$$

where we have as usual performed an integration by parts and eliminated the boundary term. Even if a generic stability condition cannot be obtained, we still can discuss sufficient stability conditions. In fact, a sufficient but not necessary condition of the stability is obtained if the potential is positive definite. On the contrary, if there is a trial function[8] Φ_0, such that $(\Phi_0, \mathcal{H}\Phi_0) < 0$, the spacetime is unstable [136].

In the case[9] where $f_{2,XF} = 0$, we found for large λ

$$V_{22} = \lambda \frac{A}{C} \frac{f_{2,F}}{f_{2,F} + 2F f_{2,FF}} + \mathcal{O}(\lambda^0)\,. \tag{6.119}$$

Considering $\Phi_0 = (0, \phi_0(r), 0)^T$ with $(\phi_0, \phi_0) < \infty$ (a normalizable trial function), we get

$$(\Phi_0, \mathcal{H}\Phi_0) = \int \mathrm{d}r_* \Big[\Big| \frac{d\phi_0}{dr_*} \Big|^2 + \lambda \frac{A}{C} \frac{f_{2,F}}{f_{2,F} + 2F f_{2,FF}} |\phi_0|^2 \Big] + \mathcal{O}(\lambda^0)\,. \tag{6.120}$$

Therefore we conclude that if

$$\frac{f_{2,F}}{f_{2,F} + 2F f_{2,FF}} < 0 \tag{6.121}$$

the integral is negative for sufficiently large λ, which implies an instability.

6.4.2 Second order Lagrangian for $\ell = 0$

Similarly to the vector perturbations, the generic analysis we have performed in the previous section is valid only for higher modes, $\ell \geq 2$. For scalar perturbations, we will see that for $\ell = 0$, we have only one perturbation related to the scalar field, the breathing mode, which is the spherically symmetric perturbation.

When $\ell = 0$, we only have the spherical harmonic $Y_0^0(\theta, \varphi)$, which is constant. Therefore,

[8] Because the lowest eigenvalue ω_0 of the spectrum of $\mathcal{H}$ gives $\forall\ \Phi$, $\omega_0^2 \leq (\Phi, \mathcal{H}\Phi)/(\Phi, \Phi)$. Therefore if a trial function Φ_0 is such that $(\Phi_0, \mathcal{H}\Phi_0) < 0$, we have $\omega_0^2 < 0$, for a normalizable trial function.

[9] Notice that this condition includes most, if not all, models studied in the literature for generic Einstein-Maxwell-dilaton theories.

the perturbations associated to the functions β_{00}, α_{00} and G_{00} vanish. The same argument apply to the gauge function transformation $\Theta(t,r)$. In the gravitational sector, there are four functions H_0, H_1, H_2 and K. As in the case of higher multipoles, ξ_r is fixed completely by setting $K_{00} = 0$. We can use ξ_t to eliminate H_0 or H_1. However, since it is not a complete gauge fixing, we will postpone it until we derive the perturbation equations from the second-order Lagrangian.

The second-order Lagrangian for the monopole perturbations can be obtained by setting $\lambda = 0$ in (6.82). Thus

$$\begin{aligned}\mathcal{L}^{(2)}_{\text{even, }\ell=0} &= a_1 H_0^2 + H_0\Big[a_2 H_2' + a_4 H_2 + a_7\delta\phi + a_9\delta\phi' + a_{10}\delta\phi'' + a_{11}(A_0' - \dot{A}_1)\Big] \\ &+ H_1\Big[b_3\dot{H}_2 + b_5\dot{\delta\phi} + b_6\dot{\delta\phi}'\Big] + c_1 H_2^2 + c_5 H_2\delta\phi + c_7 H_2\delta\phi' + c_8\dot{H}_2\dot{\delta\phi} \\ &+ c_{11}H_2(A_0' - \dot{A}_1) + e_1\dot{\delta\phi}^2 + e_2\delta\phi'^2 + e_3\delta\phi^2 + e_5\delta\phi(A_0' - \dot{A}_1) \\ &+ e_6\delta\phi'(A_0' - \dot{A}_1) + d_1(A_0' - \dot{A}_1)^2\end{aligned} \tag{6.122}$$

Variation of the action with respect to A_0 and A_1 leads to the relations $\partial_t S_e(t,r) = \partial_r S_e(t,r) = 0$, where $S_e(t,r)$ is defined in (6.85); thus, $S_e(t,r) \equiv C_1$ is constant. Variation wrt H_0, and using the previous equations, we arrive to

$$\partial_r\Big[P(r)\delta\phi + a_2 H_2 + a_{10}\delta\phi' - \frac{C_1}{2}\bar{A}_0\Big] = 0\,, \tag{6.123}$$

while variation wrt H_1 gives

$$\partial_t\Big[P(r)\delta\phi + a_2 H_2 + a_{10}\delta\phi'\Big] = 0\,. \tag{6.124}$$

Therefore, we conclude that

$$P(r)\delta\phi + a_2 H_2 + a_{10}\delta\phi' = \frac{C_1}{2}\bar{A}_0(r) + C_2 \tag{6.125}$$

where C_2 is a new integration constant. This equation will be used to eliminate H_2.

We can use the freedom on ξ_t to partially fix the gauge by choosing $H_1 = 0$, which would also leave an additional freedom, $H_0 \to H_0 - f(t)$. Taking now the variation wrt to H_2 and fixing this gauge, we obtain an expression for H_0' which can be integrated and the integration constant $g(t)$ eliminated by the remaining gauge function. These expressions are not especially illuminating and therefore will not be written. Notice that, with the above procedure, we have eliminated variables H_0, H_1, H_2, A_0, and A_1 from the Lagrangian (6.122); at the end, we only have the perturbation associated to the scalar field, which is the only

propagating degree of freedom with $\ell = 0$.

Thus, a variation in $\delta\phi$ leads to the equation

$$-K_0\ddot{\delta\phi} + \left(L_0\delta\phi'\right)' + M_0\delta\phi + N_0(r) = 0 \tag{6.126}$$

where we have defined

$$K_0 = \frac{C'^2(2P_1 - f_1)}{2\sqrt{AB}C\phi'^2}\,. \tag{6.127}$$

From the above expression, we can see that the no-ghost condition, $K_0 > 0$, is the same as the one for higher multipoles, i.e., equation (6.99). On the other hand, in the limit of a large wavenumber k, we get that the velocity of the propagation is

$$c_0^2 = \frac{L_0}{ABK_0} = \frac{C^2 f_1\left(3Bf_1'^2 - 2P_3 f_1\right)}{B\Xi^2(2P_1 - f_1)} \tag{6.128}$$

which also coincides with $c_{r_3}^2$ given in Eq. (6.102). Since only the scalar wave is excited in the monopole perturbation, this result allows to interpret $c_{r_1}^2$ and $c_{r_2}^2$ as the propagation speeds of gravitational and electromagnetic field, and $c_{r_3}^2$ as the propagation of the scalar waves.

The Eq.(6.126) admits a particular and homogeneous solution. The homogeneous solution will describe the propagation of the spherical scalar wave in the fixed background metric, while the particular solution should modify the constants of the metric. To obtain this result, let us focus on the electric Gibbons-Maeda-Garfinkle-Horowitz-Strominger (GM-GHS) BH

$$f_1 = 2\,, \quad f_2 = -2(\partial_\mu\phi)^2 - e^{-2\phi}F_{\mu\nu}F^{\mu\nu} \tag{6.129}$$

$$A = B = 1 - \frac{2M}{r}\,, \quad C = r(r - \frac{q^2}{M}) \tag{6.130}$$

$$A_0 = -\frac{q}{r}\,, \quad \phi = \frac{1}{2}\log\left(1 - \frac{q^2}{Mr}\right) \tag{6.131}$$

Using the previous equations, we found that a particular solution of Eq.(6.126) is a constant which determines (H_0, H_2) and therefore the metric perturbations have the form

$$h_{tt} = \frac{\alpha}{r}\,, \quad h_{rr} = \frac{\alpha}{r(1 - 2M/r)^2}\,, \tag{6.132}$$

where α is a real constant, $\alpha = M(C_1 q - 4c_2 M)/(8M^2 - 2q^2)$. That produces the result

$$A(r) = B(r) = 1 - \frac{2M + \alpha}{r}\,.$$

Therefore, only the mass of the black hole has been modified. Also we have

$$A_0' - \dot{A}_1 = \frac{MC_1 + 4\alpha q}{8Mr^2} \tag{6.133}$$

which shifts the electric charge as $F_{01} \to F_{01} - (MC_1 + 4\alpha q)/8Mr^2$. Therefore, we expect that for any spacetime, the particular solution shifts the constants of the spacetime while the homogeneous solution describes a scalar wave propagating in a fixed background.

6.4.3 Second order Lagrangian for $\ell = 1$

Let us analyze now the dipole perturbation. When $\ell = 1$ we have $Y_1^0 \propto \cos\theta$, and the components of the metric perturbation h_{ab} acquire the form

$$h_{\theta\theta} = (K(t,r) - G(t,r))\cos\theta \tag{6.134}$$

$$h_{\varphi\varphi} = (K(t,r) - G(t,r))\cos\theta\sin^2\theta \tag{6.135}$$

$$h_{\theta\varphi} = 0\,. \tag{6.136}$$

Therefore, h_{ab} depend on K and G only through the combination $K - G$. We can use a function of the coordinate transformation (6.66), ξ_a, to set $K - G = 0$. Similarly, we make use of the transformation ξ_t to define $\beta(t,r) = 0$. Thus, we have a remaining arbitrary function which we can use to also set $\delta\phi(t,r) = 0$. In fact, under the gauge transformation (6.18) the scalar field transforms as

$$\delta\phi \to \delta\phi - B\bar{\phi}' R.$$

Hence, we can use the transformation of coordinate ξ_r to vanish the scalar field. In this case, the gauge becomes totally fixed and therefore we can proceed as usual. The Lagrangian for the dipole mode is obtained by taking $\lambda = 2$ ($\ell = 1$) in (6.82)

$$\begin{aligned}\mathcal{L}^{(2)}_{even,\ \ell=1} = {} & a_1 H_0^2 + H_0\Big[a_2 H_2' + 2a_3\alpha' + (a_4 + 2a_5)H_2 + 2a_6\alpha + a_{11}(A_0' - \dot{A}_1)\Big] \\ & + (b_1 + 2b_2)H_1^2 + H_1\Big[b_3\dot{H}_2 + 2b_4\dot{\alpha} + b_5\dot{\delta\phi}\Big] + c_1 H_2^2 + 2c_2\alpha^2 + 2c_3 H_2\alpha \\ & + 2c_4\dot{\alpha}^2 + c_{11}H_2(A_0' - \dot{A}_1) + 2c_{12}\alpha A_0 + d_1(A_0' - \dot{A}_1)^2 + 2d_2 A_0^2 + 2d_3 A_1^2\end{aligned} \tag{6.137}$$

Performing similar calculations to those in the section of higher multipoles, after taking $\delta\phi = 0$, we get a second-order Lagrangian similar to (6.92). Again, after redefining variables,

we obtain that the Lagrangian takes the canonical form

$$\mathcal{L}^{(2)}_{even} = K^1_{ij}\dot{\chi}_i\dot{\chi}_j - L^1_{ij}\chi'_i\chi'_j + D^1_{ij}\chi'_i\chi_j + M^1_{ij}\chi_i\chi_j\,. \tag{6.138}$$

Here, χ is a two-component vector representing the two propagating degrees of freedom, (K^1, L^1, M^1) are 2×2 symmetric matrices while D^1 is anti-symmetric. The no-ghost conditions, positivity of the matrix K^1_{ij}, are the same as in the higher multipole case, i.e., given by equations (6.95) and (6.96), which are reduced to the stability condition (6.99) after taking $\lambda = 2$. Also, from this Lagrangian, we find that the propagation speeds along the radial direction are given by

$$c_1^2 = 1\,, \qquad\qquad c_s^2 = \frac{C^2 f_1\,(3Bf_1'^2 - 2P_3 f_1)}{B\Xi^2(2P_1 - f_1)} \tag{6.139}$$

which, again, both coincide with the propagation speed in the case of higher multipoles, see Eq. (6.102). We conclude that the degree of freedom associated with the scalar field travels at the same speed, regardless of the multipole order.

6.5 Application to particular models

The results obtained in this chapter are so general that they can be applied to any scalar-vector-tensor theory of the form (6.1). In this section, we will use our formalism to some particular examples that have been frequently studied in the literature.

6.5.1 Schwarzschild BH

The most simple case to analyze is the Schwarzschild solution of general relativity given by $f_1 = 2$ and $f_2 = 0$, while the metric functions are

$$A(r) = B(r) = 1 - \frac{2M}{r}\,, \qquad\qquad C(r) = r^2\,. \tag{6.140}$$

With this choice, the wave-like equations (6.45) and (6.116) reduce to a single equation for each case, since we only have two degrees of freedom. In the odd-parity sector, we get that the potential $\mathcal{V}_{11}$ (6.42), which correspond to the only non-vanishing degree of freedom in this sector, is simplified to

$$V_{RW} = A(r)\left[\frac{\ell(\ell+1)}{r^2} - \frac{6M}{r^3}\right] \tag{6.141}$$

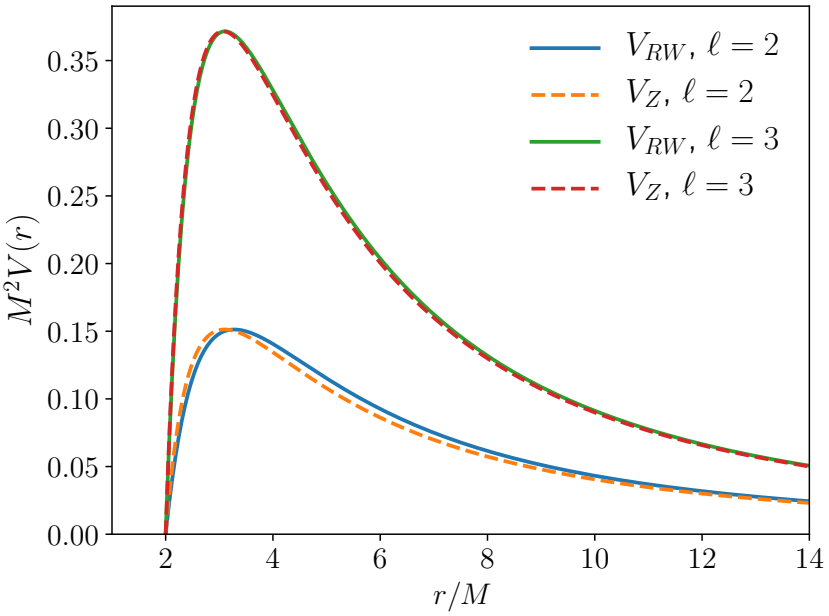

Figure 6.1: *The Regge–Wheeler potential $V_{RW}(r)$ (solid lines) and Zerilli potential $V_Z(r)$ (dashed lines), as a function of r for $\ell = (2, 3)$. The radial coordinate r is measured in units of GM/c^2 (so the horizon is at $r = 2$) and the potential is measured in units of $(GM/c^2)^{-2}$.*

which is known as the *Regge–Wheeler potential*. Now, in the even-parity sector we also get a wave-like equation. The effective potential given in (6.116) becomes

$$V_Z = A(r)\frac{6L^2Mr^2 + 2L^2(L+1)r^3 + 18LM^2r + 18M^3}{r^3(Lr+3M)^2} \tag{6.142}$$

where we defined $L = (\ell+2)(\ell-1)/2$. This is the *Zerilli potential* for scalar perturbations of Schwarzschild BHs.

It is well-known that Schwarzschild BH is classically stable. Applying the results of our analysis, the unique stability condition is $f_1 > 0$, which is trivially satisfied. Also, this conclusion can be obtained by analyzing the potentials; they are completely positive in the region outside the event horizon; thus, solutions of the wave-like equations are stable. Despite its more complicated analytic form, the Zerilli potential is numerically almost indistinguishable from the Regge–Wheeler potential, as we show in Fig. 6.1, especially at large ℓ. They also have the same asymptotic behavior

$$\begin{aligned} V_{RW} &\simeq V_Z \simeq 0\,, & r &\to 2M \\ V_{RW} &\simeq V_Z \simeq \frac{\ell(\ell+1)}{r^2}\,, & r &\to \infty\,. \end{aligned}$$

Also, QNM frequencies describing the odd- and even-parity perturbation equations are the same. We will show more details about this property in the next chapter.

6.5.2 Reissner–Nordström BH

As a second example, we take the Einstein-Hilbert action and introduce the electromagnetic field. The solution corresponds to the Reissner–Nordström BH, which is obtained by setting $f_1 = 2$ and $f_2 = 4F$. In this case, we have four degrees of freedom, two in each type of perturbations, traveling at the speed of light. The metric functions are

$$A(r) = B(r) = 1 - \frac{2M}{r} + \frac{q^2}{r^2}\,, \qquad C(r) = r^2 \tag{6.143}$$

where q denotes the electric charge. Because $f_{2,F}(\phi, X, F) = 4 > 0$, we conclude that its vector perturbations are stable. For completeness, let us write the perturbation potential for this sector

$$\mathbf{V}^{RN}_{odd}(r) = A(r)\left[\frac{1}{r^2}\left(\lambda - \frac{3M}{r} + \frac{4q^2}{r^2}\right)\mathbf{I} + \frac{1}{r^3}\begin{pmatrix} -3M & 2q\sqrt{\lambda-2} \\ 2q\sqrt{\lambda-2} & 3M \end{pmatrix}\right] \tag{6.144}$$

which corresponds exactly to the potential derived[10] originally in [121].

Focusing on the scalar perturbation sector, we have first to eliminate a row and a column of our matrices because of the absence of the scalar field. Then, we need to solve the Eq. (6.113) which gives

$$S = \begin{pmatrix} \frac{6Mr-4q^2+(\lambda-2)r^2}{r^2}c_1 & \frac{6Mr-4q^2+(\lambda-2)r^2}{r^2}c_2 \\ \frac{8c_1}{r}q + c_3 & \frac{8c_2}{r}q + c_4 \end{pmatrix} \tag{6.145}$$

where (c_1, c_2, c_3, c_4) are integration constants, which should be chosen freely as long as $c_1c_4 - c_2c_3 \neq 0$ in order for S to be invertible. Finally, the calculation of the scalar potential is trivial and we found that our potential $\mathbf{V}$ is similar to the original potential[11] derived in [122] with a change of basis matrix constant. Both matrices describe the same problem. In fact, if we write

$$-\frac{\partial^2\mathbf{\Psi}}{\partial t^2} + \frac{\partial^2\mathbf{\Psi}}{\partial r_*^2} - \mathbf{V}\mathbf{\Psi} = 0\,, \tag{6.146}$$

[10] Our perturbations (V_g, V_e) correspond respectively to $(\hat{\pi}_g, \hat{\pi}_f)$ of [121].
[11] Where our variables (S_g, S_e) correspond respectively to (Q, H) of [122]

we can always define a transformation $\mathbf{\Phi} = P\mathbf{\Psi}$ and the similar potential $\mathbf{W} = P\mathbf{V}P^{-1}$ such that

$$-\frac{\partial^2 \mathbf{\Phi}}{\partial t^2} + \frac{\partial^2 \mathbf{\Phi}}{\partial r_*^2} - \mathbf{W}\mathbf{\Phi} = 0 \tag{6.147}$$

if P is a constant matrix. From the potential, the stability can be easily obtained because of the positivity of the matrix.

Since the computation of even-parity potential is more involved, this example has been included in the MATHEMATICA® notebook [133] to show a specific application of how the formalism works and compare our results with the original paper [122].

6.5.3 Nonlinear electrodynamics

Now, let us analyze the dynamical stability of black hole solutions in self-gravitating nonlinear electrodynamics theory, given by the action

$$S = \int \mathrm{d}^4x \left[\frac{R}{4} + \mathcal{L}(F)\right] \tag{6.148}$$

where $\mathcal{L}$ is an arbitrary function of $F = -F_{\mu\nu}F^{\mu\nu}/4$. From the background equation we can find the following relation

$$\frac{A'}{A} - \frac{B'}{B} + \frac{C'}{C} - \frac{2C''}{C'} = 0\,, \tag{6.149}$$

which can be easily integrated to

$$\frac{AC}{BC'^2} = \alpha\,, \tag{6.150}$$

where α is an integration constant. If we were interested only in the background solution, we could have always reparametrized our time coordinate such that $\alpha = 1$. However, because the perturbations are time dependent, we will keep thus constant arbitrary.

In the odd-parity sector, we have that perturbations are stable if $\mathcal{L}_F \equiv \partial\mathcal{L}/\partial F > 0$. For completeness of the vector perturbations, the potential (6.42,6.43,6.44) is given by

$$\mathcal{V}_{11} = (\lambda - 2)\frac{A}{C} + \frac{ABC'}{2C}\left(\frac{C'}{C} - \frac{A'}{A}\right) \tag{6.151}$$

$$\mathcal{V}_{12} = \frac{2A}{C}\sqrt{\frac{\mathcal{G}^2(\lambda-2)}{C\mathcal{L}_F}} \tag{6.152}$$

$$\mathcal{V}_{22} = \frac{A}{C}\left(\lambda + \frac{4\mathcal{G}^2}{C\mathcal{L}_F}\right) + \frac{AB\mathcal{L}'_F}{4\mathcal{L}_F}\left(\frac{A'}{A} + \frac{B'}{B} + 2\frac{\mathcal{L}_F{}''}{\mathcal{L}_F{}'} - \frac{\mathcal{L}_F{}'}{\mathcal{L}_F}\right). \tag{6.153}$$

In [130], the perturbations for this model were studied in a gauge invariant formalism. We find exactly the same potential when $C(r) = r^2$.

Focusing on the even-parity sector, since we have only two degrees of freedom, the stability conditions reduce to (for the sake of simplicity, we have eliminated the obvious positive factors)

$$K_{11} \propto \lambda - 2 + 4\mathcal{G}^2 C^{-1} \mathcal{L}_F^{-1} > 0\,, \qquad \det(K) \propto (\lambda - 2)\mathcal{L}_F^{-1} > 0 \tag{6.154}$$

leading to the same condition as the odd-parity sector, namely $\mathcal{L}_{,F} > 0$. Continuing with the components of the potential that describe the Schrödinger-type equation, as we have shown before, we have to find the matrix S (6.113)

$$S = \begin{pmatrix} c_1\left(2\alpha\lambda + \frac{CA'}{C'} - A\right) & c_3\left(2\alpha\lambda + \frac{CA'}{C'} - A\right) \\ \frac{c_2\sqrt{C'}}{C^{3/4}\sqrt{\bar{A}_0'}} - 8c_1\mathcal{G}\sqrt{\frac{\alpha}{C}} & \frac{c_4\sqrt{C'}}{C^{3/4}\sqrt{\bar{A}_0'}} - 8c_3\mathcal{G}\sqrt{\frac{\alpha}{C}} \end{pmatrix}, \tag{6.155}$$

where, as in the previous case, the constants (c_1, c_2, c_3, c_4) can be arbitrarily chosen as long as $c_1c_4 - c_2c_3 \neq 0$. The expression of the potential in the generic case is long and not necessarily instructive. It can be straightforwardly obtained from the Eq.(6.117). It is, anyway, interesting to derive the most used expression in the literature, namely $A(r) = B(r)$ and $C(r) = r^2$, which implies from Eq.(6.150), that $\alpha = 1/4$. We will take, without any loss of generality, $c_2 = c_3 = 0$ and $c_4 = \sqrt{2Q(\lambda-2)}c_1$. We get

$$V_{11} = \frac{A[\lambda(\lambda-2) + rA'(a+2) - 2A(\lambda-2)]}{r^2(\lambda+a)} + \frac{2A^2(\lambda-2)\mathcal{B}}{r^2(\lambda+a)^2} \tag{6.156}$$

$$V_{12} = V_{21} = \frac{2A\sqrt{\mathcal{G}^2(\lambda-2)}}{r^3(\lambda+a)\sqrt{\mathcal{L}_F}}\left(\lambda - a + 2A\kappa - 4A + \frac{2A\mathcal{B}}{\lambda+a}\right) \tag{6.157}$$

$$V_{22} = A\left(\frac{\kappa\lambda}{r^2} + \frac{4\mathcal{G}^2\left(\lambda - 2A + 4\kappa A - rA'\right)}{\mathcal{L}_F\left(\lambda+a\right)r^4} + \frac{8\mathcal{G}^2A\mathcal{B}}{r^4\mathcal{L}_F\left(\lambda+a\right)^2} + \mathcal{L}_F^{1/2}\left[A(\mathcal{L}_F^{-1/2})'\right]'\right) \tag{6.158}$$

where we have defined

$$\begin{aligned} a &= rA' - 2A\,, \\ \mathcal{B} &= \lambda - 2 + 4\mathcal{G}^2/r^2\mathcal{L}_F\,, \\ \kappa &= -r\bar{A}_0''/(2\bar{A}_0') = \mathcal{L}_F/(\mathcal{L}_F + 2\bar{F}\mathcal{L}_{FF})\,. \end{aligned}$$

This potential is the same as the one discussed in [130]. From it, we can easily derive the stability condition for a specific model or calculate the QNMs.

It is important to notice that the stability will depend only on the metric function A and

its derivatives. In fact, using the equations of motion, we can eliminate the electric potential $\bar{A}_0$ and the Lagrangian $\mathcal{L}$ from all expressions, reducing the potential matrix to

$$V_{11} = \frac{A}{r^2}\Big[rA' - \lambda + 2 + \frac{2(\lambda-2)(\lambda-2A)}{rA'-2A+\lambda} + A\frac{2(\lambda-2)\left(r^2A''-2A+\lambda\right)}{\left(rA'-2A+\lambda\right)^2}\Big], \tag{6.159}$$

$$V_{12} = \sqrt{\lambda-2}\frac{A}{r^2}\sqrt{2-2A+r^2A''}\Big[\frac{\lambda-4A-rA'}{\lambda-2A+rA'} + 2A\frac{\lambda-2A+r^2A''}{(\lambda-2A+rA')^2} + A\frac{4-4A+2rA'-r^3A'''}{(\lambda-2A+rA')(2-2A+r^2A'')}\Big], \tag{6.160}$$

$$V_{22} = \frac{A}{r^2}\Big[2rA' + 7A - 2 - \lambda - r^2A'' + 2\frac{8A^2+\lambda(2+r^2A'')-A(4+4\lambda+4r^2A''+r^3A''')}{\lambda-2A+rA'} + \frac{2A(2-2A+r^2A'')(\lambda-2A+r^2A'')}{(\lambda-2A+rA')^2} - \frac{A(4-4A+2rA'-r^3A''')^2}{4(2-2A+r^2A'')^2} + \frac{(\lambda-rA')(4+2rA'-r^3A''')+A(-4\lambda+4rA'+4r^3A'''+r^4A'''')}{2(2-2A+r^2A'')}\Big]. \tag{6.161}$$

From this, we conclude that different theories (Lagrangians) having the same black hole solution will exhibit the same stability. In that direction, we found that the choice $A = B = 1 - 2M/r + q^2/r^2$, gives that the stability potential reduces to the Moncrief potential[12] which implies the stability of the Reissner-Nordström metric independently on the nonlinear electrodynamics theory considered.

6.5.4 Bardeen black hole

As an application of the above example, let us consider one of the first singularity free black hole proposed by Bardeen [137]. This metric was shown to be an exact solution of Einstein equations with a nonlinear magnetic monopole [138]. It is described by the metric

$$A(r) = B(r) = 1 - \frac{2Mr^2}{(r^2+q^2)^{3/2}} \tag{6.162}$$

and $C(r) = r^2$. In order to study black hole solutions, we consider $M > 0$. Because we have focused on an electric source, we know from the FP duality[13], that a solution can be

[12] Our potential V can be written as $V = PWP^{-1}$ with W the Moncrief potential and $P = \begin{pmatrix} 0 & 1 \\ -1 & 0 \end{pmatrix}$, therefore they are similar.

[13] The Lagrangian $\mathcal{L}(F)$ can also be written in terms of the field $P = P_{\mu\nu}P^{\mu\nu}/4$ where $P_{\mu\nu} = F_{\mu\nu}\mathcal{L}_{,F}$ [139]. This is the so-called P framework. The equations in the P framework are equivalent to the equations in the F framework by performing a transformation while the metric remains unchanged [140]. Therefore, the FP duality connects theories with different Lagrangians but similar metric. A purely magnetic solution

generated by two different Lagrangians, where one theory contains only a magnetic field and another only an electric field. It is easy to find that a Lagrangian with an electric field, generating the Bardeen spacetime, is

$$\bar{A}_0(r) = \alpha \frac{r^5}{(r^2+q^2)^{5/2}}\,, \tag{6.163}$$

$$\mathcal{L}(r) = \frac{3Mq^2(3r^2-2q^2)}{2(r^2+q^2)^{7/2}}\,, \tag{6.164}$$

where α is a constant. From this, we could obtain $\mathcal{L}(F)$, but because the expression is numerical and not analytical, we will just mention that such Lagrangian exists. We can see from the electric potential, that we will not recover the Coulomb potential at large distances, which could also be seen from the metric that reduces to

$$A(r) = 1 - 2M/r + 3Mq^2/r^3\,, \qquad r \to \infty.$$

Therefore, even at large distances, the black hole is not similar to Reissner-Nordström spacetime. Interestingly, long distance quantum corrections to the Schwarzschild black hole go like $1/r^3$ [141, 142] which is similar to the Bardeen solution if we identify q^2 to $62\hbar/45\pi$.

Looking now to the stability of this black hole, we found that odd-parity perturbations are stable if $f_{2,F} = 3M/\alpha r^2$ is positive which implies the trivially satisfied condition $M\alpha > 0$.

Considering finally the even parity sector, we have analysed the stability numerically from the potential (6.159, 6.160, 6.161). For that purpose, we redefined the variables $r \to \bar{r}q$, $M \to \bar{M}q$ such that $\bar{M}$ remains the only free parameter. Considering the normalized mass in the range $0 < \bar{M} < 10$ and for $\ell = 2, ..., 10$, we found that the potential is definite positive and therefore the black hole is stable in this range.

6.5.5 Hayward black hole

An other interesting singular free black hole is defined as [143]

$$A(r) = B(r) = 1 - \frac{2Mr^2}{r^3 + 2Ml^2}\,. \tag{6.165}$$

This black hole is known as the Hayward black hole. It reproduces the Schwarzschild spacetime at large distances with corrections $\mathcal{O}(1/r^4)$ which are not similar to loop quantum contribution as noticed in the Bardeen solution. But similarly, the black hole is regular at

in the P framework will correspond to a purely electric solution in the F framework or vice versa. This transformation exists [130] if $\mathcal{L}_{,F}(\mathcal{L}_{,F} + 2F\mathcal{L}_{,FF}) \neq 0$.

the origin and has a de Sitter core, $A \simeq 1 - r^2/l^2$.

As in the previous case, the solution can be derived from various theories. We will consider nonlinear electrodynamics. It is easy to find that a Lagrangian exists, numerically, which gives this metric

$$\bar{A}_0(r) = -\alpha \frac{6l^2M^2(r^3 + Ml^2)}{(r^3 + 2Ml^2)^2}\,, \tag{6.166}$$

$$\mathcal{L}(r) = \frac{12M^2l^2(r^3 - Ml^2)}{(r^3 + 2Ml^2)^3}\,, \tag{6.167}$$

where α is a constant.

Within this theory, we would like to know if the black hole is stable. The odd-parity sector is trivially stable because $f_{2,F} = (r^3 + 2Ml^2)^3/18\alpha^2M^2l^2r^7 > 0$.

As for the Bardeen black hole, the even-parity perturbations will be studied numerically. Interestingly, this spacetime is invariant under a scaling transformation [144]. Therefore, we can renormalize our variables, $r \to l\sqrt{M}r$, $M \to M^{3/2}l$, which reduces the solution to only one parameter. We have checked the stability for $0 < (M/l)^{2/3} \leq 10$ and $2 \leq l \leq 10$. We found that the potential is definite positive and therefore the black hole is stable in this range.

6.5.6 Scalar-tensor theory

After studying spacetimes with the presence of an electric charge, we will consider another particular case of our general analysis for which only the scalar field is present. Let us take

$$\mathcal{S} = \int \mathrm{d}^4x\sqrt{-g}\Big[f_1(\phi)\frac{R}{2} + f_2(\phi, X)\Big] \tag{6.168}$$

$$= \int \mathrm{d}^4x\sqrt{-g}\Big[F(\phi)\frac{R}{2} + K(\phi, X)\Big]\,, \tag{6.169}$$

where in the second line, we have redefined the functions of the Lagrangian in a more standard notation used in the framework of k-*essence* theory (see Chapter 4).

As in the previous cases, the odd-parity sector is trivial. Indeed, we only need to fulfill the condition $F(\phi) > 0$ outside the black hole. For example, any theory expressed in the string frame [145] where $F(\phi) = e^{-\phi}$ would be trivially stable under odd-parity perturbations. A generic sufficient condition for the stability of even-parity perturbations has not been found in closed form but we will work out particular examples. This analysis can be easily generalized to any BH within this class of theories with the MATHEMATICA® notebook file provided in [133].

Among all these theories, it was shown that Horndeski theories and Lovelock gravity are weakly hyperbolic, but might fail to be strongly hyperbolic [146, 94]. The only sub-class which is strongly hyperbolic are the K-field models defined in Eq. (6.169). Unfortunately, for most of these models, a non trivial black hole seems to be impossible. For example, it was shown that if the model is shift invariant, i.e. $f_1 = 1$ and $f_2 = f_2(X)$ (as in Chapter 4), the only solution is the Schwarzschild one [147]. For that reason, it was assumed that the area of a constant r sphere should neither be infinite or zero at the horizon. Violating this condition, the so-called cold black holes (with zero surface gravity) can be constructed [148]. Thus, we have to violate the null energy condition by choosing $f_1 = 1$ and $f_2 = -X$, where the scalar field has the "wrong" sign for the kinetic term. The solution is

$$\mathrm{d}s^2 = -\left(1 - \frac{2k}{r}\right)^{m/k} \mathrm{d}t^2 + \left(1 - \frac{2k}{r}\right)^{-m/k} \mathrm{d}r^2 + r^2 \left(1 - \frac{2k}{r}\right)^{1-m/k} \mathrm{d}\Omega^2 \tag{6.170}$$

with

$$\phi(r) = -\frac{\sqrt{\frac{m^2}{k^2} - 1}}{\sqrt{2}} \ln\left(1 - \frac{2k}{r}\right), \tag{6.171}$$

where m is the ADM mass and k is related to the scalar charge. Indeed, we have at infinity $\phi \simeq \frac{\sqrt{2m^2 - 2k^2}}{r}$.

Even if very interesting, this black hole violates the no-ghost condition (6.94). In fact, it is easy to show that $\det(K) < 0$. Maybe a stable black hole could be constructed in that framework by using a non-linear kinetic term.

Another way to escape the no-go theorem previously mentioned is to break the shift invariance and assume a non-vanishing potential. We know that important no-hair theorems restrict the existence of non-trivial black holes, see e.g. [149, 150, 151, 152].

6.5.7 Bocharova-Bronnikov-Melnikov-Bekenstein (BBMB) solution

Our following example is a scalar-tensor theory with a conformally coupled scalar field given by the action (6.1) with functions

$$f_1 = M_{Pl}^2 - \frac{\phi^2}{6}, \qquad f_2 = X. \tag{6.172}$$

Assuming a spherically symmetric background, the line element that satisfies the background equations is

$$\mathrm{d}s^2 = -\left(1-\frac{M}{r}\right)^2 \mathrm{d}t^2 + \frac{\mathrm{d}r^2}{(1-M/r)^2} + r^2\mathrm{d}\Omega^2, \tag{6.173}$$

$$\phi = \pm\frac{\sqrt{6}M_{Pl}M}{r-M}, \tag{6.174}$$

where M is the mass of the black hole. This solution is known as the BBMB black hole and has been found by Bocharova, Bronnikov, and Melnikov [153] and independently by Bekenstein [154]. This is a BH solution with a secondary scalar hair. As we can see, the line element has the same form as the extremal Reissner-Nordström black hole with $R_{\mu\nu} \neq 0$, but the conformal scalar hair blows up at the horizon.

Since we added only a scalar field, we analyze solely even-parity perturbations. The stability condition (6.99) reads

$$2\mathcal{P}_1 - \mathcal{F} = \frac{3M_{Pl}^2M^2r(r-2M)}{(r^2-3Mr+3M^2)^2} \tag{6.175}$$

which is positive only for $r > 2M$. Because the event horizon is located at $r = M$, there is an unstable region outside the horizon. Therefore, this solution is classically unstable. This result was found in [155, 156] for monopole perturbations, and in [131] for higher multipoles.

6.5.8 BH in Einstein-Maxwell-dilaton theory

Another interesting BH solution is obtained in the Einstein-Maxwell-dilaton (EMd) theory. The action in the Einstein frame is given by

$$S = \int d^4x\,\sqrt{-g}\left(R - 2g^{\mu\nu}\partial_\mu\phi\partial_\nu\phi - e^{-2a\phi}F_{\mu\nu}F^{\mu\nu}\right), \tag{6.176}$$

where a is the dilaton coupling constant. For $a = 0$, the theory reduces to Einstein-Maxwell theory and the BH solution is the Reissner-Nordström metric. The model appears as a low energy limit of the heterotic string theory for $a = 1$ and as the dimensionally reduced five dimensional vacuum Einstein action in the Einstein frame, for $a = \sqrt{3}$.

The static and spherically symmetric black hole solution in the case where the Maxwell

field is electric is given by [119, 120]

$$\begin{aligned} A(r) &= B(r) = \left(1-\frac{r_+}{r}\right)\left(1-\frac{r_-}{r}\right)^{\frac{1-a^2}{1+a^2}}, \\ C(r) &= r^2\left(1-\frac{r_-}{r}\right)^{\frac{2a^2}{1+a^2}}, \end{aligned} \tag{6.177}$$

where r_+ is the position of the event horizon and r_- corresponds to a curvature singularity $R_{\mu\nu\rho\sigma}R^{\mu\nu\rho\sigma} \propto (r-r_-)^{-2(1+3a^2)(1+a^2)}$ except for $a=0$ where the solution reduces to Reissner-Nordström metric. The two parameters (r_+, r_-) are related to the ADM mass M and the electric charge Q by solving [157]

$$M = \frac{r_+}{2} + \left(\frac{1-a^2}{1+a^2}\right)\frac{r_-}{2}, \qquad Q^2 = \frac{r_+ r_-}{1+a^2}\, e^{-2a\varphi_0}. \tag{6.178}$$

On the other hand, the only non-zero component of the electromagnetic four-potential A_μ and the scalar field ϕ are given by

$$\bar{A}_0(r) = -\frac{1}{r}\sqrt{\frac{r_+ r_-}{1+a^2}}, \qquad \phi(r) = \frac{a}{1+a^2}\ln\left(1-\frac{r_-}{r}\right). \tag{6.179}$$

Given the background solution, we can perform the analysis of perturbation theory. As a first step, we focus on odd-parity perturbations. The no-ghost conditions (6.39) are trivially satisfied since $f_1(\phi) = 2$ and $f_{2,F}(\phi, X, F) = 4\exp[-2a\phi(r)] > 0$. We conclude that the odd-parity perturbations are stable. From Eqs. (6.42) – (6.44), we get that the components of the potential associated with this type of perturbations are

$$\begin{aligned} \mathcal{V}_{11} &= \mathcal{V}_{22} + \frac{\mathcal{T}}{r}\left[\frac{(a^2-3)\, r_-}{1+a^2} - 3r_+\right] \\ \mathcal{V}_{12} &= \mathcal{V}_{21} = \frac{2\mathcal{T}}{r}\sqrt{\frac{(\lambda-2) r_- r_+}{a^2+1}} \\ \mathcal{V}_{22} &= \mathcal{T}\left[\lambda + \frac{r_-}{(a^2+1)^2\, r}\left(\frac{a^4(2r+r_--3r_+)}{r-r_-} + 2a^2 + \frac{a^2 r_+}{r} + \frac{4r_+}{r}\right)\right] \end{aligned}$$

where we have defined

$$\mathcal{T}(r) = \frac{A(r)}{(r-r_-)^2}\left(1-\frac{r_-}{r}\right)^{2/(a^2+1)}. \tag{6.180}$$

It can be checked that the potential matrix has constant eigenvalues; therefore, we can diagonalize this matrix to obtain a decoupled system of wave-like equations. After the

diagonalization, the potentials are

$$V_{\pm}^{\mathrm{EMd}} = \frac{\mathcal{T}}{r}\left[\lambda r + \frac{3a^4(r-r_+)r_-^2}{r(a^2+1)^2(r-r_-)} + \frac{(4-3a^2)\,r_-r_+}{(a^2+1)r} + \frac{(5a^2-3)\,r_-}{2\,(a^2+1)} - \frac{3r_+}{2} \pm \frac{1}{2}\sqrt{9r_+^2 + \frac{(a^2-3)^2\,r_-^2}{(a^2+1)^2} - \frac{2\,(7+3a^2-8\lambda)\,r_-r_+}{a^2+1}}\right]. \tag{6.181}$$

As a specific case, setting $a = 1$, we recover the potential computed in [158]. Now, we turn to the problem of even-parity perturbations. The no-ghost condition (6.99) is

$$2P_1 - f_1 = \frac{2r_-^2}{(2r-r_-)^2} > 0\,. \tag{6.182}$$

Therefore, the even-parity perturbations are well-defined. It can also be checked that all perturbations propagate at the speed of light. In order to study completely the stability of these modes, we need to compute the matrix S (6.113) in order to obtain the potential associated to these perturbations. Unfortunately, in these type of models, the integration of Eq. (6.113) is not easy and we have to rely on a numerical analysis. To this end, we integrate numerically Eq. (6.113) assuming any initial condition such that $\det(S) \neq 0$. From this we can easily obtain the potential (6.117). We found that the eigenvectors of the matrix (6.117) $-\mathbf{S}^{-1}\mathbf{K}^{-1}\mathbf{B}\mathbf{S}$ are constant and therefore the system has the same eigenvalues as the matrix $-\mathbf{K}^{-1}\mathbf{B}$. As a consequence, we do not need to calculate the matrix S, but only the eigenvalues of the matrix $-\mathbf{K}^{-1}\mathbf{B}$. Each eigenvalue will be the effective potential of one of the three perturbations.

From these effective potentials, we have calculated the QNMs using the sixth order WKB method (we will explain this numerical method in the next Chapter). We see in the Fig.(6.2), the real and imaginary part of the QNMs associated to this black hole compared to the Reissner-Nordström solution. We observe that, contrary to the Reissner-Nordström solution, the electric charge breaks the isospectrality[14]. From the numerical results, we found that $\mathrm{Im}(\omega) < 0$, for a large number of ℓ, and therefore we conclude that the black hole is linearly stable. As an example, we have represented, in Figs.(6.2,6.3), the real and imaginary parts of the QNM for $a = 1$ and $a = 0.5$ respectively. These results coincide with [158] for $a = 1$ and with [159, 160] in the case $a = 0.5$.

[14]Same spectrum of quasinormal modes for even and odd perturbations.

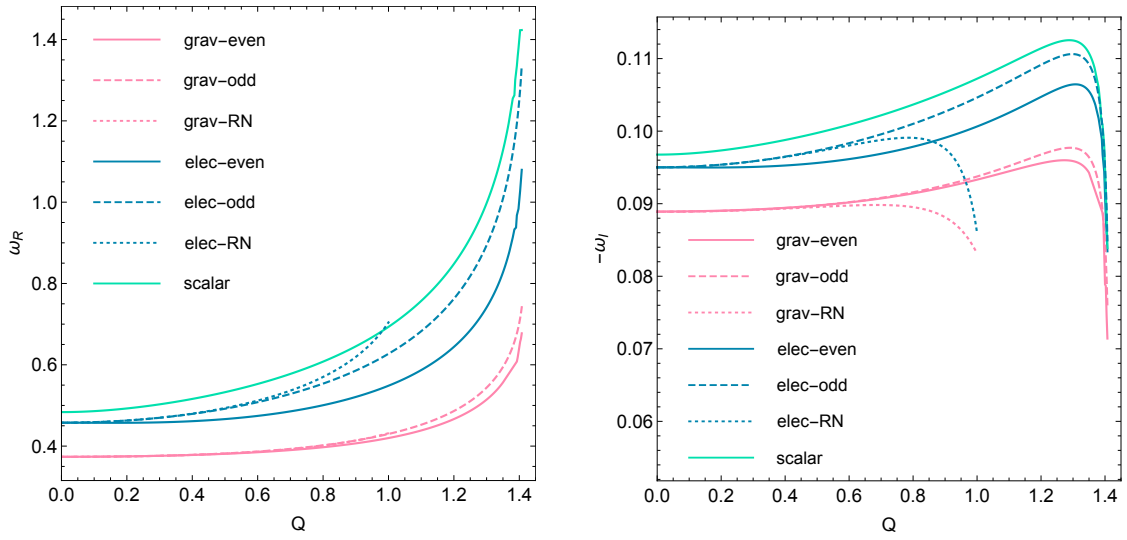

Figure 6.2: *Fundamental mode (lowest QNMs) for the EMd black hole as a function of the charge Q in units $M = 1$ and for $\ell = 2$. In pink, we have the modes associated to the gravitational sector, which reduce to the Regge-Wheeler and Zerilli potentials. In blue, we presented the QNMs associated to the electromagnetic sector and, finally, in blue we draw the modes associated to the scalar field. These perturbations are compared to the Reissner-Nordstrom black hole in dotted line. The QNMs have been calculated with a step size of* 0.0025 *for the charge.*

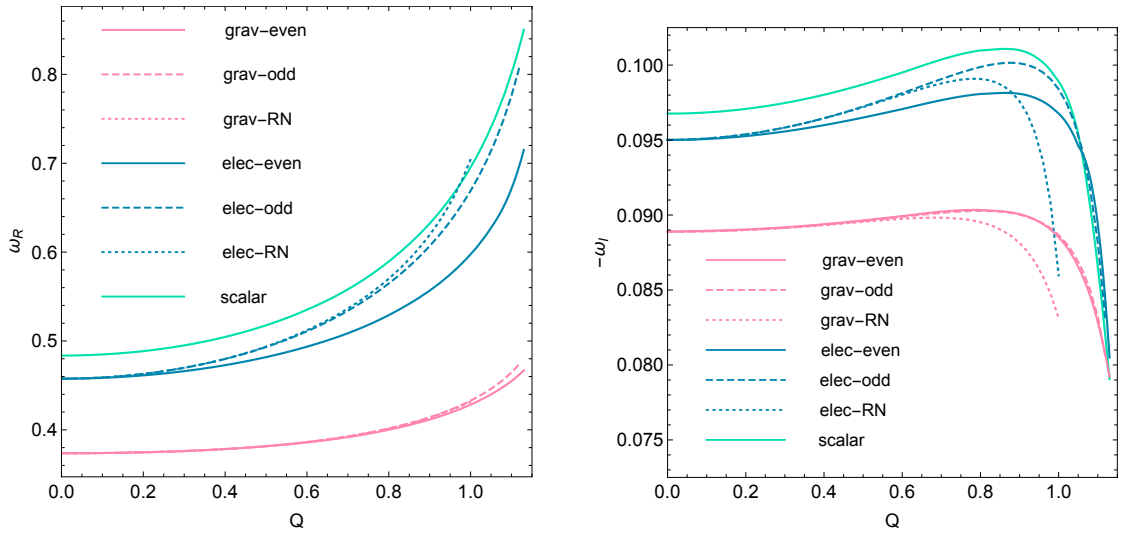

Figure 6.3: *Fundamental mode (lowest QNM), for $\ell = 2$ and $a = 0.5$, as a function of the charge Q, in units $M = 1$. In pink, we have the modes associated to the gravitational sector, which reduce to the Regge-Wheeler and Zerilli potentials. In blue, the QNMs are associated to the electromagnetic sector and finally in blue we have the mode associated to the scalar field. These perturbations are compared to the Reissner-Nordstrom black hole in dotted line. The QNMs have been calculated with a step size of* 0.0025 *for the charge.*

6.6 Discussions

We have studied the stability of static spherically symmetric black holes in generalized Einstein-Maxwell-scalar theories with an electrically charged Maxwell field. We have obtained the master equations in the odd and even parity sectors. We found that the ghost free conditions reduce to

$$f_1 > 0\,, \qquad f_{2,F} > 0\,, \qquad 3f_{1,\phi}^{\,2} + 2f_1 f_{2,X} > 0\,. \tag{6.183}$$

We found that four degrees of freedom propagate at the speed of light, while a degree of freedom associated to the scalar field could propagate faster or slower than the speed of light, as its expression is given by Eq. (6.107). From it, we also obtained a subclass of generalized Einstein-Maxwell-scalar theories where all degrees of freedom propagate at the speed of light, see Eq. (6.110). Imposing the ghost free conditions, we found that odd-parity perturbations are always stable and we obtained explicitly the effective potential matrix. Considering the even-parity sector, we derived the master equation and the procedure to calculate the effective potential matrix for a given model. We also found that assuming ghost free conditions, the perturbations are unstable if $f_{2,F} + 2\bar{F} f_{2,FF} < 0$ for models with $f_{2,XF} = 0$. Finally, we have applied this formalism for several BHs for which we could easily obtain the stability conditions and calculate the QNMs.

By using our method, we could recover all previously derived results in the literature, which guarantees the correctness of our calculations. As an application, our investigation can be used to study the QNMs of gravitational waves, electromagnetic radiation and scalar radiation. The presence of these three fields appears naturally in higher dimensional theories of gravity such as supergravity or string theory. Interestingly, we did not find any stable hairy black hole in scalar tensor theories.

Chapter 7

Pure Lovelock black hole in higher dimensions

A possibility that the spacetime may have more than four dimensions has become a trendy topic in the last decades. Gravitational theories built in dimensions other than four have a strong theoretical interest for several reasons, including the formulation of consistent string theories or understanding how field equations depend on an extra parameter, in this case, the spacetime dimension. The most simple extension of general relativity to higher dimensions is given by the Einstein-Hilbert action in d dimensions

$$\mathcal{S} = \frac{1}{\kappa}\int \mathrm{d}^d x\sqrt{-g}\, R\,. \tag{7.1}$$

It has been shown in [54] that this theory admits the Schwarzschild's vacuum solution, and it is stable under metric perturbations in all dimensions ≥ 4. In this black hole, the gravitational potential goes as $1/r^{d-3}$ with $d-3 \geq 1$ always. Therefore, as long as the potential falls faster than $1/r$, the black hole solution is stable. Using the same principles as the ones from which general relativity has been constructed, the Einstein-Hilbert action is not unique in higher dimensions. In $d > 4$, one can add new curvature terms that still preserve the following features, we expected from a theory of gravity: (a) general covariance —the Lagrangian is a scalar density constructed from the Riemann curvature, which yields a non-trivial equation of motion, (b) field equations are expressed in terms of a divergence-free symmetric rank-2 tensor, and (c) equations of motion remain second-order in the metric.

Taking into account the fact that there is no reason to discard such nonlinear in the curvature terms in the action, David Lovelock constructed the most natural generalization of Einstein's gravity in higher dimensions. The Lovelock Lagrangian [16] is a linear combination

of homogeneous polynomials in the Riemann curvature of arbitrary degree N. The Lovelock action with $N = 1$ reduces to the Einstein-Hilbert action (7.1), thus, Einstein's theory of general relativity is included as a particular case in this generalization; the polynomial with $N = 2$ is the quadratic Gauss-Bonnet (GB) term, so the Lovelock action, in that case, is a linear combination of two terms, thus it has two integrations constants. Unlike theories in which additional fundamental fields are added into the gravity sector, Lovelock theory provides a new exciting scenario to study how gravity is corrected at high energies due to the presence of higher curvature terms [161]. It has been shown in [162] that the addition of the quadratic GB term in the action is relevant to the low energy limit of string theory. This suggests that the correct theory of classical gravity is the Lovelock theory, while GR is an effective theory that arises in the low energy limit.

The general feature of the Lovelock theory is that, for $d = 2N$, equation of motion is trivial, meaning that the corresponding Einstein tensor $G_{\mu\nu}$ vanishes identically. It is kinematic for $d = 2N + 1$, implying that the corresponding Riemann is entirely given in terms of Ricci tensor and hence there can exist no non-trivial vacuum solution [163]. Gravity could have dynamics admitting non-trivial vacuum solution only in dimensions $d \geq 2N + 2$. That means, it is a quintessentially higher-dimensional generalization of gravity; i.e. the term corresponding to $N > 1$ will make a non-zero contribution to equations of motion only in dimension greater than four.

Lovelock theory admits general solutions describing static black holes [161]. Black holes are by far the most interesting solutions of gravitational theories. A natural question that arises is, can these solutions be stable in generalizations of Einstein's gravity? To show the stability of a black hole solution, as we saw in Chapter 6, a frequently used method is to apply linear perturbation theory and prove that its dynamic is governed by a positive self-adjoint operator. In that way, we guarantee that perturbations radiate and decay sufficiently fast in time. Studying the stability of a black hole with a horizon having a spherical topology, we found that metric perturbations are classified into tensor, vector, and scalar perturbations. The last two types correspond to the odd- and even-parity modes in the four-dimensional case, while tensor perturbations are new and emerge only in higher dimensions.

Following the scheme introduced in [54, 55], the stability of higher-dimensional black holes has been an active research topic in recent years. For example, tensor perturbations of Einstein-Gauss-Bonnet (EGB) gravity were studied in [164, 165]. Then, the results were generalized to third-order Lovelock in [166] and to any Lovelock order in [167]. On the other hand, the stability analysis of EGB gravity under scalar and vector perturbations has been carried out in [168], and it was later generalized to any Lovelock [169]. It was proved in

[129] that Lovelock black holes with small mass are unstable under tensor perturbations in even-dimensions and under scalar perturbations in odd-dimensions.

Recently, there has been much attention to a particular case of Lovelock gravity, the *Pure Lovelock* theory. Instead of considering the full Lovelock polynomial, only the term proportional to the curvature of order N has been taken into account. As an example, pure Gauss-Bonnet gravity has only the Gauss-Bonnet term without the Einstein-Hilbert term. Pure Lovelock gravity has several interesting and remarkable features; see e.g. [170] for degrees of freedom count. One of the most attractive feature of these theories is that their black hole solutions are indistinguishable from the ones appearing in General Relativity. As we will show later, in particular dimensions, we can always recover the 4D Schwarzschild solution, even when $d > 4$. Based on this remarkable result, we will study the stability of these particular higher dimensional Schwarzschild black holes, to see whether they share stability features with their 4D cousins..

For this purpose, in section 7.1, we review the Lovelock theory and then restrict the action to Pure Lovelock Lagrangian. In section 7.2, we apply perturbation theory to this particular solution and determine the stability of these black holes. We also generalize the formalism of linear perturbation theory given in 6.2 to a higher-dimensional spacetime. To go further in our results, we apply numerical techniques to get the spectrum, the quasinormal-mode frequencies, of these black holes. The three most common numerical techniques found in the literature are described in section 7.5. In section 7.6, we obtain the frequencies for scalar, vector and tensor perturbations for pure Gauss-Bonnet gravity in $d = 7$, before generalizing them to any critical dimension in section 7.7.

7.1 Lovelock Black Holes

Lovelock theory of gravity [16] is the generalization of Einstein's theory of general relativity in higher dimensions. The Lagrangian of this theory is constructed with a single symmetric metric tensor field g endowed with a Levi-Civita connection, which gives a divergence-free geometric operator and leads to equations of motion that do not contain derivatives of the metric tensor of order higher than two. These two properties are fundamental because they are related to the conservation of the energy-momentum tensor and the absence of any ghost modes in the theory, avoiding the well-known Ostrogradski instability [40, 41].

The corresponding action in d dimensions is

$$\mathcal{S}[g] = \int d^d x \sum_{k=0}^{n} c_k \mathcal{L}_k \tag{7.2}$$

where $\mathcal{L}_k$ is the dimensionally continued Euler density of order k in the curvature

$$\mathcal{L}_k \equiv \frac{1}{2^k}\sqrt{-g}\,\delta^{\mu_1\nu_1\cdots\mu_k\nu_k}_{\alpha_1\beta_1\cdots\alpha_k\beta_k}\,R_{\mu_1\nu_1}{}^{\alpha_1\beta_1}\cdots R_{\mu_k\nu_k}{}^{\alpha_k\beta_k}\,, \tag{7.3}$$

$R_{\mu\nu}{}^{\alpha\beta}$ is the Riemann tensor and $\delta^{\mu_1\cdots\mu_p}_{\alpha_1\cdots\alpha_p}$ is the generalized totally antisymmetric Kronecker delta of order p ($0 \leq p \leq d$). In (7.2) we defined the maximal order of the Lovelock polynomial, $n \equiv [(d-1)/2]$, where $[z]$ denotes the greatest integer function satisfying $[z] \leq z$, and c_k are arbitrary constants. As examples, $\mathcal{L}_0$ represents the identity, so c_0 is just the cosmological constant. $\mathcal{L}_1$ gives the usual scalar curvature term, while $\mathcal{L}_2$ is just the Gauss-Bonnet term. Any term of order greater than N in the action (7.2) is either zero or at best a topological invariant and hence it does not contribute to the classical field equations.

It has been shown in [171] that, for particular values of the constants c_k, a degeneracy can appear in the space of solutions when the field equations do not entirely determine the metric. This problem can be avoided by a suitable choice of the coefficients c_k. The simplest example choice corresponds to the Einstein-Hilbert term alone with the cosmological constant (Λ), which has a unique Minkowski, de Sitter, or anti-de Sitter vacuum depending on the sign of Λ. As showed in [172], another way to fix the coefficients is to restrict the theory to have a unique degenerate vacuum, leading to a family of gravity theories [173]. Requiring that Lovelock gravity has the maximum number of degrees of freedom, in odd dimensions the Lovelock Lagrangian can be written as a Chern-Simons form [174]; while, in even dimensions, the Lagrangian can be written as a Born-Infeld gravity [175]. In those theories all couplings are expressed only in terms of the gravitational interaction and the cosmological constant.

Another way to fix the constants c_k is to demand that there is a non-degenerate vacuum [176]. Such condition leads to Pure Lovelock theory [53] which consists in the particular case where the polynomial reduces to a monomial of order N, thus the action is simplified to

$$\mathcal{S}_{PL}[g] = \int d^d x\, c_N \mathcal{L}_N\,. \tag{7.4}$$

Pure Lovelock gravity has been scarcely discussed in the literature. Their black hole solutions are asymptotically indistinguishable from the ones appearing in GR [172] even though the Einstein-Hilbert term is not present in the action. The stability of black holes in this theory has been analyzed in [177]. Pure Lovelock gravity is also singled out by another property; it admits bound orbits around a static object [178]. In Einstein gravity, the gravitational potential goes as $1/r^{d-3}$ in d non-compactified spacetime dimensions, and bound orbits could exist only if $d-3<2$, the condition required for centrifugal potential to be able to counter-balance gravitational pull. Thus, for Einstein gravity, bound orbits can

exist only in $d = 4$. However, the situation changes in Pure Lovelock gravity because for it the potential goes as $1/r^{\alpha}$ where $\alpha = (d - 2N - 1)/N$ [172]. Clearly, for Pure Lovelock gravity in dimensions $d \geq 2N + 2$, we have $\alpha < 2$ and bound orbits always exist.

From the above discussion, we observe another exciting property of pure Lovelock gravity. Namely, its potential has the same fall off as four-dimensional GR, $1/r$, in $d = 3N + 1$ [179]. In all $d > 3N + 1$, it would fall sharper than $1/r$. Therefore, as stated in [179], from a purely gravitational standpoint, there is no way to distinguish whether solar system observations correspond to four-dimensional Einstein or $(3N+1)-$dimensional pure $N-$th order Lovelock gravity. Furthermore, since we have the same inverse square law for the potential in both theories, it is expected that the cosmological dynamics remains the same. Focusing on this property, the natural question that arises is whether pure Lovelock black hole in $d = 3N + 1$ are stable? This is the question we wish to address in this investigation, thus in the rest of the chapter we will focus on Pure Lovelock theory.

A variation of the action (7.4) with respect to the metric leads to the equations of motion

$$\mathcal{G}_A^B = \delta^{B\mu_1\nu_1\cdots\mu_N\nu_N}_{A\alpha_1\beta_1\cdots\alpha_N\beta_N} R_{\mu_1\nu_1}{}^{\alpha_1\beta_1} \cdots R_{\mu_N\nu_N}{}^{\alpha_N\beta_N} = 0\,. \tag{7.5}$$

As shown in [171, 180], there exist static spherically symmetric solutions to this equation in any d, given by

$$\mathrm{d}s^2 = -f(r)dt^2 + \frac{dr^2}{f(r)} + r^2 d\Omega_{d-2}^2 \tag{7.6}$$

where $d\Omega_{d-2}^2 = \gamma_{ab}\mathrm{d}x^a\mathrm{d}x^b$ is the line element of the $(d-2)-$dimensional unit sphere. Using this metric ansatz, we can compute the Riemann tensor components

$$\begin{aligned} R_{tr}{}^{tr} &= -\frac{f''}{2}\,, \quad R_{ta}{}^{tb} = R_{ra}{}^{rb} = -\frac{f'}{2r}\delta_a{}^b\,, \\ R_{ab}{}^{cd} &= \left(\frac{1-f}{r^2}\right)\delta_{ab}^{cd} \end{aligned} \tag{7.7}$$

where indices $(a, b, \dots)$ denote angular coordinates. Substituting (7.7) into (7.5) we get

$$f(r) = 1 - \left(\frac{r_s}{r}\right)^{(d-2N-1)/N} \tag{7.8}$$

where r_s is the location of the event horizon. Notice that the critical dimension $d = 3N + 1$ gives the Schwarzschild solution, but the action does not correspond to GR. In the rest of the chapter, we will consider, for each pure Lovelock of order N, the critical dimension

corresponding to $d = 3N + 1$, which describes Schwarzschild spacetime at any order N.

7.2 Perturbations and stability

Studying how a BH reacts to external perturbations has been the starting point to analyze the classical stability of a given solution. Through this approach, we can constrain the parameters of a given theory to a valid range. As we saw in Chapter 6, the study of perturbation theory in general relativity has its root in the seminal work done by Regge and Wheeler [47] for axial modes, and subsequently by Zerilli [48] for polar modes. This perturbative analyses of black hole spacetimes have provided valuable tools for investigating astrophysical problems, such as gravitational wave emission from gravitational collapse, and more fundamental problems, such as the stability and uniqueness of black holes.

The perturbation analysis in four dimensions relies on the properties of a spherically symmetry spacetime; hence this formalism can be extended to other theories. The extension of the classical stability of higher-dimensional black holes has been intensively studied by Kodama and Ishibashi [54, 55]. They showed that in four or more spacetime dimensions, the Einstein equations for gravitational perturbations of maximally symmetric vacuum black holes can be reduced to a single second-order wave equation in a two-dimensional static spacetime, irrespective of the mode of perturbations.

Aimed to this interesting conclusion, we analyzed the stability of higher-dimensional black holes given by Pure Lovelock gravity in this section. We consider a perturbation ($h_{\mu\nu}$) to the previous background solution (7.6) described by the metric

$$g_{\mu\nu} = \bar{g}_{\mu\nu} + h_{\mu\nu}\,.$$

In the higher-dimensional case, the role of the two-sphere is played by an $n-$sphere. According to how they transform under $SO(d-2,1)$ [181], the perturbations $h_{\mu\nu}$ can be decomposed into scalar and vector perturbations which correspond to the axial and polar modes in the four-dimensional case. However, a new type of perturbations appears in dimensions larger than four, known as tensor perturbations. In order to verify the stability of higher-dimensional Schwarzschild black holes (7.8), we have to investigate their stability with respect to all types of perturbations. Since the Lagrangian is invariant under parity transformations, perturbations are decoupled from each other at the level of the equations; thus, we can analyze each of them separately.

7.2.1 Scalar perturbations

For scalar perturbations, instead of working with the Uniform curvature gauge as we did in section 6.4, we use the metric in the Zerilli gauge (spatially diagonal gauge) that takes the following form

$$h_{\mu\nu} = \begin{pmatrix} fH_0 & H_1 & \mathbf{0} \\ H_1 & H_2/f & \mathbf{0} \\ \mathbf{0} & \mathbf{0} & r^2 K\gamma_{ab} \end{pmatrix} \tag{7.9}$$

where γ_{ab} is the metric of the $n-$sphere and it depends only on the angular coordinates. As done in section 6.2, we decompose each perturbation function into higher-dimensional scalar harmonics which satisfy

$$\nabla_a \nabla^a Y = -\gamma_s Y \qquad \text{with} \qquad \gamma_s = \ell(\ell + d - 3) \tag{7.10}$$

where ∇_a is the covariant derivative associated to the metric γ_{ab}. Working at the level of the equations of motion, as shown in [169, 129], all perturbations (H_0, H_1, H_2, K) can be expressed in terms of a single master function ψ solution of the equation

$$\frac{d^2\psi}{dr_*^2} + (\omega^2 - V_s(r))\psi = 0 \tag{7.11}$$

where r_* is the tortoise coordinate, ω comes from the fact that we have assumed that each perturbation function has a time dependence of the form $H(t, r) \to e^{-i\omega t}H(r)$ and $V_s(r)$ is an effective potential for scalar perturbation

$$V_s(r) = f(r)\frac{2\lambda^2(\lambda+1)r^3 + 6\lambda^2 M r^2 + 18\lambda M^2 r + 18M^3}{r^3(\lambda r + 3M)^2} \tag{7.12}$$

which, we notice, has exactly the same form as the Zerilli potential (6.142), defining

$$\lambda = \frac{(\ell + d - 2)(\ell - 1)}{d - 2}\,. \tag{7.13}$$

Since this potential is completely positive for $r > r_s$ (see Fig. 7.1a), we can easily conclude that higher-dimensional Schwarzschild BH (7.8) is stable relative to scalar perturbations. In the literature, it is common to call equation (7.11) as the master equation for perturbations.

7.2.2 Vector perturbations

A general vector perturbation is given by

$$h_{ij} = 0\,, \qquad h_{ia} = r f_i V_a\,, \qquad h_{ab} = 2r^2 H_T V_{ab} \tag{7.14}$$

where f_i and H_T are functions of (r,t), V_a is a divergence-free vector harmonic field and V_{ab} is a symmetric harmonic tensor; both defined on the $n-$sphere. For higher multipoles, we can always choose a gauge where $H_T = 0$. This generalizes the Regge-Wheeler gauge for odd perturbations to higher dimensions, which simplifies the metric perturbation to

$$h_{\mu\nu} = \begin{pmatrix} 0 & 0 & \mathbf{v}_a \\ 0 & 0 & \mathbf{w}_a \\ \mathbf{v}_a & \mathbf{w}_a & \mathbf{0} \end{pmatrix} \tag{7.15}$$

with $\bar{\nabla}_a v^a = \bar{\nabla}_a w^a = 0$. Each perturbation can be decomposed in terms of vector harmonics which satisfy the equation

$$\bar{\nabla}_a \bar{\nabla}^a Y_i = -\gamma_v Y_i \qquad \text{with} \qquad \gamma_v = \ell(\ell + d - 3) - 1\,. \tag{7.16}$$

As for scalar perturbations, we can reduce the problem to a single function ψ solution of

$$\frac{d^2\psi}{dr_*^2} + (\omega^2 - V_v(r))\psi = 0 \tag{7.17}$$

with

$$V_v = f(r)\Big[\frac{(\ell + d - 4)(\ell + 1)}{(d-3)r^2} - \frac{6M}{r^3}\Big] \tag{7.18}$$

which is also a generalization of the Regge-Wheeler equation (6.141) to any dimension. Therefore we can conclude that vector perturbations decay with time in any $d \geq 4$, because $V_v(r) > 0$ for $r > r_s$, see Fig. 7.1b.

7.2.3 Tensor perturbations

Finally, tensor perturbations around the solution (7.6) are characterized by

$$h_{\mu\nu} = \begin{pmatrix} \mathbf{0} & \mathbf{0} \\ \mathbf{0} & r^2\phi(t,r)h_{ab} \end{pmatrix} \tag{7.19}$$

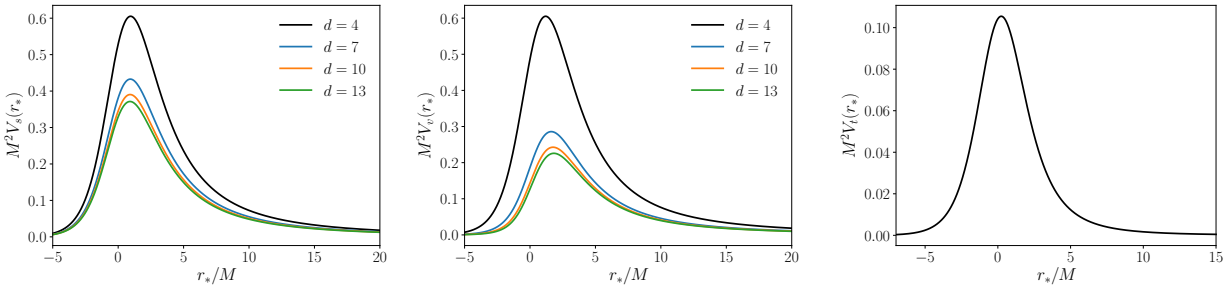

(a) *Scalar potential for* $\ell = 2$ **(b)** *Vector potential for* $\ell = 2$ **(c)** *Tensor potential for any* d *and* ℓ

Figure 7.1: *Form of the potential perturbations for various dimensions as a function of tortoise coordinates* r_**. The radial coordinate* r *is measured in units of* GM/c^2*.*

where h_{ab} is the traceless, transverse tensor harmonics solution of

$$\bar{\nabla}_c\bar{\nabla}^c h_{ab} = -\gamma_t h_{ab} \qquad \text{with} \qquad \gamma_t = \ell(\ell + d - 3) - 2\,, \tag{7.20}$$

and $\phi(t, r)$ represents the dynamical degrees of freedom. From the mathematical point of view, this is the most simple perturbation. Similarly, we can define a new function ψ related to the perturbation ϕ, which is a solution of the master equation

$$\frac{d^2\psi}{dr_*^2} + (\omega^2 - V_t(r))\psi = 0 \tag{7.21}$$

with

$$V_t = f(r)\frac{2M}{r^3}\,. \tag{7.22}$$

This is a new perturbation inexistent in four dimensions. This perturbation is independent of the angular momentum ℓ, there is no angular dependence. These perturbations are also stable because $V_t(r) > 0$ for $r > r_s$, see Fig. 7.1c.

Therefore, we have found that **for any critical dimension,** $d = 3N+1$**, the Schwarzschild solution is always stable**.

7.3 Isospectrality

In the previous subsection, we studied the stability of the Schwarzschild black hole in the critical dimensions from an analytical point of view. As we will see in the next section, another way of exploring this problem is to find the corresponding frequencies ω using numerical techniques. As we saw, all perturbations reduce to a master equation, which can be

written in the form

$$\left[-\frac{d^2}{dr_*^2}+V(r)\right]\psi=\omega^2\psi\,. \tag{7.23}$$

This, the equation is reduced to an eigenvalue problem, where the wavefunction ψ is the eigenvector and ω the eigenvalue of the corresponding operator. In general, any value of ω can solve the master equation. But, when physically motivated boundary conditions at the horizon and infinity are imposed, only few discrete complex values of ω can solve equation (7.23). These particular solutions are called quasi-normal mode (QNM) frequencies.

In four dimensions, the scalar and vector potentials are quite different for the Schwarzschild solution, but the QNM frequencies are the same. This is known as Isospectral property. It is a significant result specific to Schwarzschild black hole and does not hold for neutron stars or other gravitational theories. The proof of this unexpected fact can be found in [49]. The underlying reason is that a differential transformation relates scalar and vector perturbations, and both potentials emerge from a single potential W

$$W=\frac{2M}{r^2}-\frac{3+2c}{3r}+\frac{c(3+2c)}{3(3M+cr)}-\frac{c(c+1)}{3M} \tag{7.24}$$

$$\beta=-\frac{c^2(c+1)^2}{9M^2} \tag{7.25}$$

$$c=\frac{(l+2)(l-1)}{2} \tag{7.26}$$

Using this, the vector and scalar potential for the Schwarzschild black hole in 4 dimensions can be obtained as

$$V_s(r)=W^2-f(r)\frac{\mathrm{d}W}{\mathrm{d}r}+\beta \tag{7.27}$$

$$V_v(r)=W^2+f(r)\frac{\mathrm{d}W}{\mathrm{d}r}+\beta\,. \tag{7.28}$$

If ψ_v is an eigenfunction of the wavelike equation (7.17), then the eigenfunction for the potential V_s is given by

$$\psi_s\propto\left(W-f(r)\frac{\mathrm{d}}{\mathrm{d}r}\right)\psi_v \tag{7.29}$$

and it corresponds to the same eigenvalue ω. Therefore, the quasinormal spectrum is the same for both kinds of perturbations.

Returning to our case of Schwarzschild-type black hole in higher dimensions, we found an almost isospectral behavior. All potentials can be derived from the same form of W (7.24)

and the potentials can be obtained in the following way

$$V_s(r) = W^2 - f(r)\frac{\mathrm{d}W}{\mathrm{d}r} + \beta\,, \tag{7.30}$$

$$V_v(r) = W^2 + f(r)\frac{\mathrm{d}W}{\mathrm{d}r} + \beta\,, \tag{7.31}$$

$$V_t(r) = W^2 - f(r)\frac{\mathrm{d}W}{\mathrm{d}r} + \beta\,, \tag{7.32}$$

but the spectrum of each operator is different because the constant c differs for each type of perturbations, namely

$$\begin{aligned} c &= \frac{(\ell+d-2)(\ell-1)}{d-2}\,, && \text{for scalar perturbations} \\ c &= \frac{(\ell+d-4)(\ell+1)}{2(d-3)} - 1\,, && \text{for vector perturbations} \\ c &= 0\,, && \text{for tensor perturbations} \end{aligned}$$

Strictly speaking, the potentials are not obtained from the same potential W, because c is different. In $d = 4$, tensor modes do not exist and c takes the same value for scalar and vector perturbations. We, therefore, recover the standard result. In any other critical dimension, the spectrum will be different.

7.4 Quasinormal modes

As we have shown previously, to get Eqs. (7.23), we assumed a harmonic time dependence for each perturbation variable of the form

$$\Psi(t,r) = \sum_n e^{-i\omega_n t}\psi_n(r)\,. \tag{7.33}$$

Analyzing this equation from the numerical point of view, we get important conclusions about how a BH reacts under small perturbations. If it admits solutions whose amplitudes grow in time, then the black hole is unstable; otherwise, it is stable, at least under the assumptions made in the analysis.

To get solutions of equation (7.23) we must assign boundary conditions. In general, there are various possible ways of choosing boundary conditions of a second-order differential equation defined in the range $r_* \in (-\infty, \infty)$, and the appropriate choice depends on the physics of the problem. Considering an asymptotically flat or dS spacetime, the choice of the boundary conditions are ingoing near the horizon ($r_* = -\infty$) and outgoing at infinity or

at the cosmological horizon ($r_* = +\infty$). Mathematically[1]

$$\begin{aligned} \psi_n(r_*) &\propto e^{-i\omega_n r_*}\,, \qquad \text{when } r_* = -\infty \qquad \text{and} \\ \psi_n(r_*) &\propto e^{+i\omega_n r_*}\,, \qquad \text{when } r_* = +\infty\,. \end{aligned} \tag{7.34}$$

Ingoing at the horizon means that there is no signal which comes from the black hole. Equivalently, we should not have a wave coming from a source at infinity. As proved in [182], assumption of these boundary conditions selects discrete complex values of ω

$$\omega_{QNM} = \omega_R + i\omega_I$$

called Quasinormal frequencies. The solutions constructed from them are the Quasinormal modes (QNM), see [183] for a complete review and references therein. The imaginary part of ω_{QNM} comes from the fact that Eqs. (7.23) does not admit stationary solutions since the spacetime is unbounded and energy is radiated away to infinity. QNMs were first pointed out by Vishveshwara [50] in calculations of the scattering of gravitational waves by a Schwarzschild black hole. The study of these discrete frequencies has been investigated in a wide range of solutions employing the linear analysis, in which the fields are treated as a perturbation in the single black hole spacetime (as we did in section 7.2 and in Chapter 6), but also on fully numerical simulations of black hole-black hole collision processes, and stellar collapse. The most exciting conclusion is that the frequency and damping of these oscillations depend only on the parameters characterizing the black hole. They are entirely independent of the particular initial configuration that caused the excitation of such vibrations.

Boundary conditions (7.34) imply that an initial BH perturbation decays and disappears into gravitational radiation at infinity or approaching the horizon; this means that the perturbation amplitude must eventually go to zero at each fixed point in the space to ensure the stability of the solution. Thus, ω_{QNM} must have a negative imaginary part, $\omega_I < 0$. Perturbations with imaginary frequencies that grow exponentially with time are physically unacceptable.

This conclusion can be derived in the following way. Let us multiply the equation (7.23) by $\bar{\psi}_n$ —the complex conjugate of ψ_n— and integrate over the tortoise coordinate. We obtain after an integration by parts

$$-\bar{\psi}_n \frac{d\psi_n}{dr^*}\Big|_{-\infty}^{+\infty} + \int_{\mathbb{R}} \mathrm{d}r^* \left[\left| \frac{d\psi_n}{dr^*} \right|^2 + V|\psi_n|^2 \right] = \omega_n^2 A^2\,, \tag{7.35}$$

[1]For an AdS spacetime, the condition at the horizon is the same but the Dirichlet one at infinity.

where $A^2 = \int_{\mathbb{R}} \mathrm{d}r^* |\psi_n|^2 > 0$. Using boundary conditions (7.34), we have

$$-\bar{\psi}_n \frac{d\psi_n}{dr^*}\Big|_{-\infty}^{+\infty} = -i\omega_n B^2 \,, \tag{7.36}$$

where $B^2 = |\psi_n(+\infty)|^2 + |\psi_n(-\infty)|^2$ is always a real positive number. Therefore, Eq. (7.35) becomes

$$\int_{\mathbb{R}} \mathrm{d}r^* \Big[\Big| \frac{d\psi_n}{dr^*} \Big|^2 + V|\psi_n|^2 \Big] = \omega_n^2 A^2 + i\omega_n B^2 \,. \tag{7.37}$$

The imaginary part of this equation reads

$$\mathrm{Re}\,(\omega_n)\Big(2\,\mathrm{Im}\,(\omega_n)A^2 + B^2\Big) = 0 \,. \tag{7.38}$$

In general, this equation has non-trivial solution if $\mathrm{Im}(\omega_n) < 0$; therefore, perturbations decay with time. On the other hand, when $\mathrm{Re}(\omega) = 0$, we conclude that growing modes, which give unstable solutions, do not oscillate. Now, the real part of (7.37) reads

$$\int_{\mathbb{R}} \mathrm{d}r^* \Big[\Big| \frac{d\psi_n}{dr^*} \Big|^2 + V|\psi_n|^2 \Big] = (\mathrm{Re}\,(\omega_n)^2 - \mathrm{Im}\,(\omega_n)^2)A^2 - \mathrm{Im}\,(\omega_n)B^2 \,. \tag{7.39}$$

For growing modes, $\mathrm{Im}(\omega) > 0$ and $\mathrm{Re}(\omega) = 0$, the right hand side of the above relation is negative. Thus, we obtain unstable solutions if the left-hand side of Eq. (7.39) is negative, and therefore this condition can be fulfilled only if the potential in Eq. (7.39) is negative. On the contrary, a stable of the solution is obtained if the potential is positive. To prove the positivity of the potential, we can use the $S-$deformation technique showed in section 6.3.2.

With the previous analysis, we have shown that the stability of a solution can be analytically demonstrated by the positivity of the potential or numerically, showing that perturbations decay in time. It should be noted that both approaches are equivalent.

7.5 Numerical Techniques to compute QNM

In section (7.2), we showed that Schwarzschild BHs in critical dimensions $d = 3N + 1$ are stable under scalar, vector, and tensor perturbations using the analytical procedure. However, using the fact that QNM frequencies decay with time, $\omega_I < 0$, we can prove the stability of a solution from the numerical point of view. In general, it is possible to prove stability analytically only of some relatively simple solutions of the Einstein equations. That is why the numerical test is essential for the study of black holes. In addition, as we will see,

these numerical techniques allow us to obtain more exciting conclusions.

In what follows, we will briefly describe three numerical methods to determine the quasinormal mode frequencies, also known as the spectrum of the BH. These are the three widely used methods found in the literature.

7.5.1 WKB method

The WKB (Wentzel, Kramers and Brillouin) method is an approximate method to solve linear differential equations. The motivation to apply this numerical procedure is the similarity between the master equation of black hole perturbation theory and the time-independent Schrödinger equation for a potential barrier. This method is widely applied to compute quasinormal frequencies since it provides good accuracy and easy numerical implementation. To review this method, let us rewrite the master equation (7.23) in the following form

$$\frac{d^2\Psi}{dx^2} + Q(x)\Psi = 0\,, \qquad\qquad Q(x) = \omega^2 - V(x) \tag{7.40}$$

where x is the tortoise coordinates r_*, ω corresponds to the quasinormal mode frequency and $V(x)$ is the radial potential that takes constant values at $x = \pm\infty$, and has a maximum at $x = x_0$. Now, the key feature of this method consists in approximating the solution in a single exponential power series of the type

$$\Psi(x) \approx \exp\left[\frac{1}{\epsilon}\sum_{n=0}^{\infty}\epsilon^n S_n(x)\right]\,, \tag{7.41}$$

where the parameter ϵ tracks the order of the WKB expansion. Substituting the expansion (7.41) into the equation (7.40), and equating the same powers of ϵ, we can find the solution of the equation at any order. It can be checked that the first two terms of the above series are given by

$$S_0(x) = \pm i\int^x \sqrt{Q(x')}\,dx'\,, \qquad S_1(x) = -\frac{1}{4}\ln Q(x) \tag{7.42}$$

where the signs correspond to either incoming or outgoing waves at either of the infinities $x = \pm\infty$. Analyzing the equation (7.40) as a wave scattering problem due to a barrier potential, and noting that potentials obtained from different perturbations have a similar form (see Fig. 7.1), we can see in Fig. 7.2 that we have two turning points that divide the radial coordinates into three zones. The quasinormal frequencies are obtained applying purely outgoing waves boundary conditions (7.34) into regions I and III. Then, we need to match both WKB solutions with a solution in region II, through the two turning points $\{x_1, x_2\}$. Since this is a long calculation, we refer to [183] for more details.

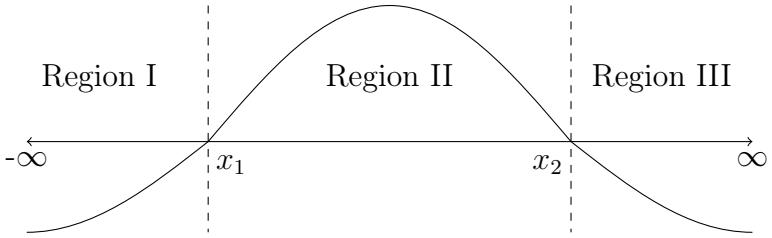

Figure 7.2: *A sketch of a general potential $V(r)$ with two turning points, x_1 and x_2.*

Considering only the first order in the WKB approximation, Schutz and Will [184] found that the quasinormal frequencies are given by the solution of

$$-\frac{iQ_0}{\sqrt{2Q_0''}} = n + \frac{1}{2}, \quad n = 0, 1, 2, ... \tag{7.43}$$

where the subscript 0 represents the function $Q(x_0)$ evaluated at its maximum. The factor n is known as the overtone number, which is a discrete quantity, and the fundamental oscillation mode is given by $n = 0$. Notice that the frequencies enter in the above equation through the definition of $Q(x)$ (7.40). This approach was extended to the third WKB order beyond the eikonal approximation by Iyer and Will [185] and to the sixth order by Konoplya [186, 187]. Using the definition of $Q(x)$, we can write an explicit expression for the QNM frequency. The sixth order WKB formula has the form

$$\frac{i(\omega^2 - V_0)}{\sqrt{-2V_0''}} - \Lambda_2 - \Lambda_3 - \Lambda_4 - \Lambda_5 - \Lambda_6 = n + \frac{1}{2}, \quad n = 0, 1, 2, .. \tag{7.44}$$

where the correction terms Λ_i depend on the value of the effective potential and its derivatives (up to the $2i$-th order) in the maximum. They are long expressions given in [186].

As a final remark, to apply the WKB method the following conditions must be fulfilled:

(i) The potential must possess two turning points;

(ii) The potential must have a maximum;

(iii) There are purely in-going waves arriving to the center and outgoing waves departing in the spatial infinity.

It is clear from Fig. 7.1, that black hole solution analyzed here satisfies each condition above. Hence, the WKB method may be correctly applied to these cases.

7.5.2 Continued fraction method

This method was applied for the first time by E. W. Leaver to compute the QNM frequencies for Schwarzschild and Kerr black holes [188]. This is the most accurate method for searching the eigenvalues of the equation (7.23) with arbitrary precision.

To review this method, we will work in radial coordinate r instead of r_*. Thus, the master equation is rewritten as

$$r(r-1)\frac{\partial^2\Psi_l}{\partial r^2}+\frac{\partial\Psi_l}{\partial r}+\frac{r^3}{r-1}\left[\omega^2-V(r)\right]\Psi_l=0\,. \tag{7.45}$$

To simplify the notation, we have rescaled the coordinate r in such a way that the event horizon is located at $r=1$. Thus, we have a second order differential equation with two regular points ($r=0$ and $r=1$) and one confluent singular regular point ($r=\infty$). This types of equations are known as *generalized spheroidal wave equation*. Again, the quasinormal mode frequencies are obtained after applying the outgoing boundary conditions (7.34), which read in the radial coordinates

$$\Psi_l\sim(r-1)^{\rho}\qquad r\to 1\qquad\qquad\text{and}\qquad\qquad \Psi_l\sim r^{-\rho}e^{-\rho r}\qquad r\to\infty\,, \tag{7.46}$$

where we have defined $\rho=-i\omega$ to simplify the notation. This method consists in solving the differential equation (7.45) using a series expansion around the event horizon ($r=1$) that respects the behavior of the solution at the boundaries

$$\Psi=(r-1)^{\rho}e^{-\rho(r-1)}r^{-2\rho}\sum_{n=0}^{\infty}a_n\left(\frac{r-1}{r}\right)^n. \tag{7.47}$$

The first two terms outside the sum ensure the behavior at $r\to 1$ and $r\to\infty$, while the third one repairs the subleading behavior at infinity coming from the change of variable from tortoise coordinates. Substituting (7.47) into the differential equation (7.45), we obtain that expansion coefficients a_n satisfy a three-term recurrence relation

$$\begin{aligned}\alpha_0 a_1+\beta_0 a_0&=0\\ \alpha_n a_{n+1}+\beta_n a_n+\gamma_n a_{n-1}&=0\end{aligned} \tag{7.48}$$

where the coefficients α_n, β_n, γ_n are simple functions of the frequency ω and their expressions depend on the particular solution since the potential in (7.45) is different for each perturbation for each solution. For example, the expressions of coefficients α_n, β_n, γ_n for the Schwarzschild and Kerr BH can be found in [188]. Applying this procedure to our case of

higher dimensional Schwarzschild BH for vector perturbations, where the potential is given by (7.18), we found that the coefficients are

$$\begin{aligned}\alpha_n &= n^2 - 4in\omega - 4\omega^2 - 4\\ \beta_n &= -\frac{\gamma_v}{d-3} - 2n^2 - n(2-8i\omega) + 8\omega^2 + 4i\omega + 2\\ \gamma_n &= n^2 + n(2-2i\omega) - 2i\omega + 1\end{aligned}$$

where d is the critical dimension. Now that we have the three-term recurrence relation (7.48) for determining the expansion coefficients a_n, we can invoke the continued fraction method [189, 188], which gives an algebraic equation to determine ω_{QNM}

$$\beta_0 - \frac{\alpha_0\gamma_1}{\beta_1 -}\frac{\alpha_1\gamma_2}{\beta_2 -}\frac{\alpha_2\gamma_3}{\beta_3 -}\ldots \equiv \beta_0 - \cfrac{\alpha_0\gamma_1}{\beta_1 - \cfrac{\alpha_1\gamma_2}{\beta_2 - \cfrac{\alpha_2\gamma_3}{\beta_3 - \ldots}}} = 0\,, \tag{7.49}$$

where the first equality is a notational definition commonly used in the literature for infinite continued fractions. This equation has an infinite number of roots corresponding to the quasinormal spectrum. The continued fraction method is very powerful to compute higher overtones because the $n-$th overtone turns out to be the most stable numerical root of the $n-$th inversion of the radial continued fraction.

7.5.3 Direct integration method

Another method to compute quasinormal modes was developed by Chandrasekhar and Detweiler [190]. This method consists in integrating the differential equations within two different regions: near the event horizon up to some point r_m (that is somewhere between the horizon and spatial infinity), and from this point to infinity. To integrate the equation, we employ the boundary conditions (7.34) with a given choice of ω. The QNM frequencies are obtained when we compare the two numerical solutions at the matching point r_m and impose that the master function Ψ and their radial derivatives are continuous there.

As described in [190, 191], this approach is numerically difficult to implement due to inherent numerical instabilities. To overcome this obstacle and improve the numerical scheme, we find asymptotic analytic solutions to the perturbation equations around the spatial in-

finity and the horizon

$$\Psi \propto \begin{cases} e^{-i\omega r_*} \sum_{k=0}^{\infty} \alpha_k (r - r_H)^k \,, & r \to r_H \,, \\ e^{i\omega r_*} \sum_{k=0}^{\infty} \beta_k r^{-k} \,, & r \to \infty \,, \end{cases} \tag{7.50}$$

where the coefficients α_k and β_k can be determined order by order in a series expansion of the perturbation equations. The QNM frequencies can be found through

$$\begin{aligned} \mathbf{\Psi}^{-}(r)\big|_{r=r_m} &= \mathbf{\Psi}^{+}(r)\big|_{r=r_m} \,, \\ \mathbf{\Psi}^{-\prime}(r)\big|_{r=r_m} &= \mathbf{\Psi}^{+\prime}(r)\big|_{r=r_m} \,, \end{aligned} \tag{7.51}$$

The conditions (7.51) generate a system of $2N$ equations for the $2N$ coefficients α_n, β_n and for ω. Since the system is linear, we can set $\alpha_0 = \beta_0 = 1$. We then use $2N - 1$ equations to find the rest of the coefficients as functions of ω. The remaining equation is then used to find the QNM frequencies. This procedure is equivalent to compute the Wronskian W of the solutions at r_m; then, the QNM frequencies are obtained by $\det(W)\big|_{r=r_m} = 0$.

7.6 QNM of Pure Gauss-Bonnet BH

In order to determine the spectrum that characterizes a BH, we will focus on a particular example. We consider $d = 7$, which is our first new critical dimension after standard Einstein gravity in $d = 4$. In this case, the action is given by the $N = 2$ term in the Lovelock series, the pure Gauss-Bonnet term

$$\mathcal{S} = \int \mathrm{d}^7 x \sqrt{-g} \Big[R^2 - 4 R_{\mu\nu} R^{\mu\nu} + R_{\mu\nu\rho\sigma} R^{\mu\nu\rho\sigma} \Big] \,. \tag{7.52}$$

For each type of perturbations, we will fix the angular momentum ($\ell = 2, 3$) and calculate the first harmonic or fundamental mode ($n = 0$), the first overtone or second harmonic ($n = 1$) and finally the second overtone or third harmonic ($n = 2$). We computed the QNM spectrum using the methods described in the last section: the WKB method at sixth order, the continued fraction method and by direct integration. The quasinormal modes are compared to Schwarzschild spacetime in $d = 4$; therefore, we compare BHs with the same background while the action is modified. Also, we compared to the Schwarzschild-Tangherlini solution [192] in $d = 7$; in this way, we analyze BHs with the same dimension while the action is changed.

Scalar perturbations					
$\ell = 2$					
n	WKB method	Continued fraction method	Direct integration	Schwarzschild in $D = 4$	Schwarzschild-Tangherlini in $D = 7$
0	0.621586 - 0.174806 i	0.621745 - 0.174513 i	0.621745 - 0.174513 i	0.747415 - 0.177847 i	1.44794 - 0.46559 i
1	0.554145 - 0.546684 i	0.555450 - 0.542138 i	0.558945 - 0.546182 i	0.693431 - 0.547752 i	1.00452 - 1.49939 i
2	0.441637 - 0.974783 i	0.440166 - 0.97515 i	0.440006 - 0.969969 i	0.600099 - 0.957657 i	0.12018 - 2.94122 i
$\ell = 3$					
n	WKB method	Continued fraction method	Direct integration	Schwarzschild in $D = 4$	Schwarzschild-Tangherlini in $D = 7$
0	0.952926 - 0.182173 i	0.952919 - 0.182185 i	0.952919 - 0.182186 i	1.198887 - 0.185406 i	2.23178 - 0.54084 i
1	0.910869 - 0.555971 i	0.909113 - 0.561265 i	0.907645 - 0.557741 i	1.165284 - 0.562585 i	1.93141 - 1.68185 i
2	0.835593 - 0.956598 i	0.836303 - 0.956543 i	0.800021 - 0.949965 i	1.10319 - 0.95811 i	1.33485 - 2.99002 i
Vector perturbations					
$\ell = 2$					
n	WKB method	Continued fraction method	Direct integration	Schwarzschild in $D = 4$	Schwarzschild-Tangherlini in $D = 7$
0	0.484860 - 0.178144 i	0.489874 - 0.171145 i	0.489877 - 0.171143 i	0.747343 - 0.177925 i	1.96718 - 0.60766 i
1	0.392473 - 0.578251 i	0.395578 - 0.540791 i	0.375665 - 0.526008 i	0.693422 - 0.547830 i	1.52058 - 1.90469 i
2	0.258772 - 1.083567 i	0.211030 - 1.006590 i	0.249988 - 1.000020 i	0.602107 - 0.956554 i	0.57082 - 3.61342 i
$\ell = 3$					
n	WKB method	Continued fraction method	Direct integration	Schwarzschild in $D = 4$	Schwarzschild-Tangherlini in $D = 7$
0	0.747239 - 0.177782 i	0.747343 - 0.177925 i	0.747343 - 0.177925 i	1.198887 - 0.185406 i	2.64217 - 0.60118 i
1	0.692593 - 0.546960 i	0.693422 - 0.547830 i	0.695469 - 0.545779 i	1.165284 - 0.562581 i	2.30384 - 1.84962 i
2	0.597040 - 0.955120 i	0.602107 - 0.956554 i	0.599970 - 0.950054 i	1.10319 - 0.95809 i	1.58364 - 3.29736 i
Tensor perturbations					
For any ℓ					
n	WKB method	Continued fraction method	Direct integration	Schwarzschild in $D = 4$	Schwarzschild-Tangherlini in $D = 7$ ($\ell = 2$)
0	0.220934 - 0.201633 i	0.220910 - 0.209791 i	0.225108 - 0.214605 i	-	2.49710 - 0.63234 i
1	0.178058 - 0.689058 i	0.172234 - 0.696105 i	0.148482 - 0.678334 i	-	2.13340 - 1.98070 i
2	0.383649 - 0.952812 i	0.381050 - 0.952612 i	0.380012 - 0.95002 i	-	1.37830 - 3.64177 i

Table 7.1: *QNMs for scalar, vector and tensor perturbations for $\ell = (2, 3)$ and $n = (0, 1, 2)$ using three different methods. We added, for comparison, the QNM for Schwarzschild in $d = 4$ and Schwarzschild-Tangherlini in $d = 7$.*

The Schwarzschild-Tangherlini solution in 7 dimensions is derived from Einstein action and gives $f(r) = 1 - (r_s/r)^4$. Using exactly the same methodology described in section 7.2, the new equation for perturbations will have exactly the same structure as Eq. (7.11) with following potentials for scalar, vector and tensor perturbations respectively

$$V_s(r) = \left[1 - \left(\frac{r_s}{r}\right)^4\right]\left[\frac{5r^{12}\lambda^2(4\lambda+7) + 9r^4 r_s^8(26\lambda+3)}{4r^6(\lambda r^4 + 3r_s^4)^2} - \frac{15r^8 r_s^4\lambda(\lambda+18) + 225r_s^{12}}{4r^6(\lambda r^4 + 3r_s^4)^2}\right] \tag{7.53}$$

$$V_v(r) = \left[1 - \left(\frac{r_s}{r}\right)^4\right]\left[\frac{(2\ell+5)(2\ell+3)}{4r^2} - \frac{75r_s^4}{4r^6}\right] \tag{7.54}$$

$$V_t(r) = \left[1 - \left(\frac{r_s}{r}\right)^4\right]\left[\frac{(2\ell+5)(2\ell+3)}{4r^2} + \frac{25r_s^4}{4r^6}\right] \tag{7.55}$$

In Table 7.1, we give the quasinormal mode frequencies obtained using the numerical techniques. Notice that for all modes $\omega_I < 0$ and therefore the solution is stable. It is also interesting that the ringdown signal vanishes exponentially with a characteristic time $\tau = 1/\mathrm{Im}(\omega)$ which is very similar between the Schwarzschild solution in 7 dimensions and the Schwarzschild spacetime in four dimensions. The dimension affects very little the characteristic time, while it is very different for similar dimension $d = 7$ and within different solution, Schwarzschild-Tangherlini. The characteristic time of decay of the perturbations is faster for Schwarzschild-Tangherlini background where the gravitational potential falls faster to zero ($1/r^4$). The characteristic time at which the perturbation decay depends mostly on the background potential.

On the contrary, the frequency at which these modes oscillate ($f = \mathrm{Re}(\omega)/2\pi$) is very different for the three spacetimes considered but, again, the analogue Schwarzschild spacetime has a frequency of mode oscillation closer to Schwarzschild spacetime in $d = 4$ than Schwarzschild-Tangherlini in $d = 7$. We conclude that this parameter is more sensitive to the theory considered and to the dimension.

7.7 Higher dimensions

In this section, we generalize the previous results to any critical dimension, Lovelock of order N in dimension $d = 3N + 1$. As we can see from Eq.(7.22), tensor modes do not depend on the dimension, but they oscillate similarly in any critical dimension. On the contrary, scalar and vector perturbations depend on the dimension.

We see from Figs.(7.3,7.4) similar results as the ones found in the previous section. The characteristic time at which the perturbations die is changing very little between all

these models. Dimension does not affect the characteristic time of the ringdown, only the background gravitational potential affects it. Notice that for $\ell = 2$, the characteristic time $(1/\mathrm{Im}(\omega))$ becomes maximum for $d = 10$ for scalar and vector perturbations.

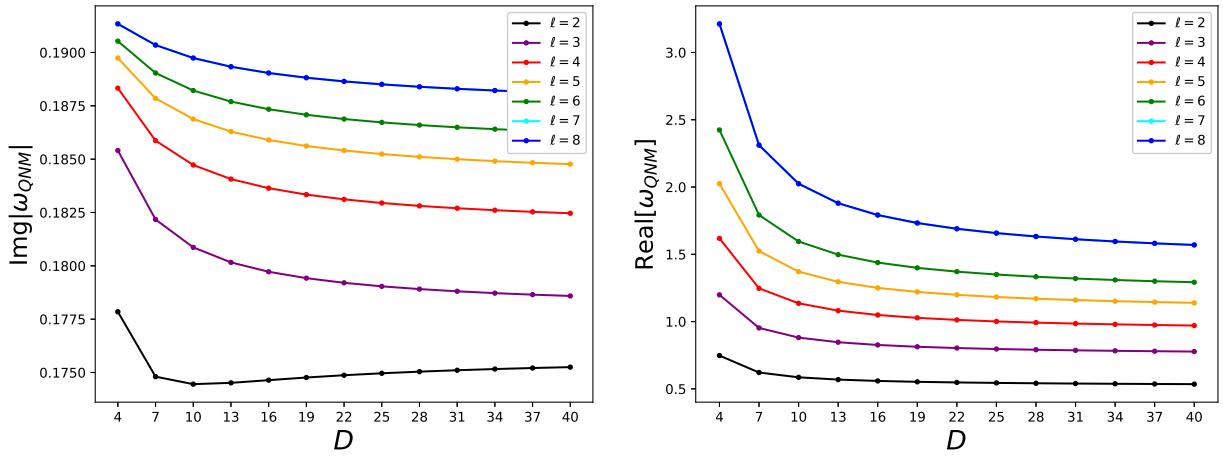

Figure 7.3: *Imaginary part of QNM (left) and real part of QNM (right) for scalar perturbations in all critical dimensions from $d = 4$ to $d = 40$ using WKB method of order 6 for the fundamental tone $n = 0$ and angular momentum $\ell = 2, ..., 8$.*

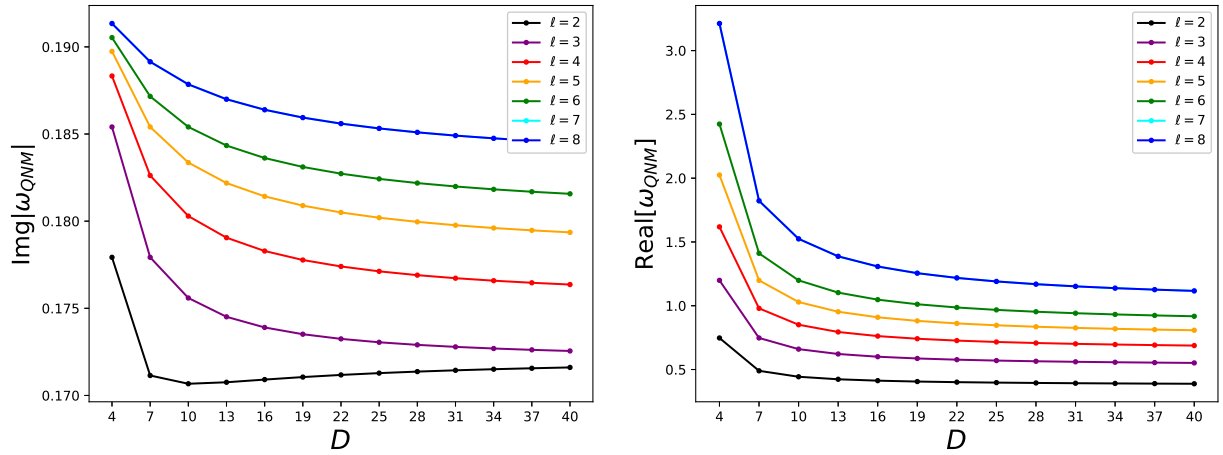

Figure 7.4: *Imaginary part of QNM (left) and real part of QNM (right) for vector perturbations in all critical dimensions from $d = 4$ to $d = 40$ using Leaver's method for the fundamental tone $n = 0$ and angular momentum $\ell = 2, ..., 8$.*

On the contrary, the frequency of oscillation is changing much more. It depends on the type of the action, and therefore on the dimension of the spacetime. The larger the dimension, the lower the frequency. Notice also that larger angular momentum ℓ increases these effects. Finally, we can notice that all values settle to some asymptotic value. This is

due to the fact that V_s and V_v have well defined limit when $d \to \infty$, e.g. we have

$$V_v = f(r)\Big[\frac{\ell+1}{r^2} - \frac{6M}{r^2}\Big] + \mathcal{O}(\frac{1}{d}) \tag{7.56}$$

and therefore the results of Figs.(7.3,7.4) could be obtained analytically by an $1/d$ expansion in higher $d-$dimensional spacetime.

7.8 Discussions

We have shown that for any dimension $d = 3N+1$, Schwarzschild spacetime is stable in the corresponding Nth order pure Lovelock gravity. And it is an exact solution of pure Lovelock equation in $d = 3N+1$. We have studied stability of this static spherically symmetric spacetime for linear perturbations. We have derived perturbation equation and shown that isospectrality holds only in $d = 4$. In any other dimension, the scalar, vector and tensor perturbations oscillate with different frequencies. We have also studied QNMs for all critical dimensions from $d = 4$ to $d = 40$ and we found that tensor perturbations are isotropic and do not depend on the dimension of the spacetime, while scalar and vector ones decay to zero with a characteristic time which depends weakly on dimension. This is because perturbations depend only on the gravitational potential while frequency of oscillation of these perturbations does depend on dimension. The larger the dimension, the lower is the frequency. We have also shown that all QNMs converge to an asymptotic value for large a dimension, because the potentials (V_s, V_v) have well-defined limit for large d, and therefore could be tackled analytically using $1/d$ expansion.

Pure Lovelock gravity is dynamical in $d \geq 2N+2$, however, static black hole is stable only in dimension $d \geq 3N+1$. This means in dimensions $2N+2 \leq d < 3N+1$, black hole would be unstable. However, for Einstein gravity $N = 1$, the two limits coincide. For $N > 1$, there would always be a dimension window of instability for pure Lovelock black holes. It would be interesting to study in a future work if third order Lovelock, $N = 3$, is unstable in dimension $d = 8, 9$.

Chapter 8

Concluding remarks

In this thesis, we have studied classical stability and the formation of black holes in theories beyond general relativity, focusing on their existence, signature and properties when they are formed.

Part of the investigation centered on the numerical study of gravitational collapse of *k-essence* model with additional shift symmetry. The main feature of a *k-essence* model is the inclusion of non-canonical kinetic terms of the scalar field in the action. We saw that *k-essence* field propagates through the effective metric, $\tilde{g}_{\mu\nu}$ given by (3.7), which is different from the gravitational metric $g_{\mu\nu}$, if the Lagrangian K is a non-linear function of X and the background is nontrivial, $\partial_\mu\phi = 0$. As we stated in Chapter 4, the *k-essence* field can propagate faster than light, provided $K_{,XX}/K_{,X} < 0$. However, we considered a particular model in which the propagation is subluminal to be consistent with basic requirements of quantum field theory, such as Lorentz invariance, unitarity and analyticity [110, 111].

For numerical purposes, we focused on a particular model defined by $K = X + \beta X^2$. In the numerical evolution, we detect two regimes, similar to the Choptuik case (in which a canonical scalar field is considered): in the weak field limit, the scalar field pulse disperses beyond the integration domain; instead, in the strong field limit, a geometric horizon begins to form. In the latter scenario, two situations occur, either only a sonic horizon forms (collapse of the effective metric) or both horizons form at the same time. In this last case, the exterior solution is always Schwarzschild and we never observed formation of caustics. Near the threshold of sonic horizon formation, we detect a loss of hyperbolicity, but, surprisingly we also found that the sonic horizon satisfies a universal power-law scaling (5.2).

Since theories of gravity can be constructed by adding other extra fundamentals fields, we also studied the classical stability of black holes in generalized Einstein-Maxwell-Scalar theories, in which a scalar and a vector field are added into the gravity sector. These theories

play a crucial role in understanding fundamental properties of modified theories of gravity since they arise in the low energy limit of Kaluza-Klein models and string theories. Following a theoretical procedure, we applied linear perturbation theory around static and spherically symmetric spacetime, in which perturbations are classified into odd- and even-parity modes. Expanding the action up to second order in perturbation and appealing to the absence of ghosts, we have derived conditions to the action (6.1) to get the classical stability of the theory. In particular, for odd-parity modes, we got that all perturbations propagate at the speed of light. The stability of the BH is obtained if the conditions $f_1(\phi) > 0$ and $f_{2,F}(\phi, X, F) > 0$ are imposed in the action (6.1). In the even-parity sector, we got that perturbations of the gravitational and electromagnetic fields propagate at the speed of light. Still, the perturbation associated with the scalar field differs from unity but is the same irrespective of the multipole order. It is necessary to remark that our formulation can be applied to any theories belonging to the Einstein-Maxwell-Scalar action of the form (6.1). As a demonstration, we have considered several concrete models including GR, a nonminimally coupled scalar field, a black hole without scalar hair, the BBMB solution, and the non-linear electrodynamic theory.

Finally, to complete our study of stability and signature of BHs, we analyze BH solutions in Pure Lovelock gravity in critical dimensions, $d = 3N + 1$. The main feature of these BHs is that the background solution is the same as GR, the Schwarzschild solution, in which the potential falls off as $1/r$. We have studied the stability of this static spherically symmetric spacetime for linear perturbations, getting that this solution is stable under scalar, vector and tensor perturbations; the last one arising only in dimensions greater than 4. Using numerical techniques, we determined the spectrum – quasinormal modes – of these BHs for all critical dimensions from $d = 4$ to $d = 40$ and we found that tensor perturbations are isotropic and do not depend on the dimension of the spacetime, while scalar and vector decay to zero with a characteristic time that depends weakly on the dimension.

Appendix A

Choptuik's Equatios in d dimensions

As described in the main text, Choptuik studied the gravitational collapse of a massless scalar field in four dimensions [34]. However, we can perform the same analysis in higher dimensions. In fact, the gravitational collapse of a massless scalar field minimally coupled to gravity in $d > 4$ was studied in [39, 70]. In this section, we deduce the Einstein tensor for a spacetime in any dimension d. The generalization to higher dimensions of the Choptuik problem will serve as another check of our numerical code. The action is given by

$$\mathcal{S} = \int d^d x \sqrt{-g} \left(\frac{R}{2k} - \frac{1}{2} \partial_\mu \phi \partial^\mu \phi \right) . \tag{A.1}$$

As a metric ansatz, we use the line element given by

$$\mathrm{d}s^2 = -f(t,r)\mathrm{d}t^2 + g(t,r)\mathrm{d}r^2 + r^2 \bar{\gamma}_{ab} \mathrm{d}x^a \mathrm{d}x^b \ , \tag{A.2}$$

where $\bar{\gamma}_{ab}$ is the metric of the $n \equiv (d-2)-$dimensional constant curvature space, with curvature $\kappa = 0, 1, -1$. The non zero components of Christoffel symbols (1.4) are

$$\Gamma^t_{tt} = \frac{\dot{f}}{2f} , \qquad \Gamma^r_{tt} = \frac{f'}{2g} , \qquad \Gamma^r_{ij} = -\frac{r}{g} \bar{\gamma}_{ij} , \qquad \Gamma^t_{rr} = \frac{\dot{g}}{2f}$$
$$\Gamma^r_{rr} = \frac{g'}{2g} , \qquad \Gamma^i_{jr} = \frac{1}{r} \delta^i_j , \qquad \Gamma^t_{tr} = \frac{f'}{2f} , \qquad \Gamma^r_{tt} = \frac{\dot{g}}{2g} , \qquad \Gamma^i_{jk} = \bar{\Gamma}^i_{jk}$$

where a prime and a dot denote derivative with respect to the radial and time coordinates, respectively. We have suppressed the coordinate dependence of the function $f(t,r)$ and $g(t,r)$ to simplify the notation. Now, the only non zero component of the Ricci tensor (1.5)

are

$$\begin{aligned} R_{tt} &= \frac{f\left(\dot{g}^2 - f'g'\right) + g\dot{f}\dot{g} + 2fg\left(f'' - \ddot{g}\right) - gf'^2}{4fg^2} + \frac{nf'}{2rg}\,, \\ R_{rr} &= \frac{f\left(f'g' - \dot{g}^2\right) - g\dot{f}\dot{g} - 2gf\left(f'' - \ddot{g}\right) + gf'^2}{4f^2g} + \frac{ng'}{2rg}\,, \\ R_{tr} &= \frac{n\dot{g}}{2rg}\,, \\ R_{ab} &= \frac{rfg' - rgf' + 2gf(n-1)(\kappa g - 1)}{2fg^2}\bar{\gamma}_{ab}\,. \end{aligned} \tag{A.3}$$

Here, we used the fact that for a maximally symmetric constant curvature space the Riemman tensor is $\bar{R}^{cd}_{ab} = \kappa/r^2\,\delta^{cd}_{ab}$. The Ricci scalar for this metric is

$$R = \frac{f'g'}{2fg^2} - \frac{\dot{f}\dot{g}}{2f^2g} + \frac{f'^2}{2f^2g} - \frac{f''}{fg} - \frac{\dot{g}^2}{2fg^2} + \frac{\ddot{g}}{fg} + \frac{n(n-1)(g\kappa - 1)}{gr^2} - \frac{n}{gr}\left(\frac{f'}{f} + \frac{g'}{g}\right) \tag{A.4}$$

Focusing on a spherically symmetric spacetime, where $\kappa = 1$, and choosing the metric functions as $f(t,r) = \alpha^2(t,r)$ and $g(t,r) = a^2(t,r)$ in order to get a similar expression to the line element in polar-areal coordinates (2.10), we get that the components of the Einstein tensor are

$$G_{tt} = \frac{n}{r}\frac{\alpha^2}{a^2}\left[\frac{a'}{a} + (n-1)\frac{a^2-1}{2r}\right] \tag{A.5}$$

$$G_{rr} = \frac{n}{r}\left[\frac{\alpha'}{\alpha} - (n-1)\frac{a^2-1}{2r}\right] \tag{A.6}$$

$$G_{tr} = \frac{n\dot{a}}{ra} \tag{A.7}$$

The G_{ab} component is not explicitly given since it is an extended expression but can be derived using the above relations. To complete the set of equations, variation of the action (A.1) with respect to the scalar field gives the Klein-Gordon equation

$$0 = \Box\phi = \frac{1}{\sqrt{-g}}\partial_\mu\left[\sqrt{-g}g^{\mu\nu}\partial_\nu\phi\right]$$

where the determinant of the metric is given by $\sqrt{-g} = a\alpha r^n\sqrt{\gamma}$. Since the scalar field only depends on (t,r) coordinates, for $d = 4$ the above equation reduces to (2.11).

Appendix B

Initial conditions: a review

As described in the text, we have to provide initial data to solve the equations that describe the gravitational collapse of some type of matter/fields. Initial conditions must be chosen so that they satisfy the Hamiltonian (2.18) and Momentum (2.19) constraint equations. Similarly as in chapter 2, in this section we label the initial scalar field as $\phi(0,r)$ and auxiliary fields as $\Pi(0,r)$ and $\Phi(0,r)$. The most traditional choice for the initial profile of the scalar field $\phi(0,r)$ is a Gaussian pulse

$$\phi(0,r) = \phi_o \, \exp\left[-\left(\frac{r-r_0}{\Delta}\right)^q\right] \tag{B.1}$$

where different families $\mathcal{S}[p]$ are given fixing three of the four initial parameters $\{\phi_o, r_o, q, \Delta\}$ and varying the other. It is also common to multiple the above profile by a factor of r, r^2 or r^3. With this initial profile for ϕ, we are free to choose the initial form of the auxiliary fields; typically, they are chosen as

$$\Phi(0,r) = \partial_r\phi(0,r)\,, \qquad \Pi(0,r) = 0 \tag{B.2}$$

which describe two Gaussian pulses, one traveling to the origin and the other to infinity, or

$$\Phi(0,r) = \partial_r\phi(0,r)\,, \qquad \Pi(0,r) = \partial_r\phi(0,r) + \frac{\phi(0,r)}{r} \tag{B.3}$$

which describe one single Gaussian pulse that travels to the origin.

However, in the literature, we can find other choices for the initial profile of the scalar and auxiliary fields. For example, in the pioneering work on gravitational collapse developed

by Choptuik [34], the families considered as initial data were

$$\phi(0,r) = \begin{cases} \phi_0\, r^3 \exp\left[-((r-r_0)/\sigma)^q\right] \\ \phi_0 \tanh\left[(r-r_0)/\sigma\right] \\ \phi_0\, (r-r_0)^{-5}[\exp(1/(r-r_0)) - 1]^{-1} \end{cases} \tag{B.4}$$

while the initial form for the auxiliary fields were fixed as shown in (B.2). Other option, as explained in [60], is to choose $\Phi(r,0) = 0$ and a Gaussian function (B.1) for $\Pi(r,0)$.

In Ref. [193], the gravitational collapse of a scalar field with angular momentum in spherical symmetry is analyzed using

$$\phi(0,r) = \begin{cases} A\, \exp\left(-(r-r_0)^2/\sigma^2\right) \\ -2A\, (r-r_0)/\sigma^2 \exp\left(-(r-r_0)^2/\sigma^2\right) \\ A\, r^2\, (\mathrm{atan}(r-r_0) - \mathrm{atan}(r-r_0-\sigma)) \end{cases} \tag{B.5}$$

while the auxiliary fields are fixed as

$$\Pi(0,r) = \Phi(0,r) = \frac{\partial \psi}{\partial r}(0,r). \tag{B.6}$$

On the other hand, critical phenomena in perfect fluids are analyzed in [71]. The following initial energy density was used as initial condition:

$$\rho = A\, \exp\left[-\left(\frac{r-r_0}{\Delta}\right)^2\right]. \tag{B.7}$$

This means that, in terms of the auxiliary field, what is fixed is the combination $\Pi^2 + \Phi^2$. As a last example, in Ref. [100], initial data are given by:

$$\Phi(t=0,r) = A \exp\left(-\frac{(r-r_0)^2}{\sigma^2}\right) \cos\left(\frac{\pi}{10} r\right), \qquad \Pi(t=0,r) = 0\,. \tag{B.8}$$

Appendix C

Misner-Sharp quasi-local mass

In General Relativity, definition of the mass/energy for the gravitational field is an intricate open problem. The difficulty relies on the equivalence principle. Due to this principle, any free-falling observer should sense a Minkowski spacetime, whose gravitational stress-energy should be zero. Hence, according to the diffeomorphism invariance, the gravitational stress-energy must be zero for any observer. Since there is a notorious problem to define global mass in a spacetime, it forces us to consider the quasi-local mass of gravity. After several attempts, we have many different forms of quasi-local forms of gravitational mass, see [194] for a review.

In a spherically symmetric spacetime, it is common to use the Misner-Sharp quasi-local mass [69, 195]. This mass is sometimes called the *Hawking mass* and *Misner-Sharp-Hernandez mass*. If we consider a spherically symmetric spacetime given by the line element in areal coordinates

$$\mathrm{d}s^2 = h_{ij}\mathrm{d}x^i\mathrm{d}x^j + r^2\mathrm{d}\Omega_2^2 \tag{C.1}$$

where $\mathrm{d}\Omega_2^2$ is the line element of the 2-sphere, the Misner-Sharp mass is defined by

$$1 - \frac{2m_{MS}(t,r)}{r} \equiv \nabla_i r\, \nabla^i r \quad \longrightarrow \quad m_{MS}(t,r) = \frac{r}{2}\big(1 - h^{ij}\nabla_i r\, \nabla_j r\big)\,. \tag{C.2}$$

The Misner-Sharp mass function can be interpreted as measuring the energy within a sphere of areal radius r at a time t. Therefore, this mass function gives a quasi-local definition to the concept of the curvature-producing energy contained within a black hole. We can use the Misner-Sharp mass to locate black hole horizons.

It can be shown that the Misner-sharp mass is a component of a conserved current corresponding to the timelike Killing vector in static spherically symmetric spacetime and to the Kodama vector in a general spherically symmetric spacetime [196].

Appendix D

Integral of spherical harmonics

As we mentioned in the main text, when studying perturbations around a spherically symmetry background solution, it is sufficient to set $m = 0$. This enables to rewrite the spherical harmonics in terms of Legendre polynomials

$$Y_\ell^{m=0}(\theta, \varphi) = \sqrt{\frac{(2\ell+1)}{4\pi}}\, P_\ell(\cos\theta)\,. \tag{D.1}$$

Thus, integration of the angular part of the second-order action can be performed using orthogonality and recurrence relations. We employ Legendre's differential equation

$$(1-x^2)\frac{d^2P_\ell(x)}{dx^2} - 2x\frac{dP_\ell(x)}{dx} + \ell(\ell+1)P_\ell(x) = 0 \tag{D.2}$$

to reduce the derivatives over $P_\ell(x)$. Here, to simplify notation, we denoted $x = \cos\theta$. Some integrals are equivalent to the orthogonality relation of the Legendre's polynomials

$$\int_{-1}^{1} P_\ell(x)P_m(x)dx = \frac{2}{2\ell+1}\delta_{\ell m}\,. \tag{D.3}$$

In addition, we used the following relations

$$\int_{-1}^{1} xP_\ell(x)P'_\ell(x)dx = \frac{2\ell}{2\ell+1} \tag{D.4}$$

$$\int_{-1}^{1} (1-x^2)[P'_\ell(x)]^2 dx = \frac{2\ell(\ell+1)}{2\ell+1} \tag{D.5}$$

$$\int_{-1}^{1} [P'_\ell(x)]^2 dx = \ell(\ell+1) \tag{D.6}$$

Bibliography

[1] R. Gannouji and Y. Rodríguez Baez, *Critical collapse in K-essence models*, *JHEP* **07** (2020) 132 [arXiv: 2003.13730].

[2] R. Gannouji, and Y. Rodríguez Baez, *Stability of generalized Einstein-Maxwell-scalar black holes*, *JHEP (to appear)* (2021) [arXiv: 2112.00109].

[3] R. Gannouji, Y. Rodríguez Baez and N. Dadhich, *Pure Lovelock black holes in dimensions $d = 3N + 1$ are stable*, *Phys. Rev. D* **100** (2019) 084011 [arXiv: 1907.09503].

[4] J. R. Oppenheimer and H. Snyder, *On continued gravitational contraction*, *Phys. Rev.* **56** (1939) 455.

[5] P. T. Chrusciel, J. Lopes Costa and M. Heusler, *Stationary Black Holes: Uniqueness and Beyond*, *Living Rev. Rel.* **15** (2012) 7 [arXiv: 1205.6112].

[6] K. e. a. Akiyama, *First M87 Event Horizon Telescope Results. I. The Shadow of the Supermassive Black Hole*, *Astrophys. J. Lett.* **875** (2019) L1 [arXiv: 1906.11238].

[7] B. P. e. a. Abbott, *Tests of General Relativity with the Binary Black Hole Signals from the LIGO-Virgo Catalog GWTC-1*, *Phys. Rev. D* **100** (2019) 104036 [arXiv: 1903.04467].

[8] B. P. e. a. Abbott, *Tests of general relativity with GW150914*, *Phys. Rev. Lett.* **116** (2016) 221101 [arXiv: 1602.03841].

[9] C. M. Will, *The Confrontation between General Relativity and Experiment*, *Living Reviews in Relativity* **17** (2014) [arXiv: 1403.7377].

[10] S. W. Hawking and R. Penrose, *The Singularities of gravitational collapse and cosmology*, *Proc. Roy. Soc. Lond. A* **314** (1970) 529.

[11] K. S. Stelle, *Renormalization of Higher Derivative Quantum Gravity*, *Phys. Rev. D* **16** (1977) 953.

[12] A. H. Guth, *Inflationary universe: A possible solution to the horizon and flatness problems*, *Phys. Rev. D* **23** (1981) 347.

[13] R. H. Brandenberger, *Inflationary cosmology: Progress and problems*, in *IPM School on Cosmology 1999: Large Scale Structure Formation*, 1, 1999, arXiv: hep-ph/9910410.

[14] S. e. a. Perlmutter, *Measurements of* Ω *and* Λ *from 42 high redshift supernovae*, *Astrophys. J.* **517** (1999) 565 [arXiv: astro-ph/9812133].

[15] A. G. e. a. Riess, *Observational evidence from supernovae for an accelerating universe and a cosmological constant*, *Astron. J.* **116** (1998) 1009 [arXiv: astro-ph/9805201].

[16] D. Lovelock, *The Einstein tensor and its generalizations*, *J. Math. Phys.* **12** (1971) 498.

[17] D. Lovelock, *The four-dimensionality of space and the einstein tensor*, *J. Math. Phys.* **13** (1972) 874.

[18] E. Berti, E. Barausse, V. Cardoso, L. Gualtieri, P. Pani, U. Sperhake et al., *Testing general relativity with present and future astrophysical observations*, *Classical and Quantum Gravity* **32** (2015) 243001 [arXiv: 1501.07274].

[19] C. Brans and R. H. Dicke, *Mach's principle and a relativistic theory of gravitation*, *Phys. Rev.* **124** (1961) 925.

[20] A. Avilez and C. Skordis, *Cosmological constraints on Brans-Dicke theory*, *Phys. Rev. Lett.* **113** (2014) 011101 [arXiv: 1303.4330].

[21] G. W. Horndeski, *Second-order scalar-tensor field equations in a four-dimensional space*, *Int. J. Theor. Phys.* **10** (1974) 363.

[22] B. P. e. a. Abbott, *GW170817: Observation of Gravitational Waves from a Binary Neutron Star Inspiral*, *Phys. Rev. Lett.* **119** (2017) 161101 [arXiv: 1710.05832].

[23] A. e. a. Goldstein, *An Ordinary Short Gamma-Ray Burst with Extraordinary Implications: Fermi-GBM Detection of GRB 170817A*, *Astrophys. J. Lett.* **848** (2017) L14 [arXiv: 1710.05446].

[24] P. Creminelli and F. Vernizzi, *Dark Energy after GW170817 and GRB170817A*, *Phys. Rev. Lett.* **119** (2017) 251302 [arXiv: 1710.05877].

[25] J. Sakstein and B. Jain, *Implications of the Neutron Star Merger GW170817 for Cosmological Scalar-Tensor Theories*, *Phys. Rev. Lett.* **119** (2017) 251303 [arXiv: 1710.05893].

[26] S. Arai and A. Nishizawa, *Generalized framework for testing gravity with gravitational-wave propagation. II. Constraints on Horndeski theory*, *Phys. Rev. D* **97** (2018) 104038 [arXiv: 1711.03776].

[27] C. D. Kreisch and E. Komatsu, *Cosmological Constraints on Horndeski Gravity in Light of GW170817*, *JCAP* **12** (2018) 30 [arXiv: 1712.02710].

[28] S. Myrzakul, R. Myrzakulov and L. Sebastiani, *K-essence in Horndeski models*, *Astrophys. Space Sci.* **361** (2016) 254 [arXiv: 1605.02726].

[29] H. P. Nilles, *On the Low-energy limit of string and M theory*, in *Theoretical Advanced Study Institute in Elementary Particle Physics (TASI 97): Supersymmetry, Supergravity and Supercolliders*, pp. 709–768, 2, 1998, arXiv: hep-ph/0004064.

[30] C. Armendáriz-Picón, T. Damour and V. Mukhanov, *k-Inflation*, *Physics Letters B* **458** (1999) 209 [arXiv: hep-th/9904075].

[31] C. Armendariz-Picon, V. Mukhanov and P. J. Steinhardt, *Dynamical Solution to the Problem of a Small Cosmological Constant and Late-Time Cosmic Acceleration*, *Phys. Rev. Lett.* **85** (2000) 4438.

[32] E. Babichev, V. Mukhanov and A. Vikman, *Escaping from the black hole?*, *Journal of High Energy Physics* **2006** (2006) 1 [arXiv: hep-th/0604075].

[33] M. M. May and R. H. White, *Hydrodynamic Calculations of General-Relativistic Collapse*, *Phys. Rev.* **141** (1966) 1232.

[34] M. W. Choptuik, *Universality and scaling in gravitational collapse of a massless scalar field*, *Phys. Rev. Lett.* **70** (1993) 9.

[35] J. Healy and P. Laguna, *Critical Collapse of Scalar Fields Beyond Axisymmetry*, *Gen. Rel. Grav.* **46** (2014) 1722 [arXiv: 1310.1955].

[36] P. R. Brady, C. M. Chambers and S. M. C. V. Goncalves, *Phases of massive scalar field collapse*, *Phys. Rev. D* **56** (1997) R6057 [arXiv: gr-qc/9709014].

[37] S. H. Hawley and M. W. Choptuik, *Boson stars driven to the brink of black hole formation*, *Phys. Rev. D* **62** (2000) 104024 [arXiv: gr-qc/0007039].

[38] C. R. Evans and J. S. Coleman, *Critical phenomena and self-similarity in the gravitational collapse of radiation fluid*, *Physical Review Letters* **72** (1994) 1782 [arXiv: gr-qc/9402041].

[39] E. Sorkin and Y. Oren, *Choptuik's scaling in higher dimensions*, *Physical Review D* **71** (2005) [arXiv: hep-th/0502034].

[40] M. Ostrogradsky, *Mémoires sur les équations différentielles, relatives au problème des isopérimètres*, *Mem. Acad. St. Petersbourg* **6** (1850) 385.

[41] R. P. Woodard, *Ostrogradsky's theorem on Hamiltonian instability*, *Scholarpedia* **10** (2015) 32243 [arXiv: 1506.02210].

[42] A. Nicolis, R. Rattazzi and E. Trincherini, *Galileon as a local modification of gravity*, *Physical Review D* **79** (2009) [arXiv: 0811.2197].

[43] L. Heisenberg, *Generalization of the Proca Action*, *JCAP* **05** (2014) 15 [arXiv: 1402.7026].

[44] L. Heisenberg, *Scalar-Vector-Tensor Gravity Theories*, *JCAP* **10** (2018) 54 [arXiv: 1801.01523].

[45] T. Kaluza, *Zum Unitätsproblem der Physik*, *Sitzungsber. Preuss. Akad. Wiss. Berlin (Math. Phys.)* **1921** (1921) 966 [arXiv: 1803.08616].

[46] O. Klein, *Quantum Theory and Five-Dimensional Theory of Relativity. (In German and English)*, *Z. Phys.* **37** (1926) 895.

[47] T. Regge and J. A. Wheeler, *Stability of a Schwarzschild Singularity*, *Phys. Rev.* **108** (1957) 1063.

[48] F. J. Zerilli, *Effective Potential for Even-Parity Regge-Wheeler Gravitational Perturbation Equations*, *Phys. Rev. Lett.* **24** (1970) 737.

[49] S. Chandrasekhar, *The Mathematical Theory of Black Holes*, International series of monographs on physics. Clarendon Press, 1998.

[50] C. V. Vishveshwara, *Stability of the Schwarzschild Metric*, *Phys. Rev. D* **1** (1970) 2870.

[51] R. H. Price, *Nonspherical perturbations of relativistic gravitational collapse. 1. Scalar and gravitational perturbations*, *Phys. Rev. D* **5** (1972) 2419.

[52] R. M. Wald, *Note on the stability of the Schwarzschild metric*, *J. Math. Phys.* **20** (1979) 1056.

[53] R.-G. Cai and N. Ohta, *Black Holes in Pure Lovelock Gravities*, *Phys. Rev. D* **74** (2006) 64001 [arXiv: hep-th/0604088].

[54] A. Ishibashi and H. Kodama, *Stability of higher dimensional Schwarzschild black holes*, *Prog. Theor. Phys.* **110** (2003) 901 [arXiv: hep-th/0305185].

[55] H. Kodama and A. Ishibashi, *A Master Equation for Gravitational Perturbations of Maximally Symmetric Black Holes in Higher Dimensions*, *Progress of Theoretical Physics* **110** (2003) 701 [arXiv: hep-th/0305147].

[56] D. Christodoulou, *The problem of a self-gravitating scalar field*, *Comm. Math. Phys.* **105** (1986) 337.

[57] D. Christodoulou, *Global existence of generalized solutions of the spherically symmetric Einstein-scalar equations in the large*, *Comm. Math. Phys.* **106** (1986) 587.

[58] D. Christodoulou, *A mathematical theory of gravitational collapse*, *Comm. Math. Phys.* **109** (1987) 613.

[59] C. Gundlach and J. M. Martín-García, *Critical Phenomena in Gravitational Collapse*, *Living Reviews in Relativity* **10** (2007) [arXiv: 0711.4620v1].

[60] C. Gundlach, *Critical phenomena in gravitational collapse*, *Physics Reports* **376** (2003) 339 [arXiv: gr-qc/0210101].

[61] A. M. Abrahams and C. R. Evans, *Critical behavior and scaling in vacuum axisymmetric gravitational collapse*, *Phys. Rev. Lett.* **70** (1993) 2980.

[62] C. Gundlach, *Critical phenomena in gravitational collapse*, *Adv. Theor. Math. Phys.* **2** (1998) 1 [arXiv: gr-qc/9712084].

[63] R. Arnowitt, S. Deser and C. W. Misner, *Republication of: The dynamics of general relativity*, *General Relativity and Gravitation* **40** (2008) 1997.

[64] R. M. Wald, *General Relativity*. Chicago Univ. Pr., Chicago, USA, 1984, 10.7208/chicago/9780226870373.001.0001.

[65] J. Winicour, *Characteristic evolution and matching*, *Living Rev. Rel.* **4** (2001) 3 [arXiv: gr-qc/0102085].

[66] H. Friedrich, *Conformal Einstein evolution*, *Lect. Notes Phys.* **604** (2002) 1 [arXiv: gr-qc/0209018].

[67] M. Alcubierre, *Introduction to 3+1 Numerical Relativity*, International Series of Monographs on Physics. OUP Oxford, 2008.

[68] M. Israeli and S. A. Orszag, *Approximation of radiation boundary conditions*, *Journal of Computational Physics* **41** (1981) 115.

[69] C. W. Misner and D. H. Sharp, *Relativistic equations for adiabatic, spherically symmetric gravitational collapse*, *Phys. Rev.* **136** (1964) B571.

[70] D. Garfinkle, C. Cutler and G. Comer Duncan, *Choptuik scaling in six dimensions*, *Physical Review D* **60** (1999) [arXiv: gr-qc/9908044].

[71] D. W. Neilsen and M. W. Choptuik, *Critical phenomena in perfect fluids*, *Classical and Quantum Gravity* **17** (2000) 761 [arXiv: gr-qc/9812053].

[72] M. W. Choptuik, E. W. Hirschmann, S. L. Liebling and F. Pretorius, *Critical Collapse of a Complex Scalar Field with Angular Momentum*, *Phys. Rev. Lett.* **93** (2004) 131101.

[73] J. F. Ventrella and M. W. Choptuik, *Critical phenomena in the Einstein massless Dirac system*, *Phys. Rev. D* **68** (2003) 44020 [arXiv: gr-qc/0304007].

[74] D. Garfinkle, R. B. Mann and C. Vuille, *Critical collapse of a massive vector field*, *Phys. Rev. D* **68** (2003) 064015 [arXiv: gr-qc/0305014].

[75] B. Gustafsson, H. O. Kreiss and J. Oliger, *Time-Dependent Problems and Difference Methods*, Pure and Applied Mathematics: A Wiley Series of Texts, Monographs and Tracts. Wiley, 2013.

[76] T. W. Baumgarte and S. L. Shapiro, *Numerical Relativity: Solving Einstein's Equations on the Computer*. Cambridge University Press, 2010, 10.1017/CBO9781139193344.

[77] M. Shibata, *Numerical Relativity*. World Scientific, 2015, 10.1142/9692.

[78] R. L. Burden and J. D. Faires, *Numerical Analysis*. Cengage Learning, 2010.

[79] B. P. e. a. Schmidt, *The High Z supernova search: Measuring cosmic deceleration and global curvature of the universe using type Ia supernovae*, *Astrophys. J.* **507** (1998) 46 [arXiv: astro-ph/9805200].

[80] T. Padmanabhan, *Cosmological constant: The Weight of the vacuum*, *Phys. Rept.* **380** (2003) 235 [arXiv: hep-th/0212290].

[81] S. Weinberg, *The cosmological constant problem*, *Rev. Mod. Phys.* **61** (1989) 1.

[82] C. Vafa, *The String landscape and the swampland*, arXiv: hep-th/0509212.

[83] E. Palti, *The Swampland: Introduction and Review*, *Fortschritte der Physik* **67** (2019) 1900037 [arXiv: 1903.06239].

[84] P. Agrawal, G. Obied, P. J. Steinhardt and C. Vafa, *On the cosmological implications of the string Swampland*, *Physics Letters B* **784** (2018) 271 [arXiv: 1806.09718].

[85] I. Zlatev, L. Wang and P. J. Steinhardt, *Quintessence, Cosmic Coincidence, and the Cosmological Constant*, *Physical Review Letters* **82** (1999) 896 [arXiv: astro-ph/9807002].

[86] S. M. Carroll, *Quintessence and the Rest of the World: Suppressing Long-Range Interactions*, *Phys. Rev. Lett.* **81** (1998) 3067.

[87] C. Armendariz-Picon, V. F. Mukhanov and P. J. Steinhardt, *Essentials of k essence*, *Phys. Rev. D* **63** (2001) 103510 [arXiv: astro-ph/0006373].

[88] M. Born and L. Infeld, *Foundations of the new field theory*, *Proc. Roy. Soc. Lond. A* **144** (1934) 425.

[89] J. Polchinski, *String Theory*, vol. 1 of *Cambridge Monographs on Mathematical Physics*. Cambridge University Press, 1998, 10.1017/CBO9780511816079.

[90] M. J. Duff, *Kaluza-Klein theory in perspective*, in *The Oskar Klein Centenary Symposium*, 1994, arXiv: hep-th/9410046.

[91] L. Randall and R. Sundrum, *Large Mass Hierarchy from a Small Extra Dimension*, *Physical Review Letters* **83** (1999) 3370 [arXiv: hep-ph/9905221].

[92] L. Randall and R. Sundrum, *An Alternative to Compactification*, *Physical Review Letters* **83** (1999) 4690 [arXiv: hep-th/9906064].

[93] T. Clifton, P. G. Ferreira, A. Padilla and C. Skordis, *Modified gravity and cosmology*, *Physics Reports* **513** (2012) 1 [arXiv: 1106.2476].

[94] G. Papallo and H. S. Reall, *On the local well-posedness of Lovelock and Horndeski theories*, *Physical Review D* **96** (2017) [arXiv: 1705.04370].

[95] C. Armendariz-Picon and E. A. Lim, *Haloes of k-essence*, *Journal of Cosmology and Astroparticle Physics* (2005) 113 [arXiv: astro-ph/0505207].

[96] A. D. Rendall, *Dynamics of k-essence*, *Classical and Quantum Gravity* **23** (2006) 1557 [arXiv: gr-qc/0511158].

[97] S. Myrzakul, R. Myrzakulov and L. Sebastiani, *k-essence in Horndeski models*, *Astrophysics and Space Science* **361** (2016) [arXiv: 1605.02726].

[98] C. D. Leonard, J. Ziprick, G. Kunstatter and R. B. Mann, *Gravitational collapse of K-essence matter in Painlevè-Gullstrand coordinates*, *Journal of High Energy Physics* **2011** (2011) [arXiv: 1106.2054].

[99] R. Akhoury, D. Garfinkle and R. Saotome, *Gravitational collapse of k-essence*, *Journal of High Energy Physics* **2011** (2011) [arXiv: 1103.0290].

[100] L. Bernard, L. Lehner and R. Luna, *Challenges to global solutions in Horndeski's theory*, *Physical Review D* **100** (2019) 1 [arXiv: 1904.12866].

[101] R. Akhoury, C. S. Gauthier and A. Vikman, *Stationary configurations imply shift symmetry: No Bondi accretion for quintessence/k-essence*, *Journal of High Energy Physics* **2009** (2009) [arXiv: 0811.1620].

[102] E. Babichev, S. Ramazanov and A. Vikman, *Recovering $P(X)$ from a canonical complex field*, *JCAP* **11** (2018) 023 [arXiv: 1807.10281].

[103] S. W. Hawking and G. F. R. Ellis, *The Large Scale Structure of Space-Time*, Cambridge Monographs on Mathematical Physics. Cambridge University Press, 2011, 10.1017/CBO9780511524646.

[104] S. D. H. Hsu, A. Jenkins and M. B. Wise, *Gradient instability for $w < -1$*, *Phys. Lett. B* **597** (2004) 270 [arXiv: astro-ph/0406043].

[105] R. V. Buniy, S. D. H. Hsu and B. M. Murray, *The Null energy condition and instability*, *Phys. Rev. D* **74** (2006) 063518 [arXiv: hep-th/0606091].

[106] I. Y. Aref'eva and I. V. Volovich, *On the null energy condition and cosmology*, *Theor. Math. Phys.* **155** (2008) 503 [arXiv: hep-th/0612098].

[107] Y. Aharonov, A. Komar and L. Susskind, *Superluminal behavior, causality, and instability*, *Physical Review* **182** (1969) 1400.

[108] J.-P. Bruneton, *On causality and superluminal behavior in classical field theories: Applications to k-essence theories and MOND-like theories of gravity*, *Phys. Rev.* **D75** (2007) 85013 [arXiv: gr-qc/0607055].

[109] S. Melville and J. Noller, *Positivity in the Sky: Constraining dark energy and modified gravity from the UV*, *Physical Review D* **101** (2020) .

[110] A. Adams, N. Arkani-Hamed, S. Dubovsky, A. Nicolis and R. Rattazzi, *Causality, analyticity and an IR obstruction to UV completion*, *Journal of High Energy Physics* **2006** (2006) 014 [arXiv: hep-th/0602178].

[111] A. Nicolis, R. Rattazzi and E. Trincherini, *Energy's and amplitudes' positivity*, *Journal of High Energy Physics* **2010** (2010) [arXiv: 0912.4258].

[112] B. Bellazzini, *Softness and amplitudes' positivity for spinning particles*, *Journal of High Energy Physics* **2017** (2017) [arXiv: 1605.06111].

[113] E. Babichev, *Formation of caustics in k-essence and Horndeski theory*, *Journal of High Energy Physics* **2016** (2016) 1 [arXiv: 1602.00735].

[114] C. de Rham and H. Motohashi, *Caustics for Spherical Waves*, *Phys. Rev. D* **95** (2017) 064008 [arXiv: 1611.05038].

[115] R. Courant and D. Hilbert, *Methods of Mathematical Physics*, no. v. 2 in Methods of Mathematical Physics. Interscience Publishers, 1962.

[116] J. L. Ripley and F. Pretorius, *Hyperbolicity in spherical gravitational collapse in a Horndeski theory*, *Physical Review D* **99** (2019) [arXiv: 1902.01468].

[117] P. Van Nieuwenhuizen, *Supergravity*, *Phys. Rept.* **68** (1981) 189.

[118] G. W. Gibbons, *Antigravitating Black Hole Solitons with Scalar Hair in N=4 Supergravity*, *Nucl. Phys. B* **207** (1982) 337.

[119] G. W. Gibbons and K.-i. Maeda, *Black holes and membranes in higher-dimensional theories with dilaton fields*, *Nuclear Physics B* **298** (1988) 741.

[120] D. Garfinkle, G. T. Horowitz and A. Strominger, *Charged black holes in string theory*, *Phys. Rev. D* **43** (1991) 3140.

[121] V. Moncrief, *Odd-parity stability of a Reissner-Nordström black hole*, *Phys. Rev. D* **9** (1974) 2707.

[122] V. Moncrief, *Stability of Reissner-Nordström black holes*, *Phys. Rev. D* **10** (1974) 1057.

[123] A. De Felice, L. Heisenberg, R. Kase, S. Tsujikawa, Y.-l. Zhang and G.-B. Zhao, *Screening fifth forces in generalized Proca theories*, *Phys. Rev.* **D93** (2016) 104016 [arXiv: 1602.00371].

[124] A. De Felice, T. Suyama and T. Tanaka, *Stability of Schwarzschild-like solutions in f(R,G) gravity models*, *Physical Review D* **83** (2011) [arXiv: 1102.1521].

[125] H. Motohashi and T. Suyama, *Black hole perturbation in parity violating gravitational theories*, *Phys. Rev. D* **84** (2011) 084041 [arXiv: 1107.3705].

[126] A. Ganguly, R. Gannouji, M. Gonzalez-Espinoza and C. Pizarro-Moya, *Black hole stability under odd-parity perturbations in Horndeski gravity*, *Classical and Quantum Gravity* **35** (2018) 145008 [arXiv: 1710.07669].

[127] B. P. e. a. Abbott, *Observation of Gravitational Waves from a Binary Black Hole Merger*, *Phys. Rev. Lett.* **116** (2016) 61102 [arXiv: 1602.03837].

[128] R. M. Wald, *Erratum: Note on the stability of the schwarzschild metric*, *J. Math. Phys.* **21** (1980) 218.

[129] T. Takahashi and J. Soda, *Catastrophic Instability of Small Lovelock Black Holes*, *Prog. Theor. Phys.* **124** (2010) 711 [arXiv: 1008.1618].

[130] C. Moreno and O. Sarbach, *Stability properties of black holes in selfgravitating nonlinear electrodynamics*, *Phys. Rev. D* **67** (2003) 24028 [arXiv: gr-qc/0208090].

[131] T. Kobayashi, H. Motohashi and T. Suyama, *Black hole perturbation in the most general scalar-tensor theory with second-order field equations II: the even-parity sector*, *Phys. Rev. D* **89** (2014) 84042 [arXiv: 1402.6740].

[132] R. Kase, R. Kimura, S. Sato and S. Tsujikawa, *Stability of relativistic stars with scalar hairs*, *Phys. Rev. D* **102** (2020) 84037 [arXiv: 2007.09864].

[133] Y. Rodríguez, "`Mathematica Notebook`: Even-parity coefficients." https://github.com/YolbeikerRB/Even-parity_Perturbations.git, 2021.

[134] R. Horn, R. Horn and C. Johnson, *Matrix Analysis*. Cambridge University Press, 1990.

[135] N. Afshordi, D. J. H. Chung and G. Geshnizjani, *Cuscuton: A Causal Field Theory with an Infinite Speed of Sound*, *Phys. Rev. D* **75** (2007) 83513 [arXiv: hep-th/0609150].

[136] M. S. Volkov and D. V. Galtsov, *Odd parity negative modes of Einstein Yang-Mills black holes and sphalerons*, *Phys. Lett. B* **341** (1995) 279 [arXiv: hep-th/9409041].

[137] J. M. Bardeen, *Non-singular general-relativistic gravitational collapse*, in *Proc. Int. Conf. GR5, Tbilisi*, vol. 174, 1968.

[138] E. Ayon-Beato and A. Garcia, *The Bardeen model as a nonlinear magnetic monopole*, *Phys. Lett. B* **493** (2000) 149 [arXiv: gr-qc/0009077].

[139] I. H. Salazar, A. Garcia and J. Plebanski, *Duality Rotations and Type D Solutions to Einstein Equations With Nonlinear Electromagnetic Sources*, *J. Math. Phys.* **28** (1987) 2171.

[140] K. A. Bronnikov, *Regular magnetic black holes and monopoles from nonlinear electrodynamics*, *Phys. Rev. D* **63** (2001) 044005 [arXiv: gr-qc/0006014].

[141] M. J. Duff, *Quantum corrections to the schwarzschild solution*, *Phys. Rev. D* **9** (1974) 1837.

[142] N. E. J. Bjerrum-Bohr, J. F. Donoghue and B. R. Holstein, *Quantum corrections to the Schwarzschild and Kerr metrics*, *Phys. Rev. D* **68** (2003) 084005 [arXiv: hep-th/0211071].

[143] S. A. Hayward, *Formation and evaporation of regular black holes*, *Phys. Rev. Lett.* **96** (2006) 031103 [arXiv: gr-qc/0506126].

[144] V. P. Frolov, *Notes on nonsingular models of black holes*, *Phys. Rev. D* **94** (2016) 104056 [arXiv: 1609.01758].

[145] G. Veneziano, *Inhomogeneous pre - big bang string cosmology*, *Phys. Lett. B* **406** (1997) 297 [arXiv: hep-th/9703150].

[146] G. Papallo, *On the hyperbolicity of the most general Horndeski theory*, *Phys. Rev. D* **96** (2017) 124036 [arXiv: 1710.10155].

[147] L. Hui and A. Nicolis, *No-Hair Theorem for the Galileon*, *Phys. Rev. Lett.* **110** (2013) 241104 [arXiv: 1202.1296].

[148] K. A. Bronnikov, M. S. Chernakova, J. C. Fabris, N. Pinto-Neto and M. E. Rodrigues, *Cold black holes and conformal continuations*, *Int. J. Mod. Phys. D* **17** (2008) 25 [arXiv: gr-qc/0609084].

[149] J. D. Bekenstein, *Transcendence of the law of baryon-number conservation in black hole physics*, *Phys. Rev. Lett.* **28** (1972) 452.

[150] J. D. Bekenstein, *Novel "no-scalar-hair" theorem for black holes*, *Phys. Rev. D* **51** (1995) R6608.

[151] D. Sudarsky, *A Simple proof of a no hair theorem in Einstein Higgs theory,*, *Class. Quant. Grav.* **12** (1995) 579.

[152] C. A. R. Herdeiro and E. Radu, *Asymptotically flat black holes with scalar hair: a review*, *Int. J. Mod. Phys. D* **24** (2015) 1542014 [arXiv: 1504.08209].

[153] N. M. Bocharova, K. A. Bronnikov and V. N. Melnikov, *On an exact solution of the Einstein-scalar field equations*, *Vestnik Mosk Univ., Fiz., Astron.* **6** (1970) .

[154] J. D. Bekenstein, *Exact solutions of Einstein conformal scalar equations*, *Annals Phys.* **82** (1974) 535.

[155] K. A. Bronnikov and Y. N. Kireev, *Instability of Black Holes with Scalar Charge*, *Phys. Lett. A* **67** (1978) 95.

[156] P. L. McFadden and N. G. Turok, *Effective theory approach to brane world black holes*, *Phys. Rev. D* **71** (2005) 86004 [arXiv: hep-th/0412109].

[157] M. Nozawa, T. Shiromizu, K. Izumi and S. Yamada, *Divergence equations and uniqueness theorem of static black holes*, *Class. Quant. Grav.* **35** (2018) 175009 [arXiv: 1805.11385].

[158] V. Ferrari, M. Pauri and F. Piazza, *Quasinormal modes of charged, dilaton black holes*, *Phys. Rev. D* **63** (2001) 064009 [arXiv: gr-qc/0005125].

[159] R. Brito and C. Pacilio, *Quasinormal modes of weakly charged Einstein-Maxwell-dilaton black holes*, *Phys. Rev. D* **98** (2018) 104042 [arXiv: 1807.09081].

[160] J. L. Blázquez-Salcedo, S. Kahlen and J. Kunz, *Quasinormal modes of dilatonic Reissner–Nordström black holes*, *Eur. Phys. J. C* **79** (2019) 1021 [arXiv: 1911.01943].

[161] C. Garraffo and G. Giribet, *The Lovelock Black Holes*, *Mod. Phys. Lett. A* **23** (2008) 1801 [arXiv: 0805.3575].

[162] B. Zwiebach, *Curvature squared terms and string theories*, *Physics Letters B* **156** (1985) 315.

[163] N. Dadhich, S. G. Ghosh and S. Jhingan, *The Lovelock gravity in the critical spacetime dimension*, *Phys. Lett. B* **711** (2012) 196 [arXiv: 1202.4575].

[164] G. Dotti and R. J. Gleiser, *Gravitational instability of Einstein-Gauss-Bonnet black holes under tensor mode perturbations*, *Class. Quant. Grav.* **22** (2005) L1 [arXiv: gr-qc/0409005].

[165] G. Dotti and R. J. Gleiser, *Linear stability of Einstein-Gauss-Bonnet static spacetimes. Part I. Tensor perturbations*, *Phys. Rev. D* **72** (2005) 44018 [arXiv: gr-qc/0503117].

[166] T. Takahashi and J. Soda, *Stability of Lovelock Black Holes under Tensor Perturbations*, *Phys. Rev. D* **79** (2009) 104025 [arXiv: 0902.2921].

[167] T. Takahashi and J. Soda, *Instability of Small Lovelock Black Holes in Even-dimensions*, *Phys. Rev. D* **80** (2009) 104021 [arXiv: 0907.0556].

[168] R. J. Gleiser and G. Dotti, *Linear stability of Einstein-Gauss-Bonnet static spacetimes. Part II: Vector and scalar perturbations*, *Phys. Rev. D* **72** (2005) 124002 [arXiv: gr-qc/0510069].

[169] T. Takahashi and J. Soda, *Master Equations for Gravitational Perturbations of Static Lovelock Black Holes in Higher Dimensions*, *Prog. Theor. Phys.* **124** (2010) 911 [arXiv: 1008.1385].

[170] N. Dadhich, R. Durka, N. Merino and O. Miskovic, *Dynamical structure of Pure Lovelock gravity*, *Phys. Rev. D* **93** (2016) 64009 [arXiv: 1511.02541].

[171] J. T. Wheeler, *Symmetric solutions to the maximally Gauss-Bonnet extended Einstein equations*, *Nuclear Physics B* **273** (1986) 732.

[172] N. Dadhich, J. M. Pons and K. Prabhu, *On the static Lovelock black holes*, *Gen. Rel. Grav.* **45** (2013) 1131 [arXiv: 1201.4994].

[173] J. Crisostomo, R. Troncoso and J. Zanelli, *Black hole scan*, *Phys. Rev. D* **62** (2000) 84013 [arXiv: hep-th/0003271].

[174] J. Zanelli, *Chern-Simons Forms in Gravitation Theories*, *Class. Quant. Grav.* **29** (2012) 133001 [arXiv: 1208.3353].

[175] S. Deser and G. W. Gibbons, *Born-Infeld-Einstein actions?*, *Class. Quant. Grav.* **15** (1998) L35 [arXiv: hep-th/9803049].

[176] P. Concha and E. Rodríguez, *Generalized Pure Lovelock Gravity*, *Phys. Lett. B* **774** (2017) 616 [arXiv: 1708.08827].

[177] R. Gannouji and N. Dadhich, *Stability and existence analysis of static black holes in pure Lovelock theories*, *Class. Quant. Grav.* **31** (2014) 165016 [arXiv: 1311.4543].

[178] N. Dadhich, S. G. Ghosh and S. Jhingan, *Bound orbits and gravitational theory*, *Phys. Rev. D* **88** (2013) 124040 [arXiv: 1308.4770].

[179] S. Chakraborty and N. Dadhich, *1/r potential in higher dimensions*, *Eur. Phys. J. C* **78** (2018) 81 [arXiv: 1605.01961].

[180] R.-G. Cai, *A Note on thermodynamics of black holes in Lovelock gravity*, *Phys. Lett. B* **582** (2004) 237 [arXiv: hep-th/0311240].

[181] A. Higuchi, *Symmetric Tensor Spherical Harmonics on the N Sphere and Their Application to the De Sitter Group SO(N,1)*, *J. Math. Phys.* **28** (1987) 1553.

[182] M. Maggiore, *Gravitational Waves. Vol. 2: Astrophysics and Cosmology*. Oxford University Press, 2018.

[183] R. A. Konoplya and A. Zhidenko, *Quasinormal modes of black holes: From astrophysics to string theory*, *Rev. Mod. Phys.* **83** (2011) 793 [arXiv: 1102.4014].

[184] B. F. Schutz and C. M. Will, *Black hole normal modes: A semianalytic approach*, *Astrophys. J. Lett.* **291** (1985) L33.

[185] S. Iyer and C. M. Will, *Black-hole normal modes: A WKB approach. I. foundations and application of a higher-order WKB analysis of potential-barrier scattering*, *Phys. Rev. D* **35** (1987) 3621.

[186] R. A. Konoplya, *Quasinormal behavior of the d-dimensional Schwarzschild black hole and higher order WKB approach*, *Phys. Rev. D* **68** (2003) 024018 [arXiv: gr-qc/0303052].

[187] R. A. Konoplya, *Gravitational quasinormal radiation of higher dimensional black holes*, *Phys. Rev. D* **68** (2003) 124017 [arXiv: hep-th/0309030].

[188] E. W. Leaver, *An Analytic representation for the quasi normal modes of Kerr black holes*, *Proc. Roy. Soc. Lond. A* **402** (1985) 285.

[189] W. Gautschi, *Computational Aspects of Three-Term Recurrence Relations*, *SIAM Review* **9** (1967) 24.

[190] S. Chandrasekhar and S. Detweiler, *The quasi-normal modes of the schwarzschild black hole*, *Proceedings of the Royal Society of London. Series A, Mathematical and Physical Sciences* **344** (1975) 441.

[191] C. F. B. Macedo, V. Cardoso, L. C. B. Crispino and P. Pani, *Quasinormal modes of relativistic stars and interacting fields*, *Phys. Rev. D* **93** (2016) 64053 [arXiv: 1603.02095].

[192] F. R. Tangherlini, *Schwarzschild field in n dimensions and the dimensionality of space problem*, *Nuovo Cim.* **27** (1963) 636.

[193] I. I. Olabarrieta, J. F. Ventrella, M. W. Choptuik and W. G. Unruh, *Critical behavior in the gravitational collapse of a scalar field with angular momentum in spherical symmetry*, *Physical Review D* **76** (2007) [arXiv: 0708.0513].

[194] L. B. Szabados, *Quasi-Local Energy-Momentum and Angular Momentum in GR: A Review Article*, *Living Rev. Rel.* **7** (2004) 4.

[195] M. E. Cahill and G. C. McVittie, *Spherical Symmetry and Mass-Energy in General Relativity. II. Particular Cases*, *Journal of Mathematical Physics* **11** (1970) 1392.

[196] G. Abreu and M. Visser, *Kodama time: Geometrically preferred foliations of spherically symmetric spacetimes*, *Phys. Rev. D* **82** (2010) 044027 [arXiv: 1004.1456].